FUNDAMENTAL MECHANISMS OF TENSILE FRACTURE IN ALUMINUM SHEET UNIDIRECTIONALLY REINFORCED WITH BORON FILAMENT

by

Harvey Wayne Herring

Thesis submitted to the Graduate Faculty of the

Virginia Polytechnic Institute and State University

in partial fulfillment of the requirements for the degree of

DOCTOR OF PHILOSOPHY

in

Materials Engineering Science

J. L. Lytton
Dr. J. L. Lytton, Chairman

T. P. Floridis
Dr. T. P. Floridis

A. L. Fricke
Dr. A. L. Fricke

W. C. Hackler
Dr. W. C. Hackler

C. R. Houska
Dr. C. R. Houska

J. H. Steele, Jr.
Dr. J. H. Steele, Jr.

J. P. Wightman
Dr. J. P. Wightman

December, 1971

Blacksburg, Virginia

FUNDAMENTAL MECHANISMS OF TENSILE FRACTURE IN UNIDIRECTIONAL BORON FILAMENT REINFORCED ALUMINUM SHEET

by

Harvey Wayne Herring

(ABSTRACT)

Results are presented from an experimental research effort to gain a more complete understanding of the physics of tensile fracture in unidirectionally reinforced B–Al composite sheet. By varying the degree of filament degradation resulting from fabrication, composite specimens were produced which failed in tension by the cumulative mode, the noncumulative mode, or by any desired combination of the two modes.

Radiographic and acoustic emission techniques were combined to identify and physically describe a previously unrecognized fundamental fracture mechanism which was responsible for the noncumulative mode. The tensile strength of the composite was found to be severely limited by the noncumulative mechanism which involved the initiation and sustenance of a chain reaction of filament fractures at a relatively low stress level followed by ductile fracture of the matrix. The minimum average filament stress required for initiation of the fracture mechanism was shown to be approximately 170 ksi, and appeared to be independent of filament diameter, number of filament layers, and the identity of the matrix alloy.

A comprehensive analysis of tensile fracture surfaces revealed that characteristic features of the surfaces were determined by the mode of fracture. The characteristic features were categorized, and related to the responsible fracture mechanism in such a way that subsequent fractographic analyses of B–Al tensile failures will be greatly facilitated by direct comparison with the results of this investigation.

Tests of specimens which contained flaws in the form of internally broken filaments revealed that a relatively large proportion (up to 20 percent) of the filaments in a given specimen could be broken without directly affecting fracture. Local stress concentrations resulting from internal filament breaks were apparently alleviated by matrix plasticity.

ACKNOWLEDGEMENTS

The author wishes to express his deep gratitude to Drs. Jack L. Lytton and James H. Steele, Jr. for their valuable suggestions and guidance throughout the course of this investigation. He would also like to thank the remainder of his Graduate Committee, and the various faculty members with whom he had contact, for providing an environment truly conducive to the expansion of his capability to analyze and reason. Finally, he would like to extend his appreciation to his family, especially his wife and children, for their considerable patience during his continuing pursuit of a broader understanding of his surroundings.

TABLE OF CONTENTS

LIST OF TABLES

LIST OF FIGURES

I. INTRODUCTION

Based on considerations of density, stiffness, and compressive strength, unidirectional boron filament reinforced aluminum (B–Al) composite is regarded as a potentially useful material for advanced aerospace applications. The material offers two significant advantages over composites with resinous matrices. First, B–Al can perform effectively at temperatures up to 800°F compared with a maximum of about 350°F for boron filament reinforced epoxy. Second, the increased shear and transverse stiffnesses of the aluminum matrix allows unidirectionally reinforced B–Al to effectively resist buckling loads. In resin matrix composites, a capability for withstanding buckling must be developed through a more complicated multidirectional arrangement of filaments.

A perplexing problem associated with B–Al composite has been its disappointingly low tensile strength, with tensile failures typically being observed at an average filament stress less than half the strength of the virgin filament used in fabrication of the composite. A recent investigation at the Langley Research Center of NASA[1] has shown that one commercially available B–Al composite, used in a structural element with sufficient support to prevent buckling, could routinely withstand compressive stresses on the order of 225 ksi without failure. The very same material, however, exhibited a tensile strength of only 100 ksi, suggesting that ultimate strength in tension was being limited by some peculiar

fracture mechanism which became operative at a relatively low stress level.

The problem of tensile fracture in composites containing parallel brittle filaments was analyzed by Zweben and Rosen[2,3,4] in a series of recent papers. Zweben, in particular[2] described two fundamental fracture modes. One of them, the cumulative mode, was characterized by the gradual accumulation of a considerable number of individual filament breaks in advance of total composite fracture.

The cumulative mode can occur when filaments break under the influence of stress concentrations resulting from their previously broken neighbors, or when filaments break in scattered locations according to their individual load bearing capabilities. Ultimate failure of the composite occurs almost instantaneously when the cross-sectional area of unbroken filaments becomes too small to withstand the increasing load.

The second fracture mode did not involve a significant number of individual filament breaks prior to composite fracture, and was referred to as the noncumulative mode. The actual mechanism of noncumulative fracture was not specified, but was assumed to precipitate from the fracture of only a few of the weaker filaments in the composite.

The cumulative fracture mode was observed by Rosen[5] in the tensile failure of glass filament reinforced epoxy composites. The noncumulative mode was observed by Mullin and his coworkers[6,7,8] in the failure of boron-epoxy and graphite-epoxy composites. In

Mullin's work, noncumulative fracture occurred in some composites when one of the first filaments to break initiated a matrix crack which propagated through both filaments and matrix to cause rapid, complete failure of the composite.

Most unidirectional composites of practical significance undergo tensile failure by a combination of the two modes proposed by Zweben. As load is increased, the weaker filaments break cumulatively, but above some threshold value of average filament stress, a noncumulative mechanism becomes operative to cause catastrophic fracture. The physical nature of the noncumulative mechanism depends on the local response of the matrix and the filament–matrix interfacial bond to the sudden release of elastic strain energy by a breaking filament. If the matrix responds by cracking, then ultimate composite strength can possibly be improved by toughening the matrix, or by creating internal energy sinks to absorb a portion of the energy pulse. The strength increase would result from a broadening of the stress range over which cumulative fracture may occur, and a corresponding postponement of the disastrous noncumulative mode.

Mullin was able to control the fracture mode for boron–epoxy and graphite–epoxy composites by decreasing the crack sensitivity of the epoxy, and by adjusting the filament–matrix interfacial bond strength to allow energy absorption by a small amount of debonding near the newly formed ends of a broken filament. He was able to produce composite which failed cumulatively, noncumulatively, and by combinations of the two modes.

In this thesis, results are presented from an experimental research effort to gain a more complete understanding of the physics of tensile fracture in unidirectionally reinforced B–Al composite sheet. By varying the degree of filament degradation resulting from fabrication, it was possible to produce composite specimens which failed in tension by the cumulative mode, the noncumulative mode, or by any desired combination of the two modes. Radiographic and acoustic emission techniques were combined to identify and physically describe a previously unrecognized fundamental fracture mechanism which was responsible for the noncumulative mode in unidirectional B–Al composite. A threshold value of average filament stress was determined below which the noncumulative mechanism was not operative. Common features of tensile fracture surfaces were categorized and found to be compatible with the observed mechanism of fracture. The effects of internal stress concentrations in the form of previously cut filaments were investigated, and, to a limited extent, so were the effects of variations in matrix composition, filament spacing, and internal bond strengths. Preliminary results from this research program have previously been presented by Steele and Herring[9,10].

II. LITERATURE REVIEW

The process of tensile fracture in unidirectional filamentary composites can be quite complicated, and depends to a great extent on the properties of the filaments and the matrix and the strength of the interfacial bond between them. If the filaments are brittle, as is the case for boron, then they do not possess a unique strength, and any attempt at analytical description of composite fracture must employ a statistical approach.

A. Evolution of a Statistical Strength Theory

The evolution of a statistical strength theory for unidirectional composites has involved three steps. The first was to obtain a probability density function which adequately described the strength of a single filament. It was then necessary to develop a statistical strength relationship for a group or bundle of filaments. Finally, those results were applied to an actual composite by accounting for the contributions of a matrix to composite strength.

Coleman[11] used a weakest link hypothesis to show that the cumulative distribution function of Weibull[12] was generally descriptive of the strength characteristics of individual brittle filaments. Daniels[13] considered the problem of a large bundle of parallel filaments. He found that bundle strength was characterized by a Gaussian distribution function, and that on the average,

bundle strength was less than the strength of the constituent filaments. No stress concentration or dynamic effects were considered.

1. The Cumulative Weakening Model

The first application of the statistical theory of filament and bundle strengths to composite strength was made by Gücer and Gurland[14]. They developed a so-called cumulative weakening model in which the composite was composed of a stack of transverse layers of thickness, t. Each layer contained a number of filament segments loaded uniformly in parallel. Each filament segment of length, t, was assumed to fail independently, and composite failure occurred when one of the layers contained a sufficient number of broken filaments so that the surviving filaments within that layer could no longer support the applied load. Thus the cumulative weakening model treated the composite as a chain of bundles, and failure of the composite was coincident with failure of the weakest bundle. The length of a bundle (thickness of a layer) was not defined.

Rosen[5] realized that a broken filament was rendered ineffective only over the length required for reassumption of the load by shear transfer through the matrix. That ineffective length defined the layer thickness in the cumulative weakening model because a filament break within a given layer was required by definition to render the filament ineffective only within that layer. Rosen used a shear lag analysis to determine the ineffective length, and thereby made the cumulative weakening model amenable to numerical calculations. He then proceeded to show that there was considerable

disagreement between predictions based on the model and experimental results from monolayer glass filament reinforced epoxy sheet.

The cumulative weakening model was based on Daniels' bundle strength analysis which ignored stress concentrations and dynamic effects resulting from a filament break. Hedgepeth[15] calculated static and dynamic stress concentration factors for a monolayer composite sheet containing various numbers of broken filaments. The calculations were later extended to three dimensional composites by Hedgepeth and Vandyke[16]. Zweben[2] refined the cumulative weakening model for a two dimensional composite by applying the static stress concentration factors to filaments adjacent to broken ones in a layer of the model. The three dimensional case was treated later by Zweben and Rosen[4]. Those refinements brought predictions based on the cumulative weakening model into much closer agreement with the experimental results obtained by Rosen[5] for glass–epoxy composites.

2. The Noncumulative Mode

The cumulative weakening model in its present form accurately describes the tensile failure of fiberglass reinforced epoxy composites. However, the model is not generally applicable because it does not consider internal debonding or dynamic effects produced by filament fractures. Zweben[2] also discusses a noncumulative fracture process in which ultimate composite failure is preceded by very few filament breaks at most, indicating that composite failure is precipitated by fracture of perhaps the weakest filament. No

mechanism is proposed to account for noncumulative fracture, but some of the dynamic effects ignored by the cumulative weakening model could obviously be involved.

B. Experimental Observations

Mullin and his coworkers[6,7,8] have analyzed composite fracture in terms of the elastic strain energy released when a filament breaks. They have amassed a considerable quantity of experimental information concerning fracture of both boron–epoxy and graphite–epoxy composites. By adjusting the toughness of the matrix and the strength of the filament–matrix interfacial bond, they were able to observe a variety of fracture modes. The previously described cumulative fracture mode was observed when the matrix was sufficiently tough to absorb the energy released by the majority of filament breaks without cracking. As matrix toughness was reduced, some of the higher strength filaments produced matrix cracks when they failed. In the limiting case of an extremely brittle matrix, practically any filament break would initiate a crack which immediately propagated through the composite causing catastrophic noncumulative fracture.

The role of the interfacial bond was also emphasized by Mullin. If bond strength were very low, then a broken filament could simply pull itself free of the matrix, and thus become completely ineffective, the same as for a bundle. A high bond strength was consistent with either cumulative or noncumulative fracture. An intermediate bond strength allowed a small amount of debonding to

occur near the newly formed ends of a broken filament. The debonding process absorbed a portion of the energy pulse resulting from a filament break, and served the same purpose as toughening the matrix.

Most of the experimental observations of fracture have been concerned with resinous matrix composites because those materials were amenable to study by photoelastic analysis and through transmission of visible light. Due to the inapplicability of those standard techniques, experimental studies of fracture in the B–Al system have been limited. The most significant work done thus far has probably been that of Jones[17], who was the first to make extensive use of the scanning electron microscope in the study of B–Al fracture surfaces. Jones' work consisted primarily of a phenomenological observation of fractures. He did not make a concerted attempt to deduce a mechanism to account for the fracture surface features he observed.

One unexpected feature of B–Al tensile fracture surfaces was obvious from Jones' photographs. Even though his specimens failed at very low strains, matrix fracture occurred in a ductile manner. That was surprising considering the work of Shimizu[18]. He determined that the matrix was in a complicated state of triaxial stress resulting partly from the thermal contraction mismatch between boron and aluminum during fabrication, and partly from the different Poisson's ratios of the two materials during tensile loading. The majority of the matrix was determined by photoelastic measurement to be in triaxial tension, and thus would be more sensitive to cracking than normal. Because of that, it had been supposed that

low strain failures of B–Al composite occurred in a manner similar to that observed by Mullin for a boron–epoxy composite with reduced matrix toughness. The observed ductile matrix failure was not consistent with that supposition.

C. Fracture of Internally Flawed Composites

The problem of load concentrations in an internally flawed composite was first considered by Hedgepeth[15]. His model consisted of an infinite composite sheet containing one layer of parallel filaments which supported the entire tensile load. They were uniformly spaced in an elastic matrix which carried only shear. The internal flaw took the form of a transverse slit which cut through a variable number of filaments, and Hedgepeth calculated both the static and dynamic load concentrations on the first few filaments away from each end of the slit. In a subsequent paper, Hedgepeth and Vandyke[16] extended the calculations to include three dimensional composites and the effect of matrix plasticity on reducing the load concentrations.

The problem of ultimate tensile fracture in internally flawed composites was treated by Zweben[19,20] using the load concentrations of Hedgepeth and Vandyke. For composites in which the reinforcing filaments had a unique strength, the solution was straightforward, and an exact formulation was possible. As soon as the concentrated load on the first filament adjacent to either end of the slit was more than that filament would bear, fracture of the entire composite

resulted.

With brittle filaments as the reinforcement, the problem became more complicated. The statistical strength distribution of boron filaments was associated with a definite point to point variation in strength along the lengths of all filaments. Thus, any filament subjected to a stress concentration at one point, say at the end of a slit, might very well fail at a weak point some distance away from the slit. It was also necessary to consider the magnitudes of concentrated stress several filaments away from each end of the slit, since a finite probability existed that the filament adjacent to the broken filament would survive while one of its neighbors a few filaments away broke under the influence of a less concentrated stress. Zweben accounted for those effects by assuming that the strength of boron filaments was characterized by the Weibull distribution function. On that basis he was able to arrive at an expression for a lower bound on the ultimate tensile strength of internally flawed boron filament reinforced composites.

III. MATERIALS AND SPECIMENS

The B–Al composite used most extensively in this study was fabricated at the Langley Research Center of NASA. A primary reason was that material with reproducible properties could not be procured from commercial vendors at the time the study was initiated. Filament spacing was not uniform in commercially available composites, and filament–matrix and matrix–matrix bonds varied from poor to nonexistent within just a few interfilament spacings in the material. Another reason for in–house fabrication was the desire for first–hand control of the fabrication process. Considerable flexibility was thus allowed in the choice of fabrication parameters which affected the physical and mechanical properties of the composite. A significant effort was devoted in the first phase of the research program to the development of a fabrication process which would routinely produce well bonded composite with accurately controlled filament spacing and reproducible mechanical properties. No attempt was made to produce composite with optimum mechanical properties. The primary purpose of the research program was to gain a more complete understanding of the fundamental fracture characteristics of the material. Composite fabrication procedures were altered as necessary to serve that purpose.

A. Composite Fabrication

1. Filament Winding Apparatus

A combined filament winding and diffusion bonding process was used to produce B–Al composite in the form of unidirectionally reinforced sheet. The apparatus constructed for filament winding is shown in Figure 1. Boron monofilament was taken off the manufacturer's reel, passed across a traversing mechanism, and wound onto a cylindrical mandrel covered with a single layer of aluminum foil. The mandrel was driven by a variable speed electric motor through a reduction gear. The traversing mechanism used to locate the filament on the mandrel surface was gear driven at a constant speed. Smooth filament tension was provided by magnetically braking the payoff reel. A conventional three–phase alternating current motor was converted to a magnetic brake for this purpose. The stator winding of the motor was connected so as to provide maximum magnetic coupling with the rotor when direct current was applied. The shaft of the payoff reel was coupled to the shaft of the altered motor, and continuously variable braking action was obtained by passing the alternating current output from a variable transformer through a full wave silicon rectifier into the motor.

Filament spacing was controlled by varying the speed of mandrel rotation, but the factory speed control device was not sufficiently stable against minor line voltage fluctuations to permit accurate filament placement. To eliminate that problem, a stroboscopic tachometer was set at the desired speed for the mandrel

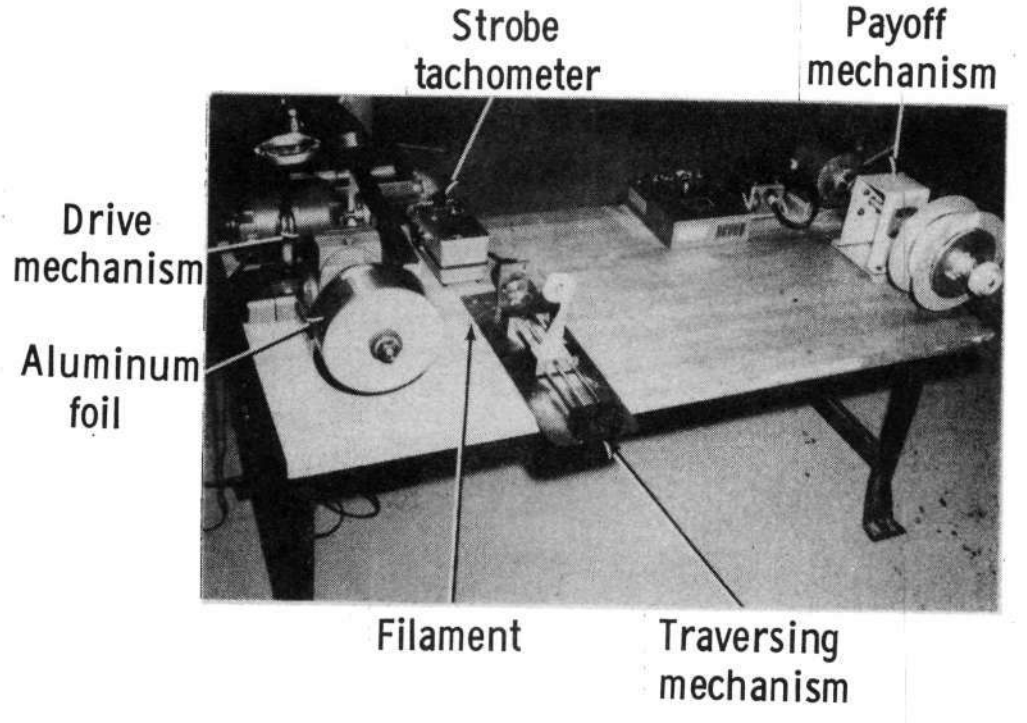

Figure 1. - Filament winding apparatus used in fabrication of B-Al composite sheet.

drive motor. Precise speed control was achieved by continuous manipulation of a ten-turn potentiometer added to the factory speed control so as to match the speed of the stroboscopic flash. Once the winding apparatus had been perfected, it was possible to make an advance calculation of desired filament spacing, and then to duplicate the calculated value in practice with an error of less than one percent per inch of traverse.

2. Fabrication of Monolayer Preform

A four inch wide sheet of three mil thick 1230 aluminum alloy foil was wrapped around the circumference of a 9.5 inch diameter wooden mandrel such that the ends butted precisely together. The 1230 aluminum alloy was chosen because it was available in copious quantities at the Langley Research Center, and because its purity (99.3% Al) would ensure the production of clean, precipitate-free fracture surfaces. The exposed surface of the foil was transversely brush painted with an air-drying acrylic resin solution (Rohm and Haas "Acryloid B-66") which dried with sufficient tack to maintain filament spacing and alignment. The resin formulation was one of several available which would evaporate completely during subsequent consolidation of the composite. Either 3.9 mil or 5.6 mil diameter boron filament was wound at 200 or 160 per inch, respectively onto the resin coated surface of the foil, and a second coating of resin was applied to the layer of filaments. Once the resin was dry, foil and filaments were removed from the mandrel as a 30 inch long unit by cutting through the filaments along the butt between foil ends. The resin binder was

sufficiently pliable when dry to allow the monolayer foil–filament preform to be flattened without laterally displacing the filaments. The flat preform was cut into three inch wide by seven inch long rectangular segments with their length parallel to the filament direction. The segments were stacked in the sequence Al–B/Al–B/– – – – –/Al as desired in preparation for consolidation by diffusion bonding.

3. Diffusion Bonding

Consolidation of filaments and foil into composite sheet was accomplished by diffusion bonding the stacked preform segments in an evacuated stainless steel retort. A thin, water–base slurry of powdered magnesium oxide was applied as a parting agent between the retort and the composite. Retort pressure was maintained below 10^{-3} mm Hg. The retort and its contents were heated from ambient temperature to 800°F under contact pressure between electrically heated platens installed in a 300 kip capacity hydraulic testing machine. That temperature was held for 15 minutes to allow the resin binder to evaporate. Pressure was then applied through the platens as they were heated to the bonding temperature. Both the temperature and the heating rate were electronically controlled during the heating portion of the diffusion bonding cycle. The heating rate was 30°F per minute, and the instantaneous temperature varied no more than $\pm$ 3°F from its intended value. The bonding temperature was maintained for one hour. The bonding pressure, however, was not relaxed until the retort had

cooled to 300°F so that buckling of individual filaments under the compressive stress generated by the different thermal contraction tendencies of aluminum and boron would be prevented. The cooling portion of the cycle was not controlled, but the time required for cooling to 300°F was approximately 2.5 hours.

B–Al composite sheets containing from one to five layers of filament were fabricated. A sheet containing one layer of filaments was referred to as a monolayer sheet. One with two layers was referred to as a bilayer, and so on. Since foil was available in only one thickness, the filament volume fraction varied with the number of layers in the composite. The variation was from 0.20 for a monolayer composite to 0.45 for a five layer composite, both containing 3.9 mil diameter filament. The 5.6 mil diameter filament was used only to fabricate monolayer sheet, and the volume fraction of filaments was 0.33.

In the great majority of cases, bonding temperature was 1100°F and bonding pressure was 10 ksi. Those conditions were made severe by design so that production of well bonded composite would be ensured. Sheet material with reproducible properties was required, and to that end, the decline in average composite strength resulting from increased filament degradation was accepted. In several instances bonding pressures as high as 15 ksi were used in a deliberate attempt to influence the degree of filament degradation resulting from consolidation. In one case, both pressure and temperature were reduced to 9 ksi and 950°F, respectively, in order to produce composite sheet in which filament–matrix and matrix–matrix

bond strengths would approximate those usually found in commercially fabricated composites.

The weakly bonded composite was inadvertantly made with substandard filament. A reel of boron filament normally contains approximately 35,000 feet of filament made up of spliced lengths not less than 1000 feet long. These smaller lengths are produced consecutively in the same run, and result from breaks which occasionally occur during production. In one reel used to fabricate specimens for this study, the manufacturer had spliced in several lengths of a 3.5 mil diameter filament at random. This filament was unusually weak as determined by the abnormally high frequency of breaks during filament winding. All except one length were detected and destroyed as they came off the reel. The remaining length found its way into the weakly bonded composite.

B. Commercially Fabricated Composite

A quantity of commercially produced B-Al composite was also included in the study. The material contained five layers of filament, and was fabricated by filament winding and diffusion bonding 4.1 mil diameter silicon carbide coated boron filament and 2024 aluminum alloy foil. Specific fabrication parameters were not available from the manufacturer, but as the general case for commercially available materials, filament-matrix and matrix-matrix bonds were relatively weak. That condition did not necessarily represent poor quality, but resulted from reduced reactivity between silicon carbide and

aluminum and the deliberate adjustment of fabrication parameters by the manufacturer to minimize filament degradation. The commercial material contained 48 percent filaments by volume.

C. Specimens

Composite tensile specimens, 0.50 inch wide with a gage length of 2.0 inches, were cut from sheet material by electrical discharge machining. A typical specimen is shown in Figure 2 prior to testing. The specimens had straight edges, and were cut so that load would be applied parallel to the filaments. Beveled fiberglass tabs with a nylon-flexibilized epoxy matrix were adhesively bonded to the specimen ends to ensure a gradual transfer of load from the grips of the testing machine into the specimen.

A number of specimens were fabricated with internal flaws in the form of intentionally cut filaments. The flaws were created by placing a monolayer preform segment under a low power stereo microscope and cutting (or crushing) the desired number of adjacent filaments with a scalpel. Filament cuts were located in the preform segment in such a way that after consolidation to produce a monolayer sheet, tensile specimens could be obtained with predetermined numbers of transverse cuts roughly centered in their gage sections.

Several cutting methods were tried for removing specimens from B-Al composite sheet, including shearing, diamond sawing, and electrical discharge machining. The electrical discharge method

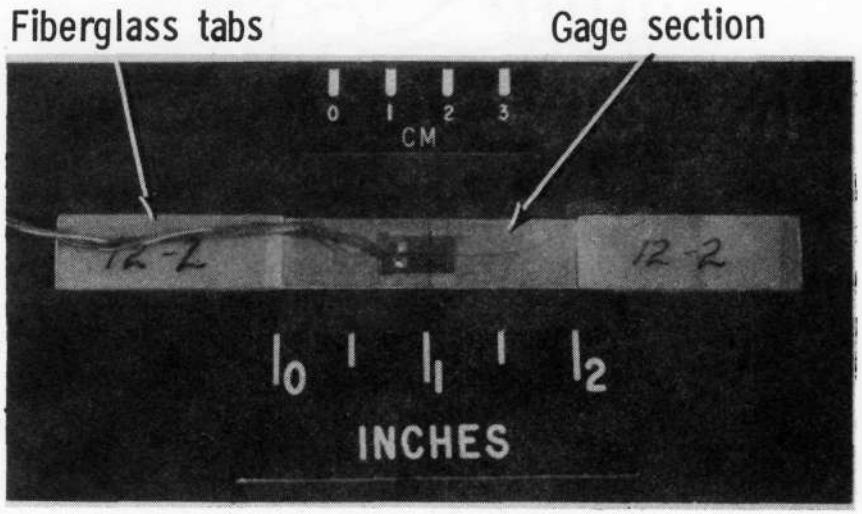

Figure 2. - Typical B-Al sheet tensile specimen prior to testing.

produced the smoothest edge and the least number of filament breaks in from a specimen edge. Figure 3 shows the typical appearance of a machined edge of a bilayer specimen. Only one filament is visible, and it has been neatly sliced parallel to its axis.

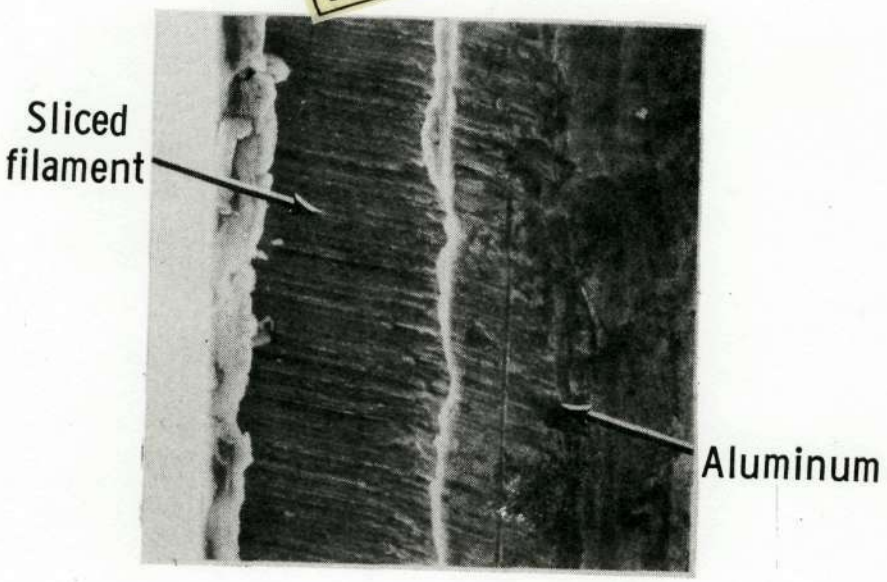

Figure 3. - Edge of bilayer B-Al composite tensile specimen cut by electrical discharge method.

IV. EXPERIMENTAL PROCEDURE

A. Composite Sheet

1. Tensile Testing

The apparatus for composite tensile testing is represented schematically in Figure 4. A specimen was mounted in a testing machine with sufficiently precise alignment so that tensile strains resulting from both in-plane and out-of-plane bending were less than two percent of the total axial strain. For the majority of tests, strain output was recorded from a single foil-type gage bonded to the center of one specimen surface. Strain was recorded autographically as a function of load. A few specimens with multiple strain gages were periodically tested to ensure that alignment was being maintained. The strain rate was 0.002 per minute for all tests.

2. Acoustic Monitoring

A capacitance microphone was placed approximately 0.030 inch away from a specimen to collect acoustic emissions during testing. Its output was amplified and routed through a loudspeaker so that sounds from filaments breaking, both individually and in groups, would be audible. The acoustic monitoring system was used to indicate the onset of fracture, and was useful only in instances where catastrophic fracture of the composite was preceded by at least a small number of filament failures. No attempt was made to record and analyze

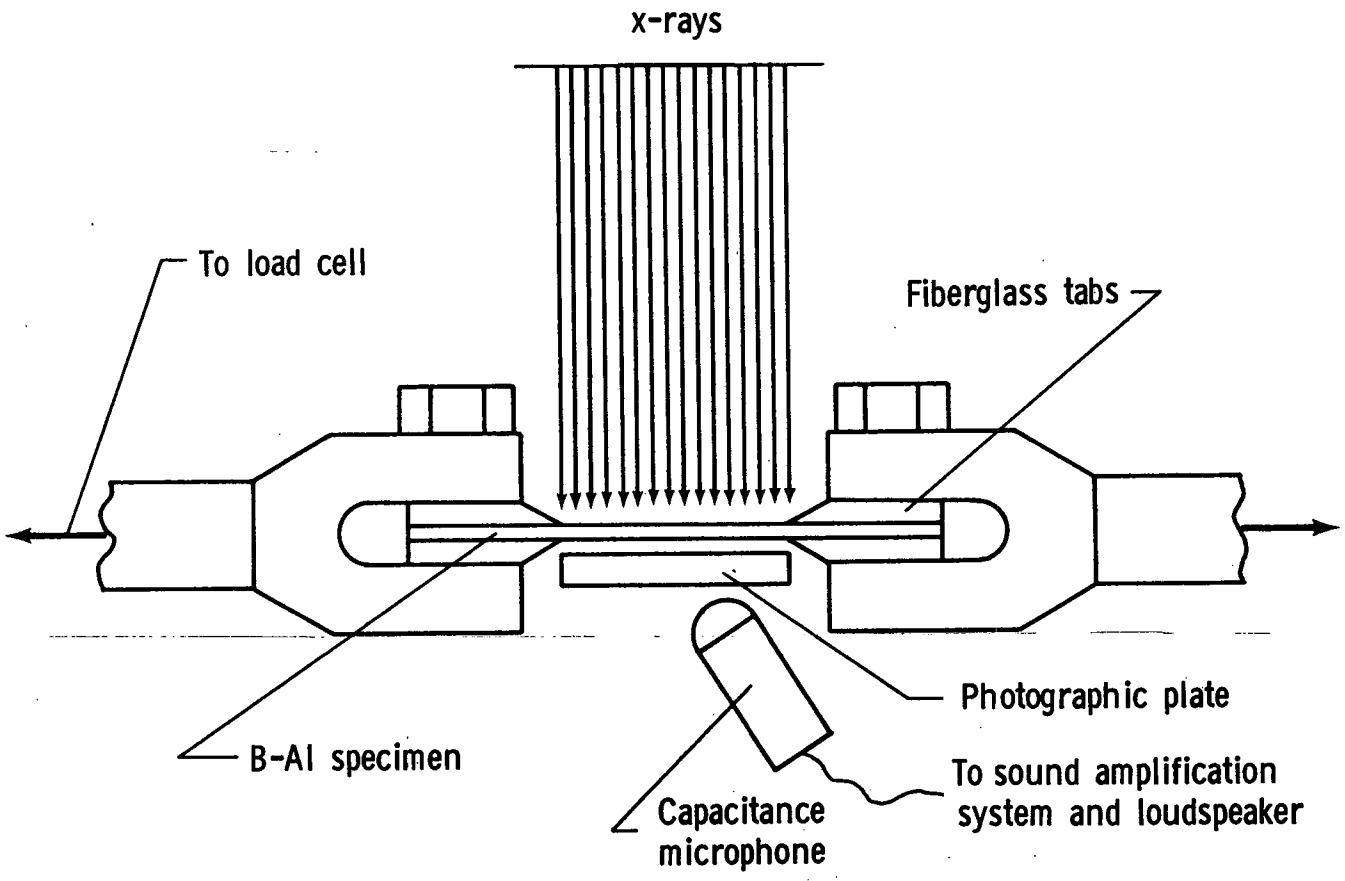

Figure 4.- Schematic drawing of apparatus used to study tensile fracture of B-Al composite sheet.

the acoustic frequency spectrum associated with fracture.

3. Radiography

A source of X-rays was placed so that a photographic plate on the opposite side of the specimen could be exposed to reveal interior details of the composite. Specimens were radiographed before loading, under load, and after failure in an attempt to establish the sequence of events involved in the fracture process. Kodak high resolution plates were exposed for 10 to 15 minutes at an X-ray tube voltage of 100 kV. Slightly better resolution could have been obtained at lower voltage, but the required exposure time would have been considerably longer. A short exposure time was desirable because of the large number of specimens involved in the program, and also because of the difficulty in maintaining a constant load on a specimen for long periods of time. Specimens in which ultimate fracture was preceded by cumulative breaking of filaments as a function of time could not be radiographed successfully at high loads because of the long exposure time required.

4. Photography

Photographs of the radiographic images were taken at magnifications up to 550X on Kodak metallographic plates. A bench metallograph was used with light transmitted through the plate containing the radiographic image. The emulsion grain of the high resolution plates could be discerned on the photographs, but did not interfere with the interpretation of the radiographic

results.

Matching fracture surfaces were observed and photographed on Polaroid film using the Cambridge Stereoscan scanning electron microscope. The B–Al composite was sufficiently conductive so that coating was not necessary. No special techniques were required.

5. Fracture Arrest

In order to effectively study the noncumulative mechanism of fracture, it was necessary to be able to stop the fracture process short of complete specimen failure. For the majority of specimens tested, fracture, once initiated, was extremely rapid. To arrest a crack by load relaxation was a trial and error process which resulted in a goodly number of fracture surfaces, but a dearth of arrested cracks. Nevertheless, that method was successful in a sufficient number of instances. In some specimens, alignment was accurate enough so that two cracks would begin simultaneously at different locations. One would invariably result in separation of the specimen, and the other would be arrested for further study.

B. Filament Tensile Tests

A quantity of B–Al composite sheet having unique fabrication parameters was referred to as a batch. At least one typical tensile specimen from each of several batches was not tested in the normal manner. Instead, the matrix was leached out in a warm sodium hydroxide solution, and the reclaimed filaments were tested

individually. Tensile strength distributions for filaments contained within each batch were thus determined. Gage length was 5.1 cm and strain rate was 0.002 per minute, the same as for the composite specimens. Filaments were gripped for testing by bonding their ends to grooved metal tabs with sealing wax according to the method prescribed by Herring[21].

V. RESULTS AND DISCUSSION

The majority of the B–Al sheet material used in this study was well bonded. A strong diffusion bond had been achieved between foil layers during consolidation, and a chemical bond had been developed between the boron filaments and the aluminum matrix. The tensile failure mode for well bonded composite was generally noncumulative provided the filaments had not been severely degraded during consolidation. Ultimate failure of the composite was preceded by very few, if any, individual filament breaks. By adjusting the pressure and temperature involved in consolidation of the composite, however, it was possible to vary the fracture mode. Fracture could be made noncumulative, cumulative, or partially cumulative as desired.

The noncumulative mode will be discussed first and most extensively because the mechanism involved was the limiting factor in the failure of nearly all the specimens tested in this investigation. The fracture of weakly bonded composites and commercially fabricated composites will be analyzed based on considerations of the two fundamental modes. A stress criterion for noncumulative fracture will be established based on experimental data obtained from all the composite types studied. Finally, the results of a brief study of the effects of internal filament damage on composite fracture will be presented and discussed.

A. Noncumulative Fracture

1. Radiographic Evidence

Noncumulative fracture was not preceded by individual filament breaks, therefore there was no acoustic signal to indicate the onset of fracture. Sequential radiographs at various stages of the fracture process were obtained in only a few instances, and then only by a combination of perseverance and good fortune. A typical sequence is represented by the pair of radiographs shown in Figure 5. Both radiographs were taken through the same region of a monolayer specimen so that identical filaments are shown in Figures 5(a) and 5(b). The vertical white lines are the tungsten boride cores. The surrounding sheaths of boron are seen as dark bands adjacent to the cores, and the aluminum matrix is represented by the lighter bands separating the boron.

The radiograph of Figure 5(a) reveals the initial stage of tensile fracture in the form of several broken filaments extending inward from the edge of the specimen. Two different filament fracture modes are observed. The third and fifth filaments from the edge of the specimen are broken cleanly, but the remaining filament breaks are characterized by the presence of wedge-shaped fragments. The matrix between the broken filaments is still continuous, and has remained visibly unaffected by the filament breaks.

In Figure 5(b), the same region is shown after complete fracture of the specimen. All the additional filament breaks

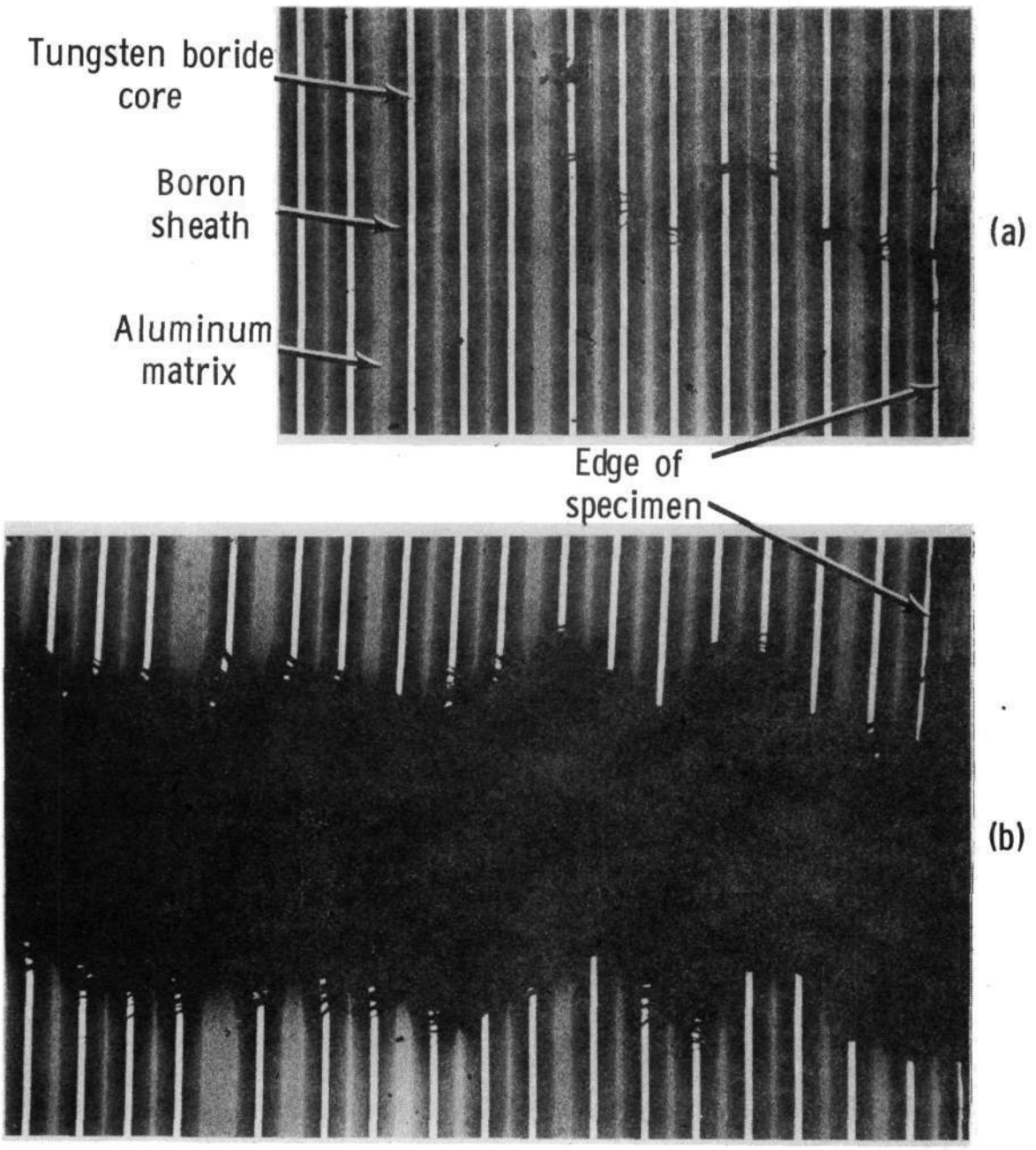

Figure 5. - Tensile fractoradiographs of monolayer B-Al composite: (a) crack initiation near edge of specimen; (b) same region after complete fracture, 0.6 mil core diameter.

were accompanied by fragmentation, and the shape and distribution of the fragments bear a definite relationship to the direction of crack propagation. The wedge-shaped fragments are displaced in the direction of propagation, and the wedges are all oriented so that they appear as arrowheads pointing opposite to the direction of propagation.

2. The Noncumulative Fracture Mechanism

Based on the radiographs of Figure 5, the following fracture scheme is proposed. The third and fifth filaments from the edge of the specimen were weak and broke first, perhaps simultaneously. The elastic strain energy stored in each filament was abruptly released, apparently in the form of transverse compressive stress waves. The stress waves propagated transversely through the matrix and impacted against adjacent filaments with sufficient force not only to shatter them, but also to displace the fragments within the matrix. Fragments from the fourth filament were not displaced because they were in a region where two waves of approximately equal energy content were oppositely directed, therefore their displacement was neutralized. As each successive filament was broken, the energy content of the original stress wave was alternately depleted and replenished. The wave was completely damped in Figure 5(a), but above some threshold value of average filament stress, the mechanism, which shall henceforth be referred to as noncumulative filament break propagation, became self sustaining and catastrophic fracture resulted.

3. The Effect of Filament Spacing

The effect of filament spacing was not investigated in the sense that composite sheets with various uniform spacings were tested. That was not possible for two reasons. The first was that precise increases in the thickness of the foil used to fabricate the composite would have been necessary in order to provide the additional aluminum required to fill the increased volume between filaments. No capability existed for making such adjustments in thickness. The second reason was concerned with a limitation of the diffusion bonding method of consolidation. It was pointed out by Dolowy[18] that the development of a strong matrix-matrix bond depended on whether the oxide films on faying foil surfaces could be ruptured before contact was made. Rupture of the films normally occurred when the aluminum was forced into the spaces between filaments under the influence of the bonding pressure. However, when the gap between filaments exceeded 1.5 diameters, rupture of the oxide films occurred only in the vicinity of the filaments where deformation was greatest. The films were left intact in the spaces between filaments, and incomplete matrix bonding was the result. It was possible, however, to fabricate B-Al sheets with small numbers of filaments missing at various locations. That was accomplished by removing filaments from monolayer preform segments before consolidation, and as many as five adjacent filaments were removed in a given location. The resulting deficiency in bond strength between matrix elements was localized, and did not seem to have a significant effect on gross specimen behavior.

A typical specimen with missing filaments is represented by the pair of radiographs presented as Figure 6. Both radiographs were taken through the same region of a monolayer specimen which contained a gap created by the removal of two adjacent filaments. In Figure 6(a), the initial stage of noncumulative filament break propagation is evident in the first three filaments in from the specimen edge. Figure 6(b) shows the same region after complete specimen fracture. The compressive stress wave was not damped as a result of the gap between filaments. The noncumulative filament break propagation mechanism described in the previous section continued across the gap to cause complete fracture of the specimen. Identical behavior was observed for specimens containing gaps produced by the removal of up to five filaments. Specimens with larger gaps were not tested, therefore the ultimate gap width required to inhibit filament break propagation was not determined. However, B-Al sheet with filaments spaced farther apart than even two filament diameters would have little practical engineering significance.

4. Correlation with Fracture Surface Features

The photograph presented as Figure 7 was taken of matching tensile fracture surfaces of a monolayer composite. The two halves of the specimen may be matched by mentally inserting the bulbous projection of the second filament up from the lower left corner (denoted by arrow) into its corresponding depression on the opposite surface. Two important features are observed which serve

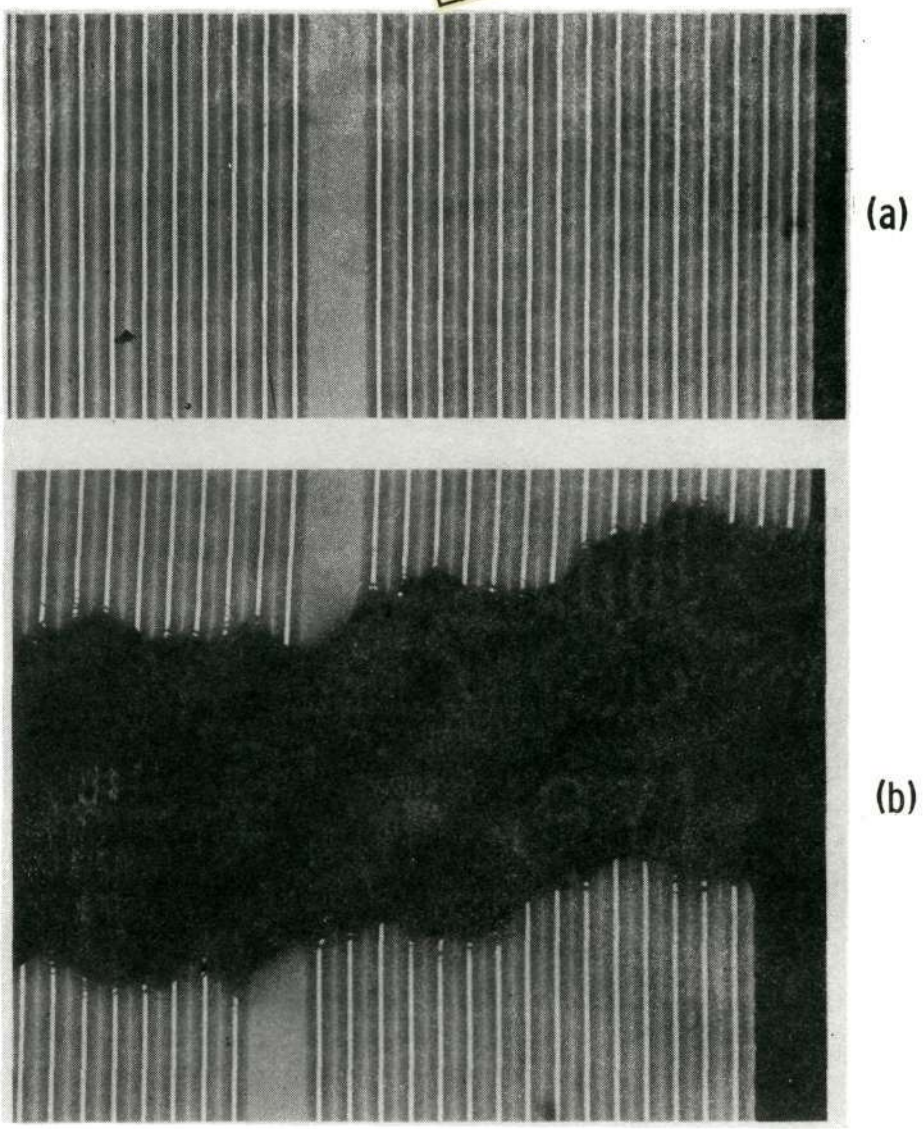

Figure 6. - Tensile fractoradiographs of monolayer B-Al composite with missing filaments: (a) crack initiation near edge of specimen; (b) same region after complete fracture, 6 mil core diameter.

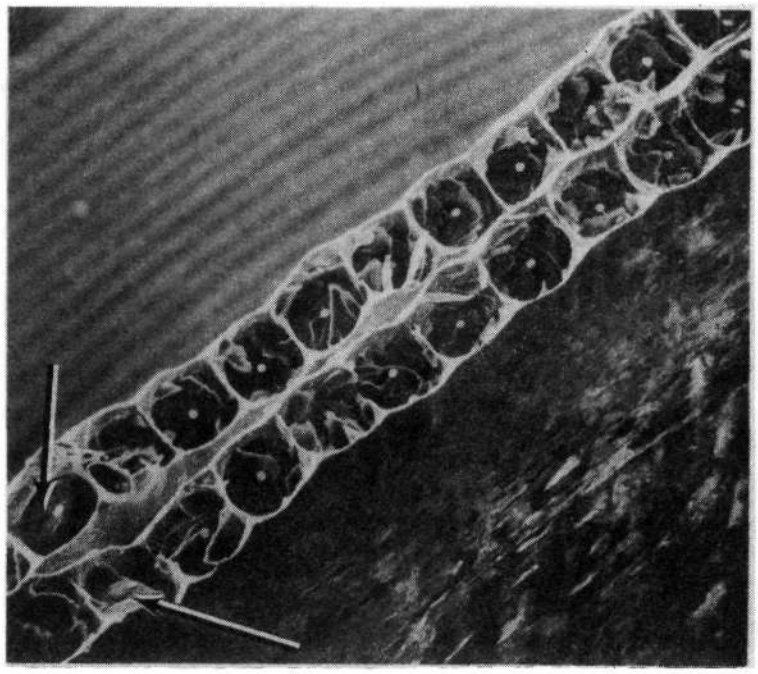

Figure 7. - General view of matching transverse fracture surfaces of monolayer B-Al composite showing filament fragmentation, 5.6 mil filament diameter.

to corroborate the noncumulative filament break propagation mechanism discussed previously. One is the presence of wedge-shaped fragments associated with each broken filament. The second is related to fracture modes exhibited by the matrix.

Details of the matrix fracture are more visible in the magnified view of Figure 8. Each broken filament lies at the bottom of an aluminum crater whose outer walls have the appearance of the shear lip in a conventional cup-cone fracture. Also, a scalloped effect is observed along the boundaries of the overall specimen fracture surface as a result of restraint imposed by the filaments on necking of the matrix. At the junctions of crater walls, gross pores resulting from microvoid coalescence are observed, indicating the fracture mode there to be ductile rupture.

All these observations indicate that matrix fracture occurred in a completely ductile manner by the normal processes of plastic flow. Combining the photographic evidence with that obtained from analysis of the radiographs, it is apparent that individual filament fractures do not initiate matrix cracks. It is also apparent that filament fracture occurs several inter-filament spacings in advance of matrix fracture. The relatively flat, transverse fracture surface is an expected result of the noncumulative filament break propagation mechanism, since the stress waves emanating from filament breaks impact against adjacent filaments at the point of closest approach.

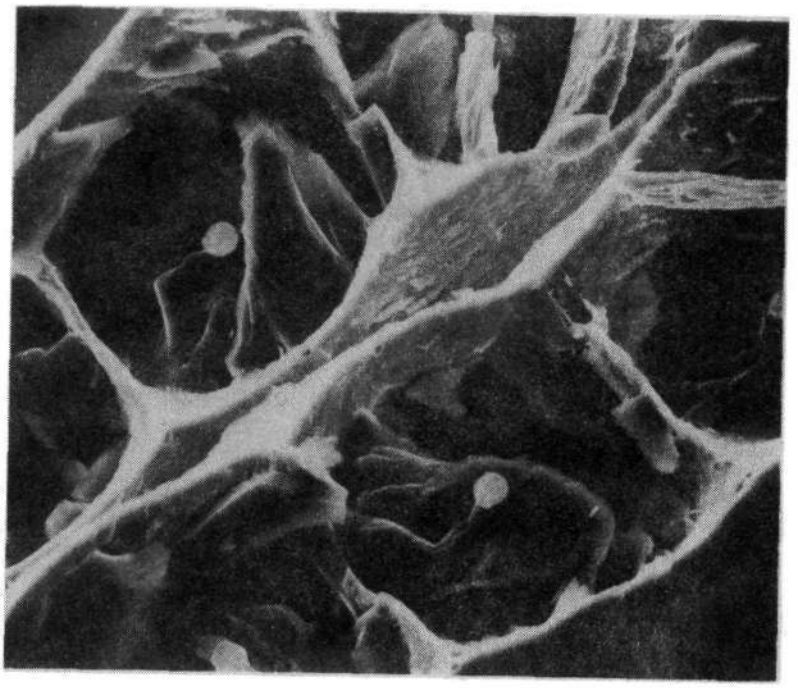

Figure 8. - Matching transverse fracture surfaces of monolayer B-Al composite showing details of matrix fracture, 5.6 mil filament diameter.

B. Modifications of Noncumulative Fracture

The noncumulative filament break propagation mechanism appeared to govern the tensile strength of well bonded composites regardless of the number of filament layers they contained. Identical evidence of its occurrence was observed on fracture surfaces of composites containing as many as five layers of filament. The interpretation of radiographs become difficult, however, for trilayer and thicker materials because of overlapping filament images. For that reason, most of the subsequent discussion is restricted to fracture of monolayer or bilayer composites. Ostensibly, no loss of generality results from this restriction.

1. Initiation

As a general rule, crack initiation occurred at a specimen edge, probably at a stress concentration produced by machining. The radiograph presented as Figure 9 shows an arrested crack extending inward from the edge of a specimen containing two layers of filaments. The apparent irregularity in filament spacing was the result of looking through superimposed filament layers. The actual irregularity was not severe as will be seen in subsequent fracture surface observations. All the features of the noncumulative filament break propagation mechanism were present, including the displaced wedge-shaped fragments and broken filaments in advance of matrix fracture. Necking of the matrix between broken filaments

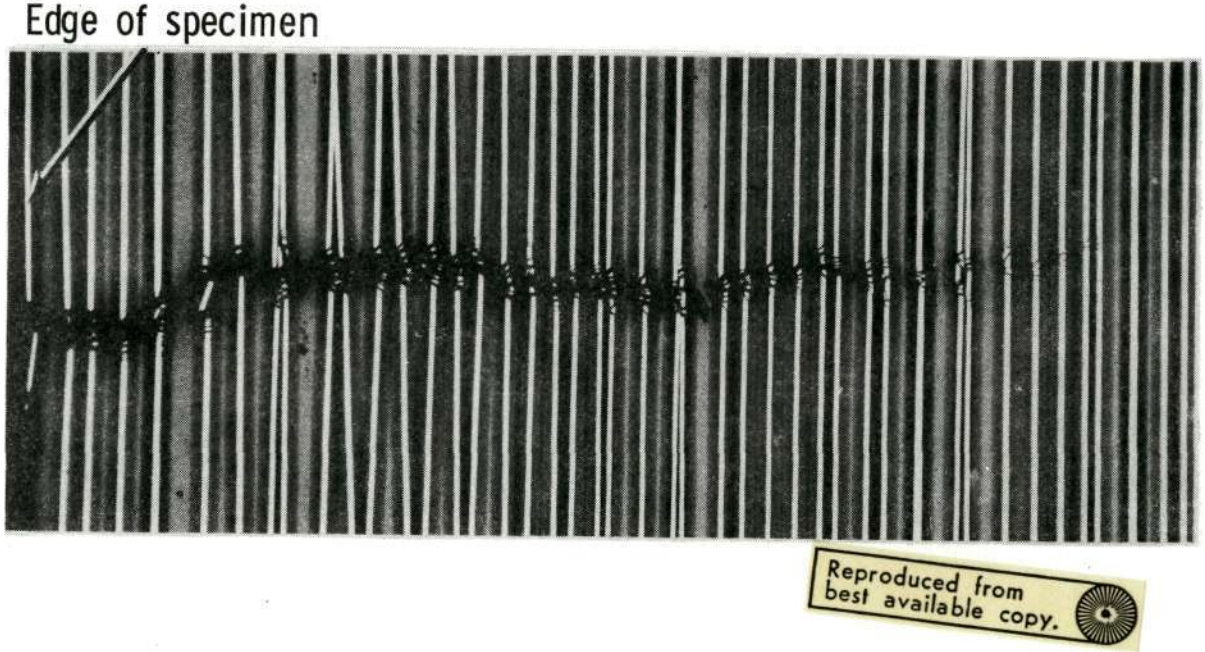

Figure 9. - Fractoradiograph showing arrested crack in bilayer B-Al composite, 0.6 mil core diameter.

could be seen in the region near the tip of the crack. Once a crack was initiated, three distinct fracture modifications were observed: transverse fracture, axial fracture, and canted fracture. Each modification was either related to or a result of the noncumulative filament break propagation mechanism. The three modifications are discussed subsequently.

2. Transverse Fracture

Transverse fracture occurred when filaments from all layers in the composite failed by noncumulative break propagation in a single plane perpendicular to the axis of loading. A typical transverse fracture surface of bilayer composite is shown in Figure 10. The fracture morphology was quite similar to that already observed for monolayer composite (Figures 7 and 8) except that in the bilayer material the crater walls intersected in a hexagonal rather than in a rectangular pattern. The magnified view of Figure 11 shows details of the interior crater wall, including the shear lip and porosity at lines and points of ultimate separation in the matrix.

The shapes and arrangements of fragments associated with the fracture of filaments were typified by those shown in Figures 12, 13, and 14. No attempt was made to interpret the markings on fragment surfaces. Figure 12 shows the general appearance of fragments in a single transverse fracture surface. Figure 13 does likewise, but also serves to focus attention on the regions of separation between constituents of well bonded composite. The matrix-matrix bond (denoted by arrow) has ruptured only within a

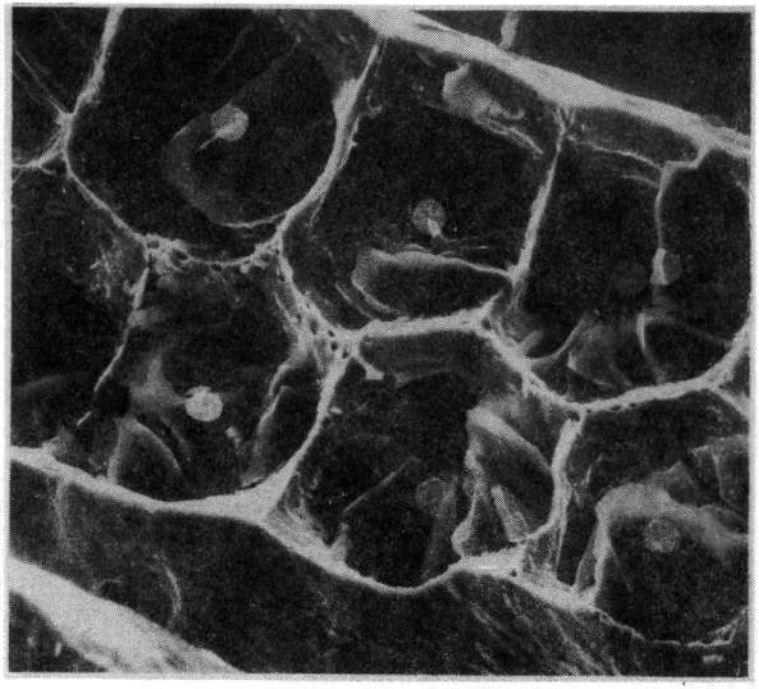

Figure 10. - General view of transverse fracture surface of bilayer B-Al composite showing filament fragmentation, 3.9 mil filament diameter.

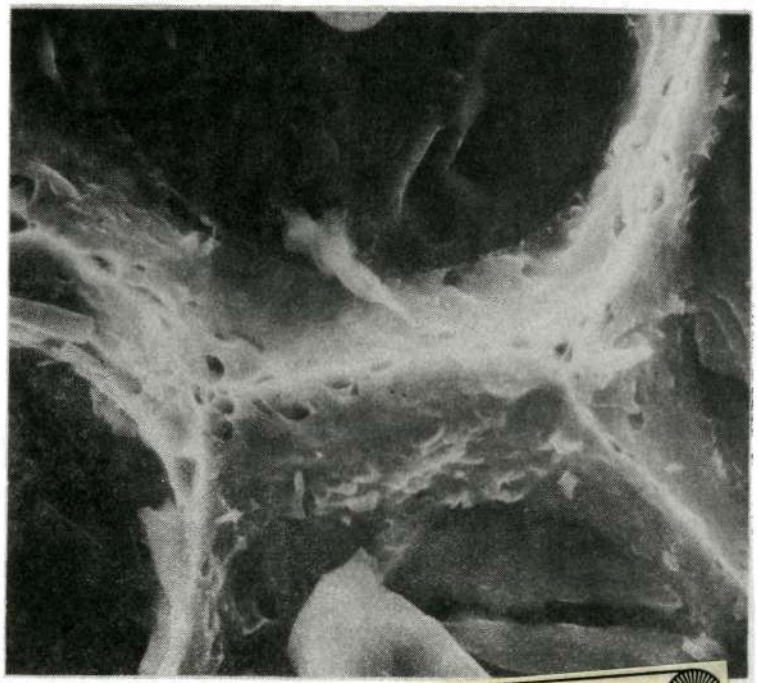

Figure 11. - Transverse fracture surface of bilayer B-Al composite showing details of matrix fracture, 3.9 mil filament diameter.

Figure 12. - Typical boron filament fragments in a transverse noncumulative fracture surface, 3.9 mil filament diameter.

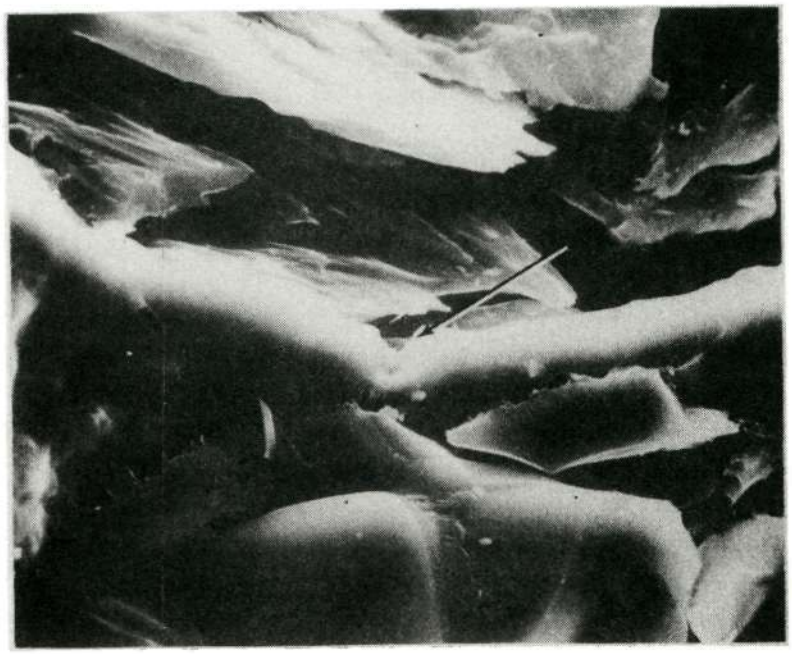

Figure 13. - Filament-matrix and matrix-matrix separation in transverse noncumulative fracture surface, 3.9 mil filament diameter.

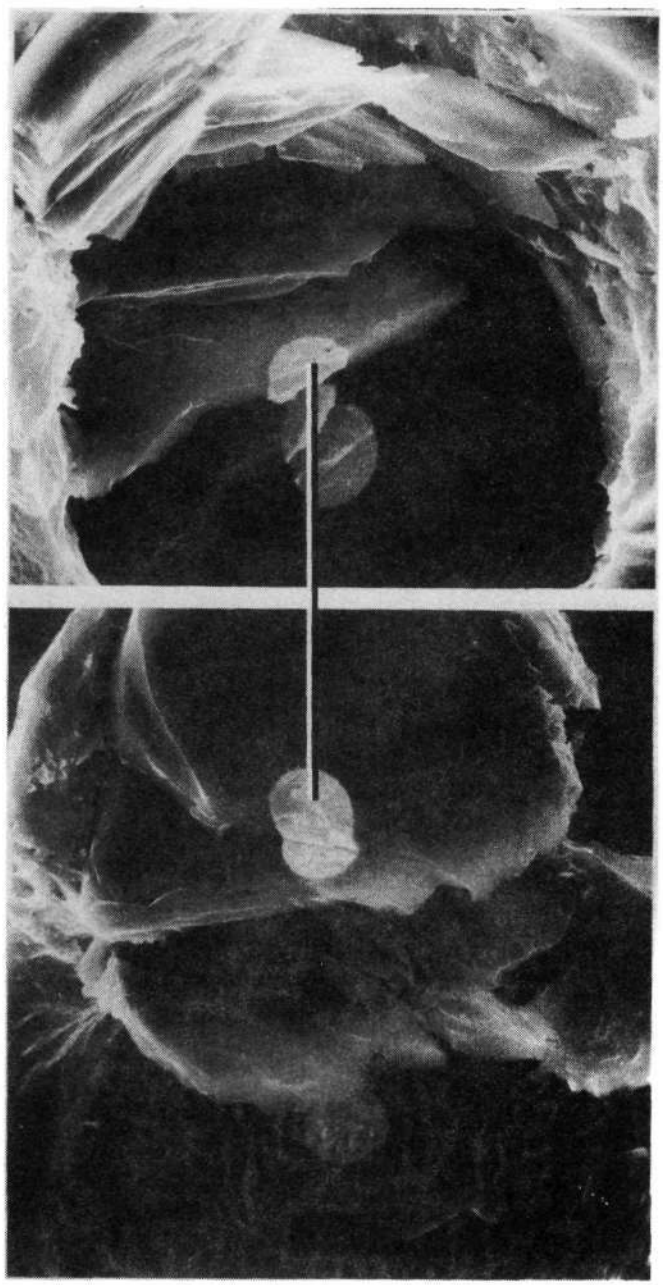

Figure 14. - Matching boron filament fragments from opposing transverse noncumulative fracture surfaces, 3.9 mil filament diameter.

very small volume in spite of the violence of a fracture process which left filament debris scattered widely. A measure of the tenacity of the filament-matrix bond was indicated by the incipient formation of dimples around the periphery of the large fragment at the bottom of the photograph. Figure 14 shows matching fragments from a single filament in two photographs taken of opposite transverse fracture surfaces. Matching core segments are connected by a line for one fragment pair.

One unusual type of transverse fracture resulting from noncumulative filament break propagation was not associated with the presence of wedge-shaped filament fragments. Instead of fragmenting under the influence of a transverse compressive stress wave, the filaments broke cleanly in at least two places to form one or more relatively long cylindrical segments. Figure 15 presents radiographic evidence of that type of transverse fracture. No wedge-shaped fragments were associated with the individual broken filaments. Instead, each filament was broken cleanly at least one additional time under the fracture surface.

A pair of matching fracture surfaces from the specimen represented in the previous radiograph are shown in Figure 16. Matching filaments are linked by a line. Each broken filament is split longitudinally to an unknown depth, probably down to the nearest transverse break under the surface. The splits are all parallel to the plane of the composite sheet, and thus were not obvious in the radiograph of Figure 15. This is an excellent example of a situation where failure to combine radiographic and

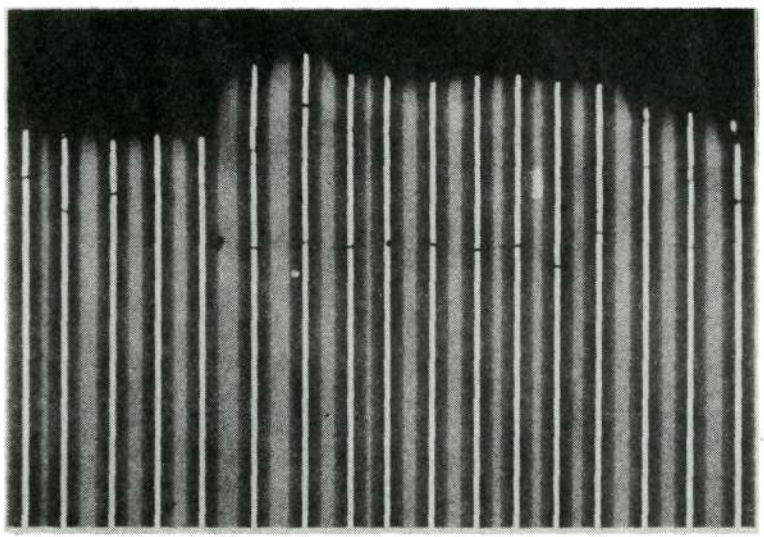

Figure 15. - Fractoradiograph showing rare transverse noncumulative fracture without wedge-shaped fragments, 0.6 mil core diameter.

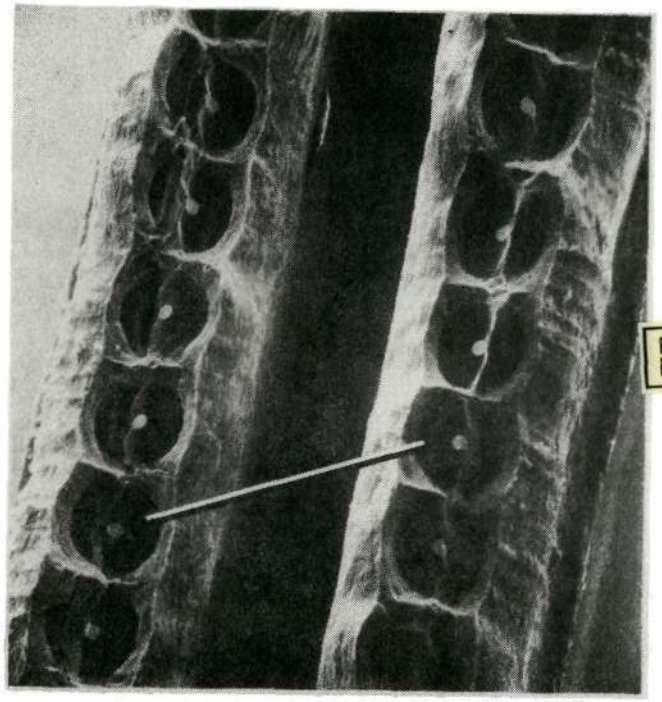

Figure 16. - Matching transverse fracture surfaces of monolayer B-Al composite showing filaments split instead of fragmented, 3.9 mil filament diameter.

microscopic observations would have led to confusion and possibly even an erroneous interpretation.

The transverse modification with wedge-shaped filament fragments was the predominant one. The great majority of fracture surface examined in the present investigation was a consequence of transverse noncumulative fracture, and wedge-shaped filament fragments were abundant in the surface. Transverse fracture involving split filaments was extremely rare. In fact, it was seen only twice during observation of nearly 1000 B-Al tensile fracture surfaces. The particular area represented by Figure 15 and 16 made up approximately one-third the total fracture surface of a well bonded monolayer specimen. The remaining two-thirds showed evidence of the more prevalent transverse fracture with wedge-shaped fragments. A study of the direction of fragment displacement indicated that crack propagation proceeded out of the region of split filaments, and that region was the first to fracture.

3. Axial Fracture

The axial modification was seen as a jog parallel to the axis of loading which connected two regions of transverse fracture at different levels. The radiograph of Figure 17 shows the axial fracture modification in a bilayer specimen as a vertical jog. Noncumulative filament break propagation proceeded from left to right until it reached the region now identified as the jog. At that point it was interrupted by the initiation and propagation

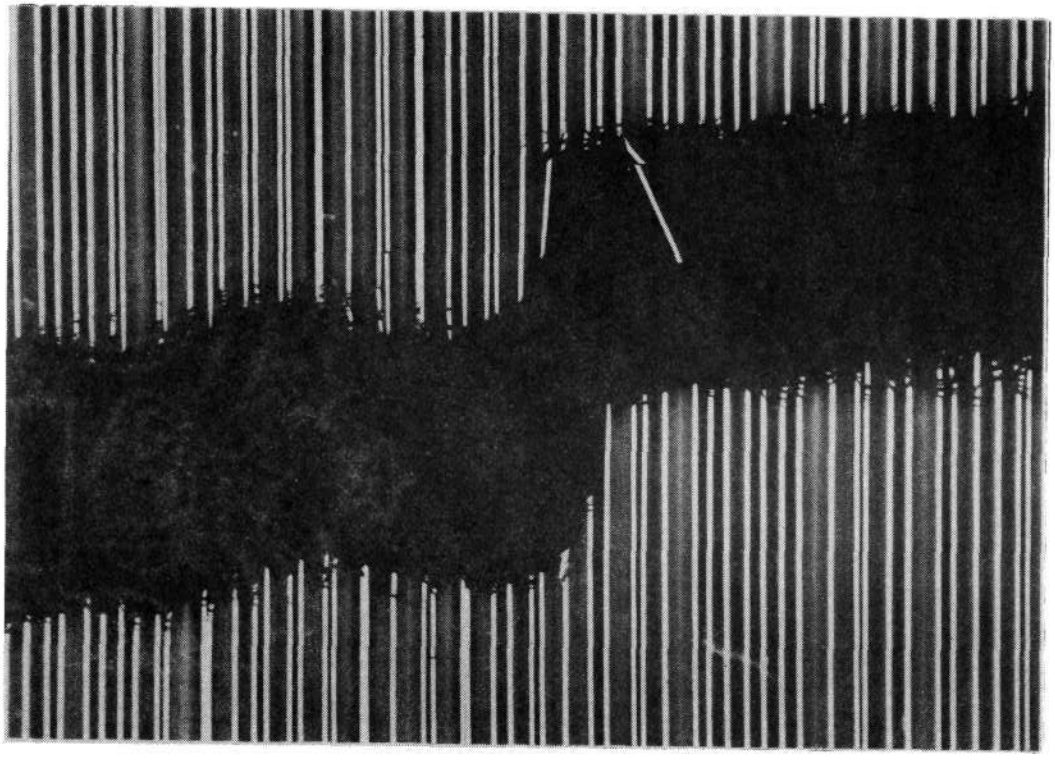

Figure 17. - Fractoradiograph of bilayer B-Al composite exhibiting axial fracture, 0.6 mil core diameter.

of filament breaks at a different level. By studying the directions of fragment displacement, it was readily seen that secondary initiation occurred three or four filaments to the right of the jog (see arrow) on the upper level. Following that, the crack continued to propagate from left to right. Fracture at the jog occurred by shear rupture of the matrix parallel to the load axis.

The characteristic appearance of the axial fracture modification is seen in the matching fracture surfaces of Figure 18 which show the jog and evidence of noncumulative filament break propagation on either side. The magnified view in Figure 19 shows details of the axial shear surface. Note that the side of the exposed filament is covered with a residual layer of aluminum. Both the surfaces of this layer and the matrix exhibit the elongated dimples which are characteristic of shear rupture in a ductile metal. The shear dimples on the exposed filament and the corresponding ones on the matching surface are shown magnified to a greater extent in Figure 20.

Axial fracture occurred locally and made up only a small part of any given fracture surface. Its occurrence was always associated with the presence of a pre-existing filament break located away from the edges of the specimen and apart from the region in which the filament break propagation mechanism was operating. For some unknown reason, the previously broken filament was able to resist the stress wave impinging on its side without fragmenting in the normal manner, thus stopping the initial transverse crack. Fragmentation sometimes occurred at a different location,

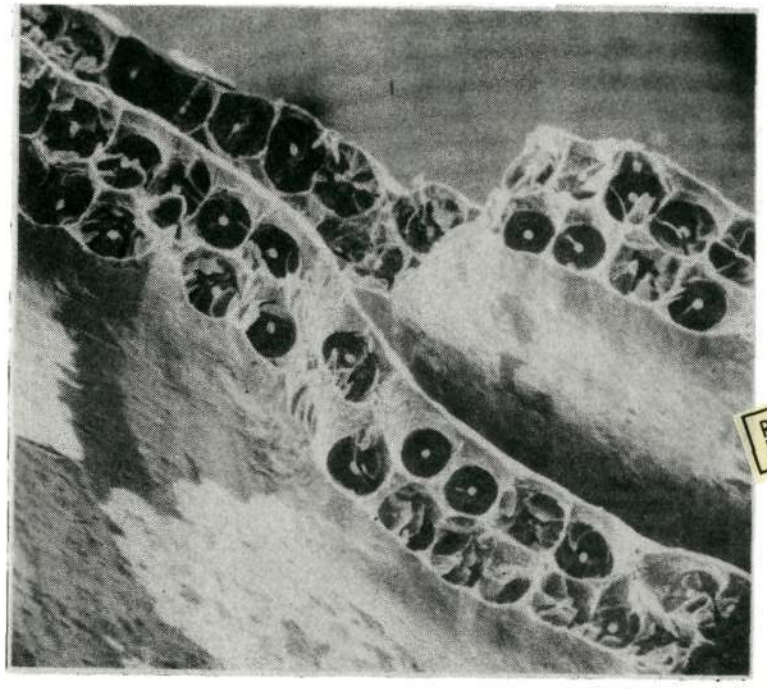

Figure 18. - General view of matching fracture surfaces of bilayer B-Al composite exhibiting axial fracture, 3.9 mil filament diameter.

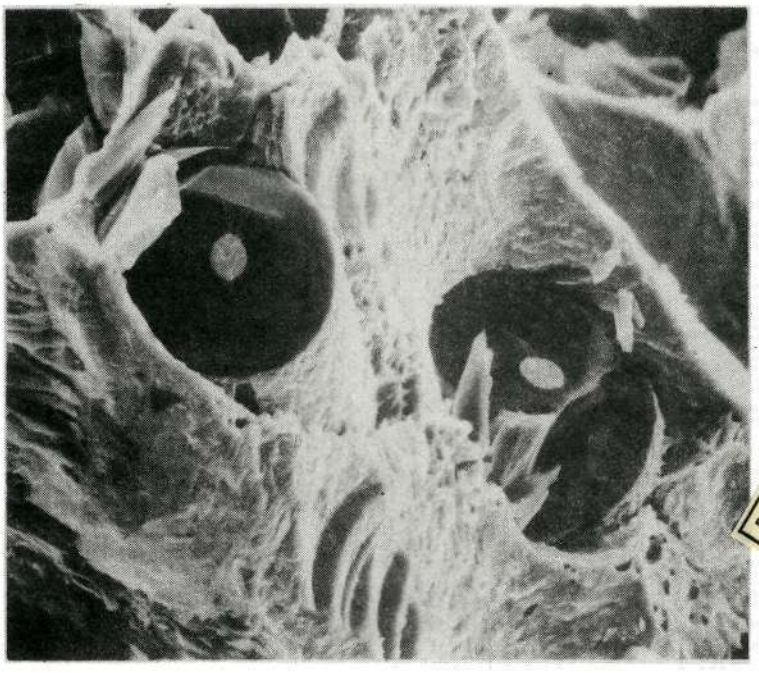

Figure 19. - Details of an axial shear surface in bilayer B-Al composite, 3.9 mil filament diameter.

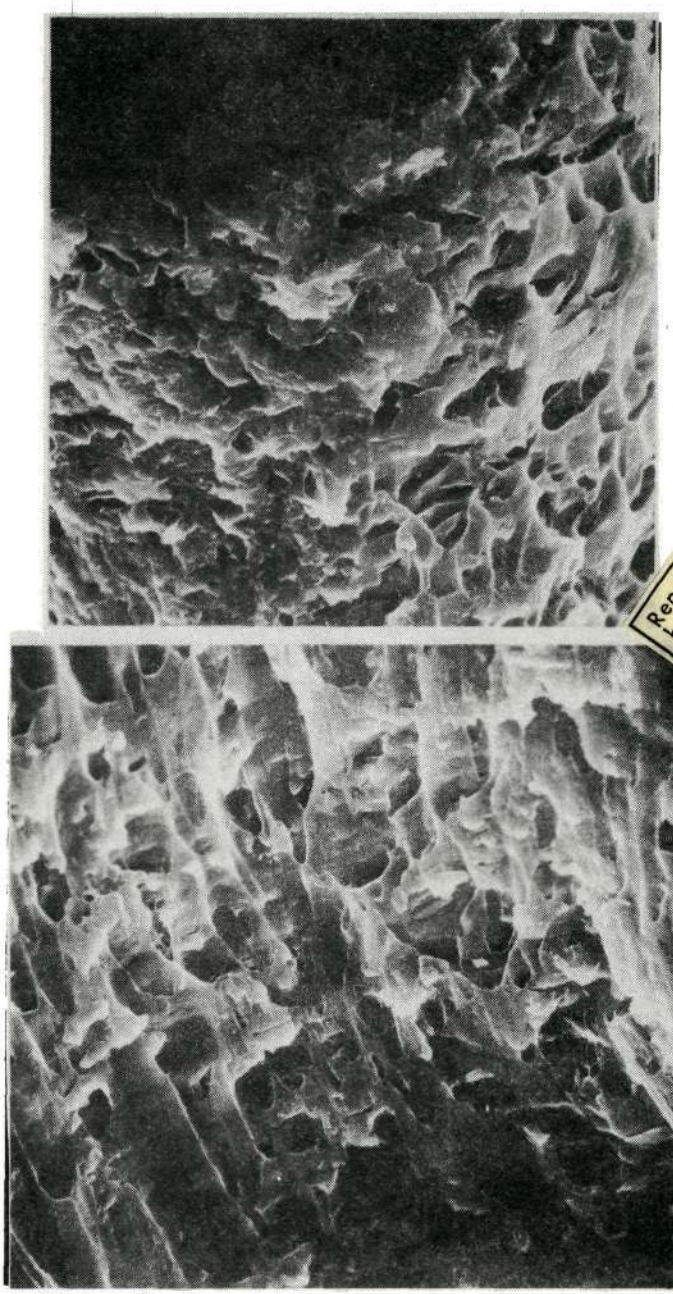

Figure 20. - Evidence of shear rupture: (a) on side of exposed filament in axial shear surface; (b) on matching surface from which exposed filament was separated, 3.9 mil filament diameter.

and occasionally the filament split, but the pre-existing break was never directly involved in the fracture of the specimen. Secondary initiation occurred immediately in the adjacent filaments because the initial crack had progressed sufficiently far into the specimen to create a significant additional increment of tensile stress due to in-plane bending. Axial separation between the two transverse fracture planes was determined by the location of the weakest point in one of the adjacent filaments which was within the region of influence of the stress concentration. Specimens which contained no pre-existing filament breaks generally did not exhibit the axial fracture mode.

An example of the role of the pre-existing filament break in the axial modification is shown in Figure 21. These are the same two radiographs presented earlier as Figure 6, but cropped differently to show the vertical jog. In addition to the three previously mentioned broken filaments at the edge of the specimen in Figure 21(a), the 27^{th} filament from the edge is also broken (see arrow). This break existed before any load was applied, and is shown in Figure 21(b) as well.

Filament break propagation proceeded from right to left until it reached the 27^{th} filament with the pre-existing break. That filament broke, split, and fragmented at a different location, but it succeeded in stopping the initial crack. A new series of filament breaks was then initiated on the lower level in the manner previously discussed. Occasionally when a split filament was involved, the axial fracture surface developed in such a way as to expose the

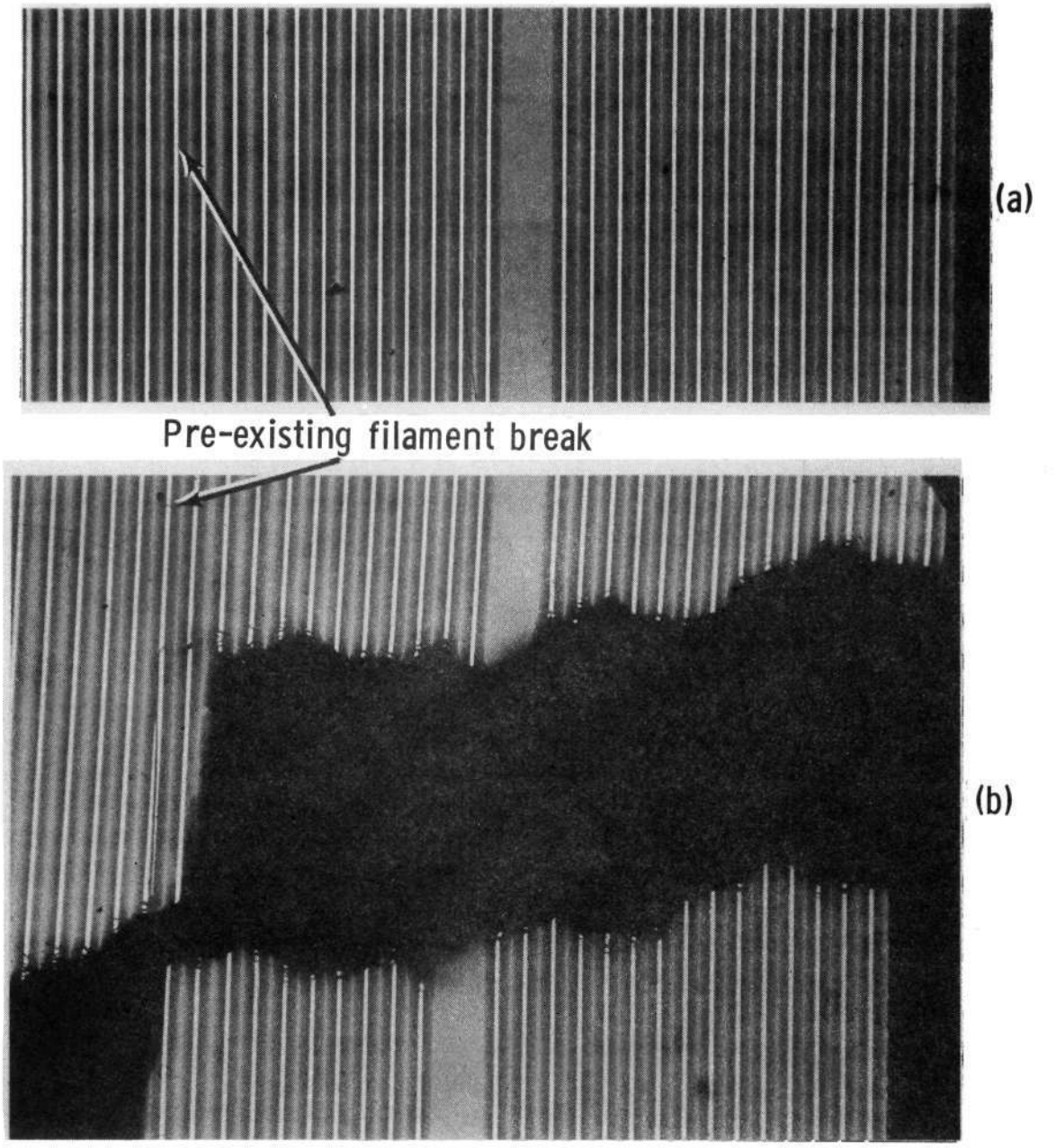

Figure 21. - Fractoradiographs of monolayer B-Al composite showing role of pre-existing filament break in promoting development of axial fracture, 0.6 mil core diameter.

filament. Successively magnified views of a typical fracture surface of that type are shown in Figures 22, 23, and 24. Figure 22 shows the general appearance of the axial fracture surface with transverse fracture at different levels on either side. Details of the overall axial surface are shown in Figure 23, and a close-up view of the split filament surface is shown in Figure 24. Apart from the filament split, the remainder of the axial surface was created by shear rupture as shown in Figures 18, 19, and 20.

4. Canted Fracture

The third noncumulative fracture modification observed was descriptively termed canted fracture because the resulting fracture surface was angled with respect to the plane of the sheet specimen. Canted fracture occurred when filaments in adjacent layers failed by transverse break propagation in separate planes perpendicular to the load axis. Matrix failure then occurred by shear along an angled surface between filament layers.

Radiographic evidence of the canted modification of noncumulative fracture is presented in Figure 25 for a bilayer specimen. In the canted region the broken ends of one filament layer extend beyond those of the other layer, and matrix thickness gradually decreases toward the extended ends. A portion of canted surface corresponding to the radiograph is presented as Figure 26. The appearance bears some similarity to the chisel point fracture observed under certain conditions in the tensile fracture of metallic sheet. Filament fracture on different transverse planes

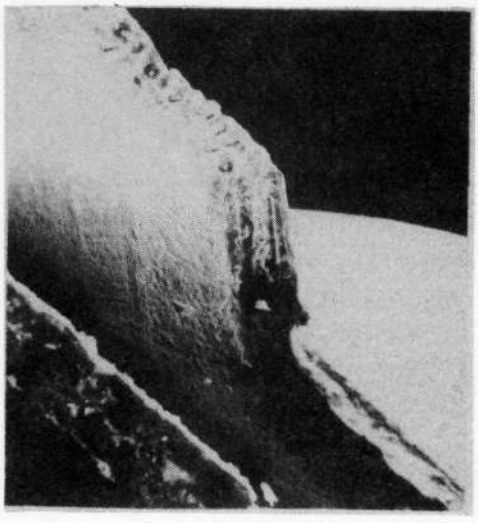

Figure 22. - General view of bilayer B-Al composite fracture surface with split filament in the axial portion, 3.9 mil filament diameter.

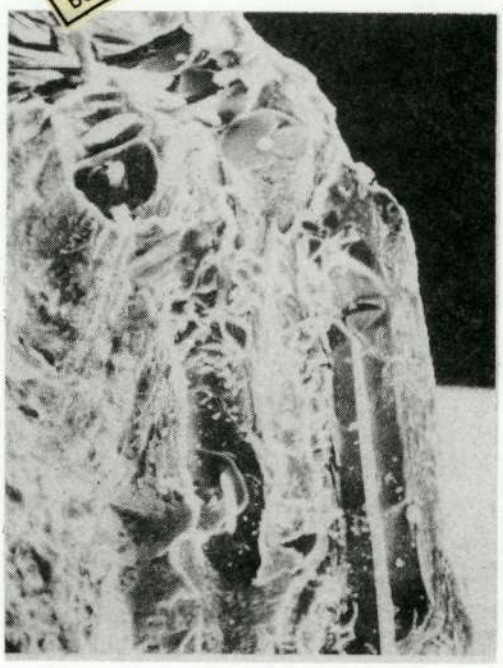

Figure 23. - Details of axial fracture surface containing split filament, 3.9 mils filament diameter.

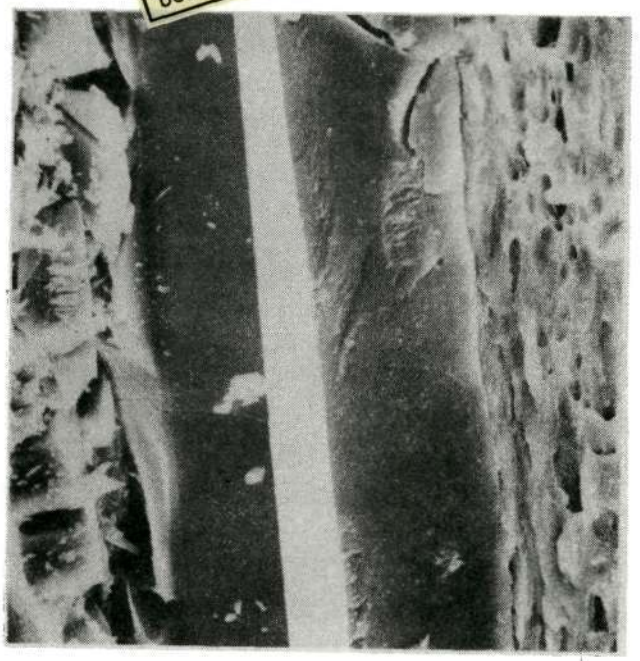

Figure 24. - Split filament in axial fracture surface.

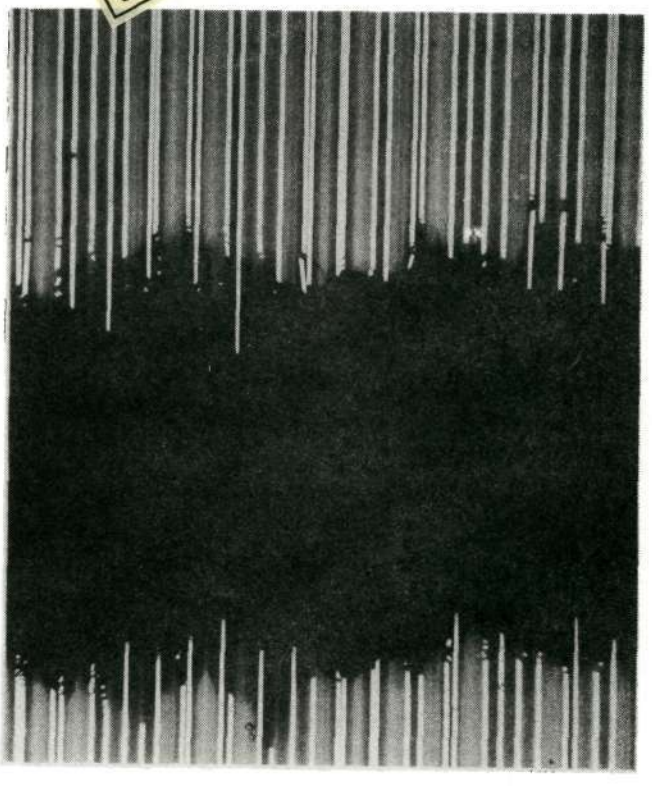

Figure 25. - Fractoradiograph of bilayer B-Al composite exhibiting canted fracture, 0.6 mil core diameter.

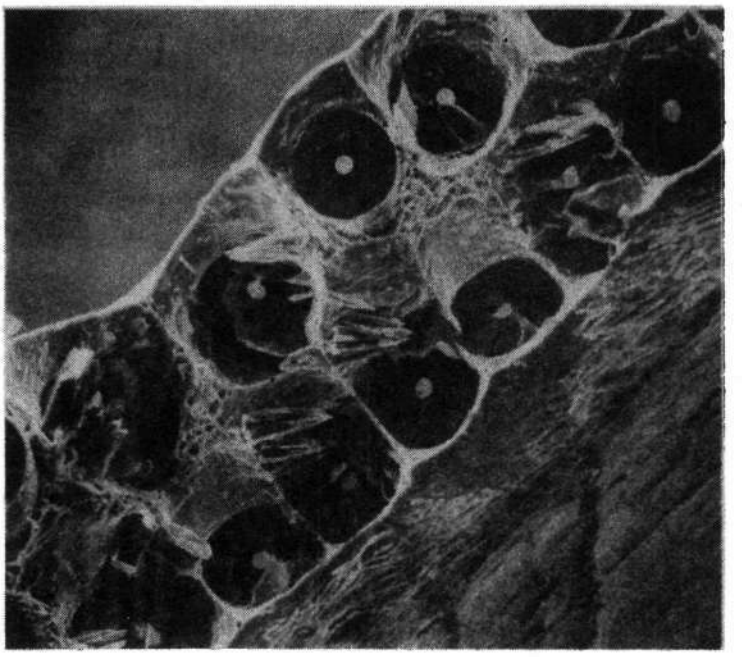

Figure 26. - Details of a canted fracture surface in bilayer B-Al composite, 3.9 mil filament diameter.

is obvious along with the canted matrix shear surface between filament layers. A magnified view of the shear surface is shown in Figure 27, and exhibits the characteristic elongated dimples seen previously for the case of axial shear.

A characteristic feature of canted fracture surfaces observed in this study is a narrow strip on exposed filament sides where no bond existed between filament and matrix. Evidence of the unbonded strip is obvious for three filaments in Figure 26, particularly the one with the greatest amount of its side exposed. The unbonded strip on the side of that filament is shown in greater detail in Figure 28(a). The opposing filament fracture surface is shown in Figure 28(b). Note the absence of shear dimples on the matrix surface where the unbonded strip pulled out. The presence of the unbonded areas is probably due to incomplete removal of the acrylic resin binder used during fabrication to maintain filament spacing and alignment. Their influence, if any exists, on the occurrence of canted fracture is not known.

Canted fracture is a local phenomenon which, by definition, can not occur in monolayer composite. However, it is almost always found to comprise a very small portion of multilayer composite fracture surfaces. The fracture surface of Figure 26 contains one filament which is apparently unfragmented. Occasionally filaments are found which exhibit whole fracture surfaces, even in a generally noncumulative fracture, indicating that failure of these filaments probably occurs as a result of simple axial tension rather than under the influence of a transverse impact.

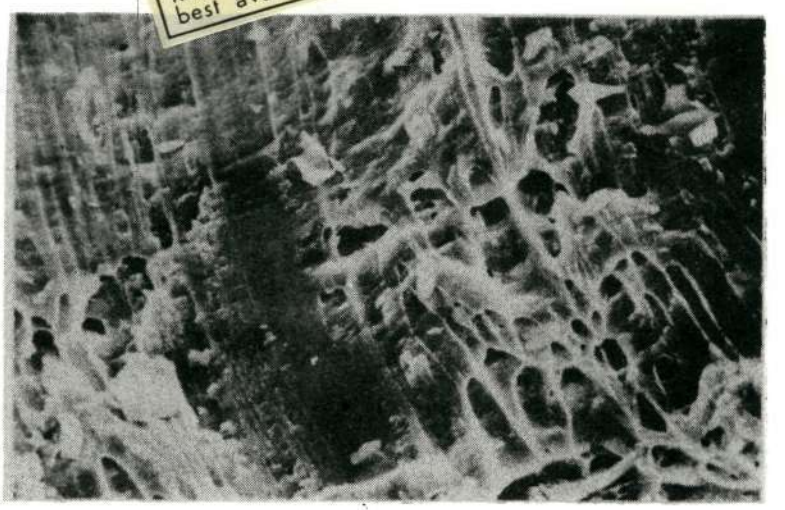

Figure 27. - Details of matrix shear in canted fracture surface.

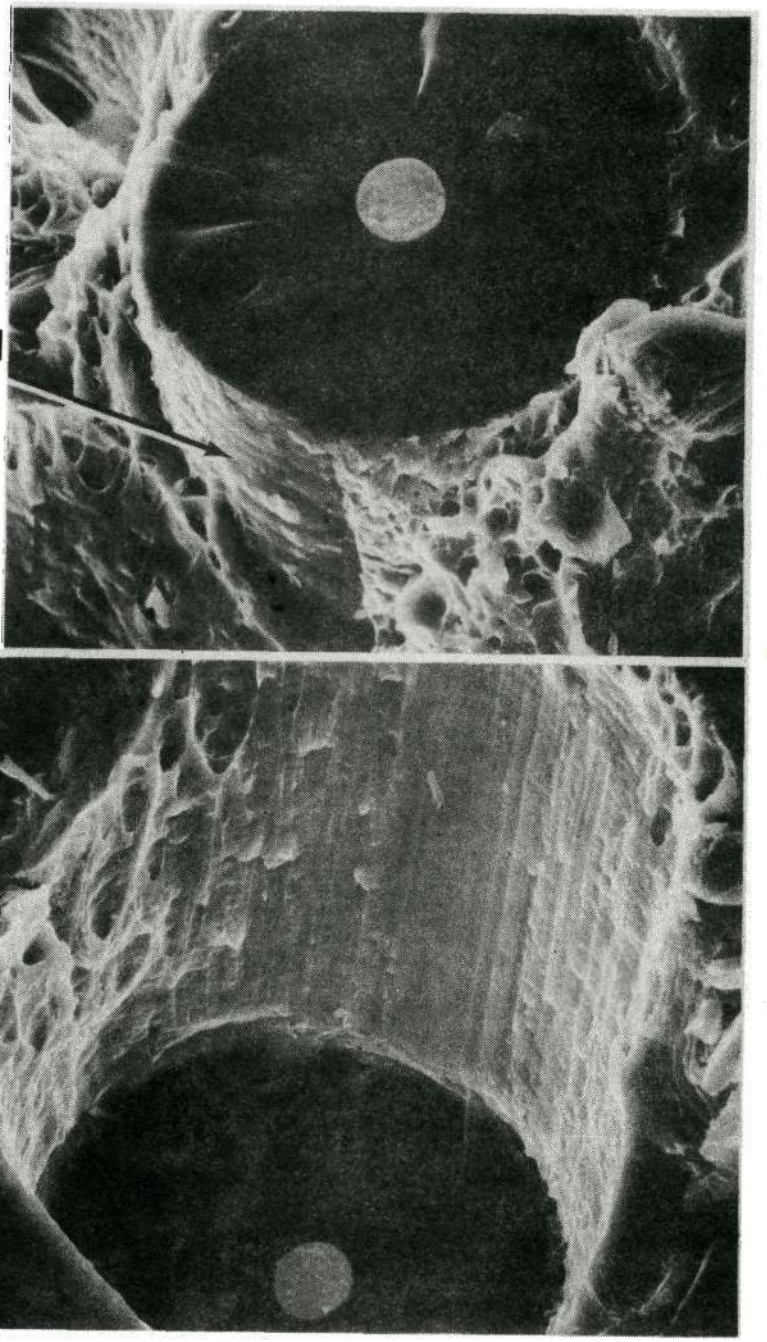

Figure 28. - Matching, 3.9 mil diameter filament fracture surfaces in canted fracture region: (a) unbonded strip on side of exposed filament; (b) corresponding unbonded area in opposing surface.

5. Unfragmented Filaments

The occasional occurrence of simple tensile fractures is not surprising, even in a largely noncumulative fracture surface, since it would be unreasonable to expect every filament to fail by fragmentation. There is at least a small stress concentration just ahead of an advancing crack in spite of the plasticity of the matrix, and the statistical distribution of filament strengths requires that occasionally a weak point in a filament will be located in such a way that simple tensile fracture might occur just ahead of filament break propagation resulting from a stress wave. A typical pair of matching whole-filament fracture surfaces are presented in Figure 29. The mechanism of filament fracture in simple tension is not completely understood. However, fracture appears to begin at an imperfection in the core which is in a state of residual triaxial tension as a result of the process by which boron filament is manufactured. The crack then proceeds through the boron sheath with a turning and climbing motion to produce a fracture surface which has the form of a spiral ramp.

C. Cumulative Fracture

The B-Al composite sheet used in the study of noncumulative fracture was consolidated by hot pressing for one hour at 1100°F under 10 ksi pressure. The hot pressing parameters were purposefully designed to produce internally well bonded composite, and in order to accomplish that purpose, it was necessary to accept a significant

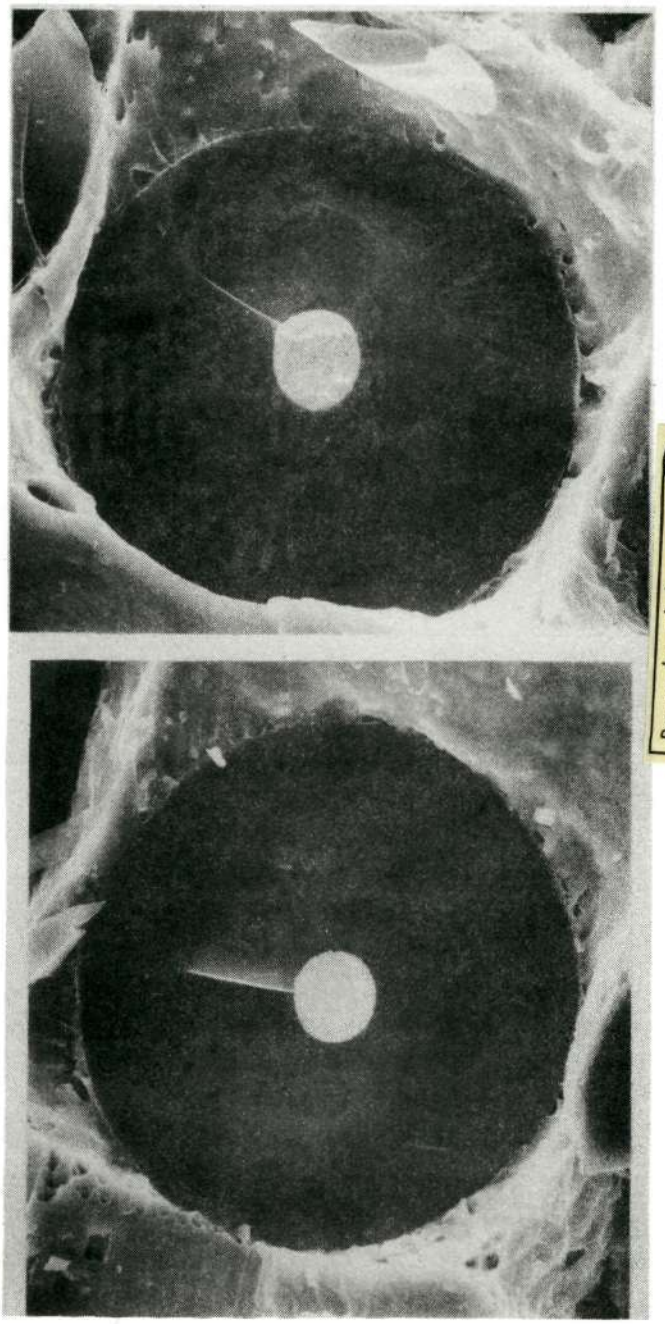

Figure 29. - Matching surfaces of unfragmented 3.9 mil diameter boron filament from transverse B-Al composite fracture surface.

degradation of filament strength resulting from chemical reaction between the boron and the aluminum matrix. When tested in tension, the material fractured suddenly and without any warning in the form of acoustic emissions. Fracture was essentially 100 percent noncumulative.

By increasing the consolidation pressure, it was possible to fabricate batches of well bonded composite with varying degrees of filament degradation. When filaments in a given batch had been degraded beyond a certain level, composite specimens from that batch no longer fractured in a completely noncumulative manner. Sporadic acoustic emissions prior to total specimen failure indicated that filaments were breaking, both individually and in groups, and that the composite fracture mode had become at least partially cumulative. Cumulative fracture occurred much more slowly than noncumulative fracture, and it was a comparatively simple task to arrest a cumulative crack for further study.

1. Radiographic Evidence

A typical cumulative crack in well bonded bilayer composite is shown in the radiograph of Figure 30, growing inward from the edge of a specimen. Most of the filaments broke without fragmenting, and when fragmentation did occur, the displacement of fragments was randomly directed. One similarity between noncumulative and cumulative fracture was that individual filament breaks did not produce matrix cracks. In both modes, broken filaments were observed several interfilament spacings in advance of ductile

separation of the matrix. A major difference between the noncumulative and cumulative modes was observed in the paths along which cracks propagated. In contrast with the relatively straight transverse crack associated with noncumulative fracture, the cumulative crack changed direction frequently as it passed through the specimen.

2. The Cumulative Fracture Mechanism

The crack shown in Figure 30 is an excellent example of cumulative filament break propagation as described by Zweben[2,20]. Fracture begins when one or two filaments break near the edge of a specimen, probably under the influence of a stress concentration produced by machining. The presence of broken filaments contributes an additional increment of stress concentration, or as Zweben explains, a load concentration which is effective over a finite length of the adjacent filaments rather than at a point. Now the strength of boron filaments varies from filament to filament, and from point to point along the length of a single filament. Thus there are two nonexclusive possibilities for subsequent filament fracture, both of which are observed near the crack tip in Figure 30. The load concentration acting over a length of a given filament resulting from a previously broken neighbor can cause the filament to break at a weak point located some distance above or below the break in the neighboring filament. Also, a weak point can be located such that several filaments immediately adjacent to a previously broken filament will remain whole while another filament breaks farther away. The load concentration is less on the more

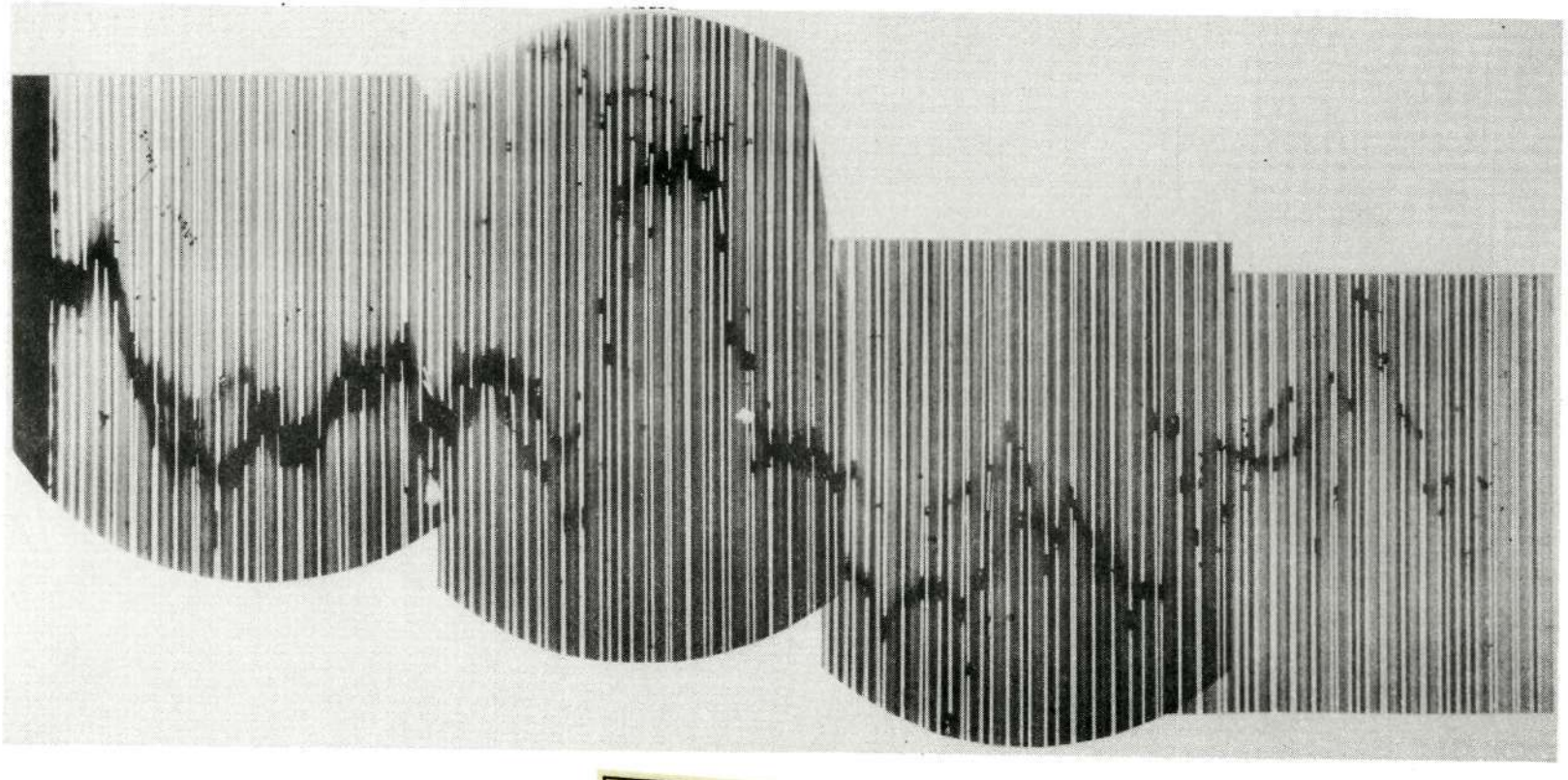

Figure 30. - Fractoradiograph showing arrested cumulative crack in bilayer B-Al composite, 0.6 mil core diameter.

remote filament, but still effective. The tortuous path of the crack is explained by this reasoning. The crack proceeds gradually from one group of broken filaments to the next wherever they may be located. If adjacent breaks or groups of breaks are widely separated in the direction parallel to the axis of loading, then matrix fracture occurs by axial shear. There is a great deal more axial shear in cumulative fracture than in the noncumulative mode.

The observation that filaments fracture several interfilament spacings in advance of matrix fracture probably holds true for any composite with a ductile metal matrix. The same behavior was observed by Cooper and Kelly[22] for tungsten wire reinforced copper composites.

A small number of filament breaks were characterized by the presence of wedge-shaped fragments, indicating that fracture of those filaments was influenced by transverse stress pulses emanating from neighboring filament failures. In the specimen of Figure 30, fragmented breaks were widely dispersed, and the direction of fragment displacement depended solely on the direction from which the stress wave came. The local stress in the regions where fragmentation occurred never reached the level required to sustain the noncumulative filament break propagation mechanism.

The radiograph of Figure 30 shows completely cumulative fracture. When fracture occurred by a combination of the cumulative and noncumulative modes, a cumulative region was developed either at an edge of a specimen or within its interior. That region grew in size until the stress in the composite became sufficiently

great to cause instantaneous fracture of the remainder of the specimen by noncumulative filament break propagation. The radiograph of Figure 31 shows a bilayer specimen after complete mixed-mode fracture. Only the cumulative region is shown, and it was bounded on both sides by transverse noncumulative fracture. This radiograph will be used in the following discussion of cumulative fracture surface features.

3. Cumulative Fracture Surfaces

The two matching fracture surfaces corresponding to the radiograph in Figure 31 are presented as Figures 32 and 33. The same surfaces are shown in both figures, but they have been rotated so that the surface hidden in one figure can be seen in the other. The fracture surfaces of Figure 32 may be related to the radiograph of Figure 31 by the segment of broken filament which protrudes horizontally from the near surface. The radiograph shows two such segments; apparently one was lost before the fracture surface was photographed. The fracture surface of Figure 33 may be related to the radiograph by the same filament segment, and also by a small piece of composite which is cantilevered from the surface at one end of the cumulative region.

Figures 32 and 33 show the irregularity and angularity of typical cumulative fracture surfaces. The filaments in the cumulative region are mostly unfragmented, and to a large extent, matrix fracture is the result of axial or nearly axial shear. On either side of the cumulative region, the fracture surfaces become transverse, and the proportion of fragmented filaments increases

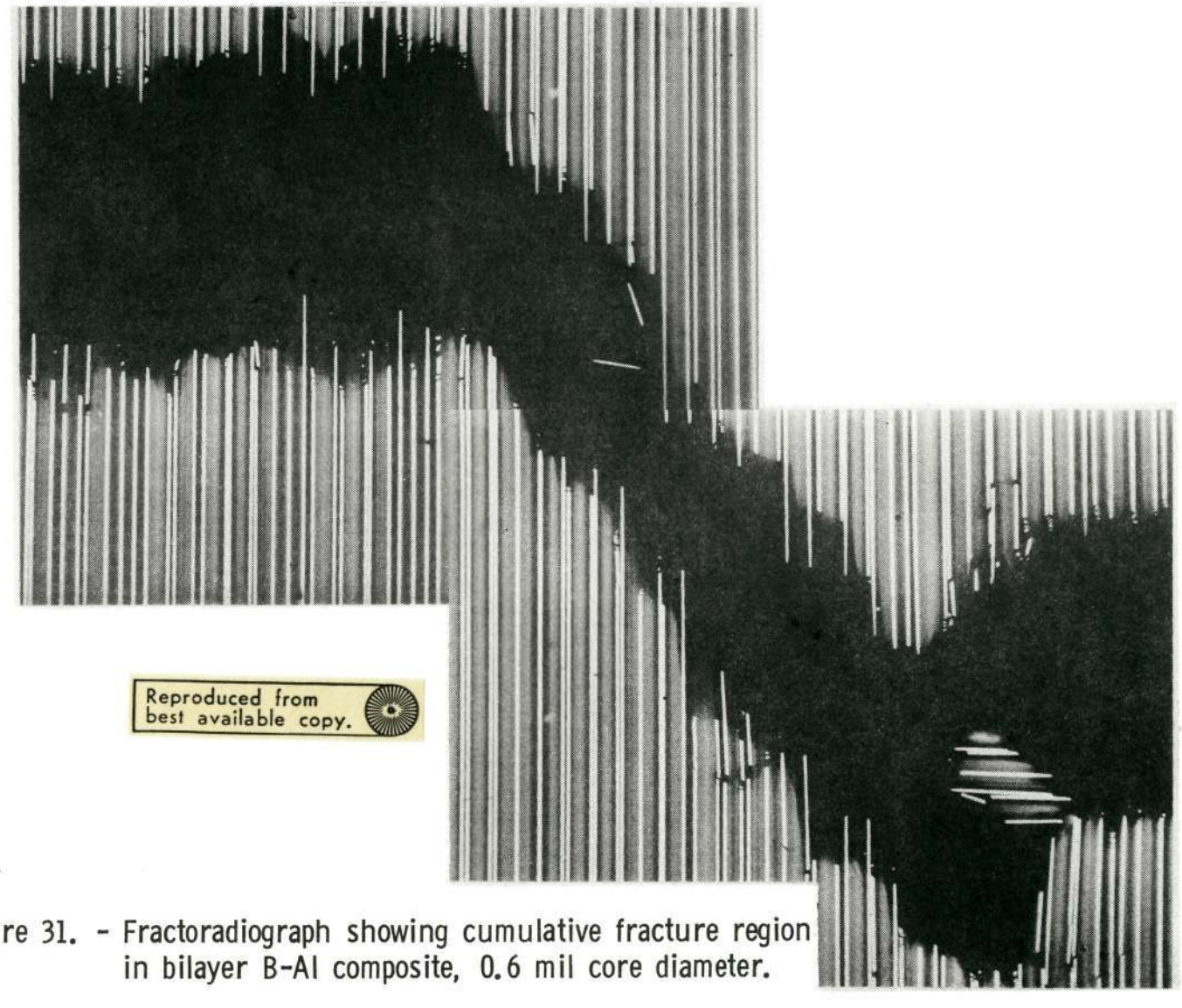

Figure 31. - Fractoradiograph showing cumulative fracture region in bilayer B-Al composite, 0.6 mil core diameter.

rapidly, indicating the onset of the noncumulative mode of fracture.

4. Canted Fracture

Canted fracture was previously described as a modification of noncumulative fracture. However, in the upper left corner of Figure 32, a region of canted fracture separates the cumulative and transverse noncumulative regions. This canted surface is isolated in Figure 34, and like all other canted fracture surfaces, it contained at least one unfragmented filament. Canted fracture probably occurred as the transition between the noncumulative and cumulative modes. In fractures which were previously referred to as being completely noncumulative, the presence of a few small regions of canted fracture probably represented incipient cumulative fracture which was denied further development by the rapidity of the noncumulative fracture mechanism.

D. Fracture of Commercially Fabricated Composites

The B-Al composite procured from a commercial vendor was characterized by moderately weak internal bonding. A portion of a typical fracture surface for the commercial material is presented as Figure 35, and gives an indication of the complexity of the fracture process for multilayer composites in general. Beginning at the left edge of the specimen, the fracture mode was transverse noncumulative. A short distance to the right, the mode became cumulative. The cumulative region blended into a second transverse

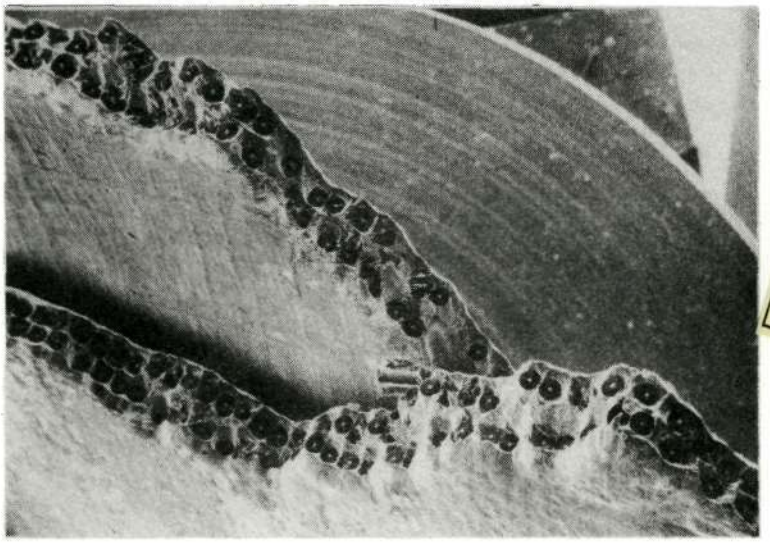

Figure 32. - General view of cumulative region in matching bilayer B-Al composite fracture surfaces, 3.9 mil filament diameter.

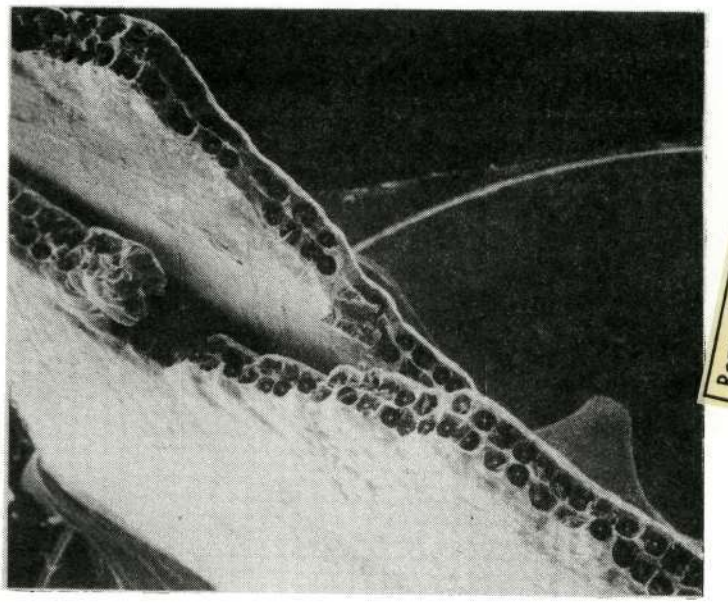

Figure 33. - General view of cumulative region in matching bilayer B-Al composite fracture surfaces, 3.9 mil filament diameter.

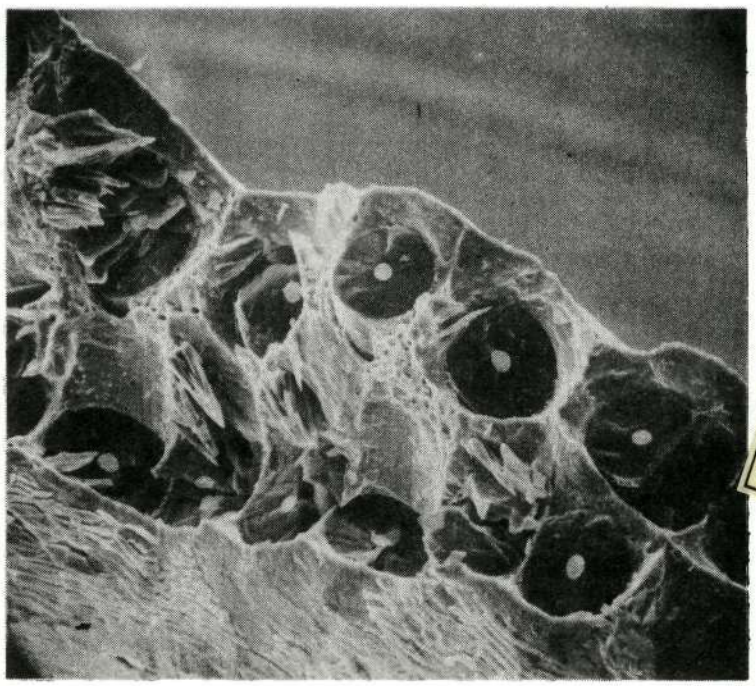

Figure 34. - Details of a canted fracture surface in bilayer B-Al composite, 3.9 mil filament diameter.

noncumulative region, and so on. All the modes and modifications of fracture discussed previously were present in the fracture surface. In addition, there was evidence of debonding between matrix layers, and between filaments and matrix resulting in filament pull-out.

Several of the more important features of the fracture surface of Figure 35 are presented for more detailed examination in the sequence of Figures 36, 37, and 38. Figure 36 shows the leftmost transition between the transverse noncumulative and cumulative modes. Transverse, axial, and canted fracture can all three be identified in the photograph, along with evidence of very poor filament-matrix bonding. Figure 37 shows the second region of transverse noncumulative fracture, and evidence of weak matrix-matrix bonding in the form of troughs which developed as individual matrix layers separated in an attempt to neck down independently. Figure 38 shows local debonding between filaments and matrix at the left edge of the second transverse noncumulative region. The rough, cluttered appearance of the matrix fracture surface is typical of a ductile fracture surface for aluminum alloys (2024 in this case), and serves to justify the choice of relatively pure aluminum (the 1230 alloy) for the majority of specimens observed in the research program.

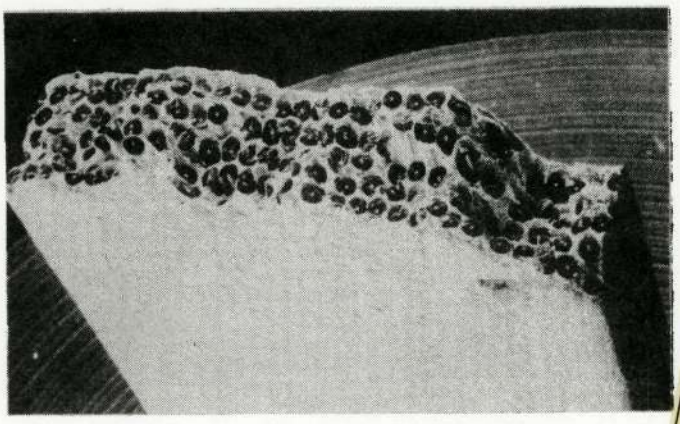

Figure 35. - General view of fracture surface of commercially fabricated composite, 4.1 mil filament diameter.

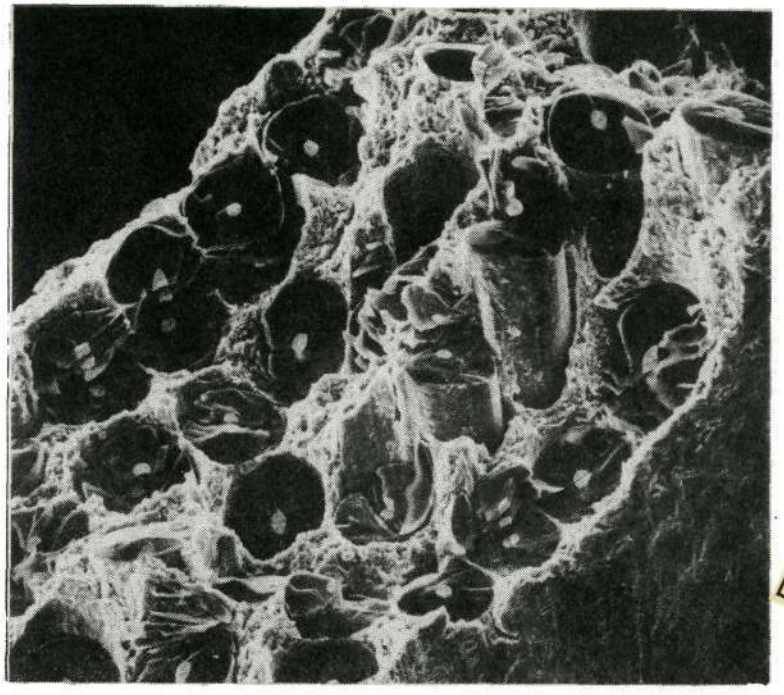

Figure 36. - Leftmost transition region between transverse noncumulative and cumulative fracture in fracture surface of Fig. 35, 4.1 mil filament diameter.

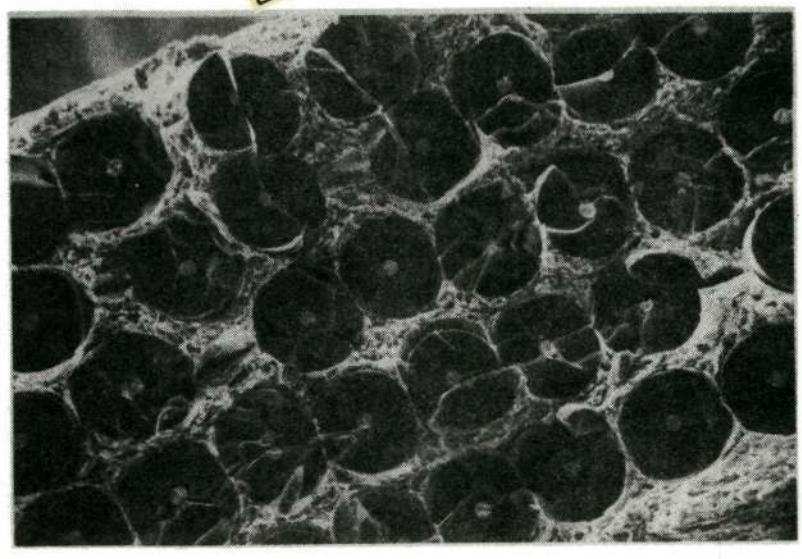

Figure 37. - Second transverse region from left edge of fracture surface of Fig. 35, 4.1 mil filament diameter.

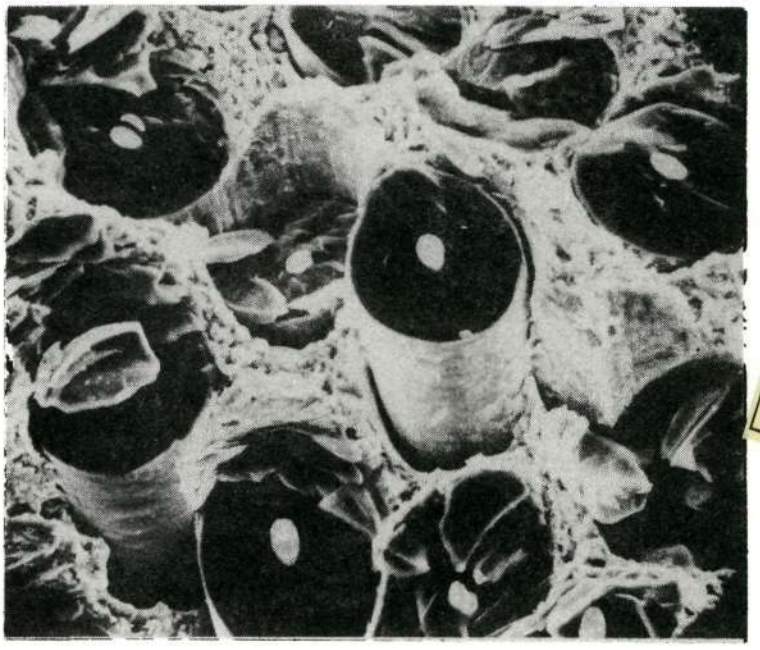

Figure 38. - Left-hand boundary of second transverse region of Fig. 35, 4.1 mil filament diameter.

E. Fracture of Weakly Bonded Composite

1. Composites with Moderately Weak Internal Bonding

One batch of B–Al composite sheet was fabricated so that internal bonding between constituents was moderately weak. That was done in an effort to approximate the extent of bond development generally observed for commercially fabricated composites. It was impossible to distinguish between fracture of well bonded and moderately weakly bonded material from observations of radiographs. The fracture surfaces, however, reflected the difference in bond strengths. A pair of matching fracture surfaces from a typical moderately weakly bonded specimen are shown in Figure 39. Tensile fracture was only partially cumulative, therefore most of the broken filaments were fragmented. Evidence of weak bonding was obvious, both in the separation of foil layers upon ductile failure of the matrix (see arrow), and in local filament–matrix debonding in the immediate vicinity of broken filaments. Debonding between filaments and matrix is more obvious in the magnified view of Figure 40 in the form of annular chasms separating the filaments from the surrounding matrix. The extent of debonding between matrix layers approximated that of the commercially fabricated composite very closely. The filament–matrix bonds were weaker in the commercial composite, resulting in filament pull–out. Reduced reactivity between the aluminum matrix and the silicon carbide coating on the filaments was probably responsible.

In Mullin's work on fracture of boron–epoxy composites[6,7],

matrix cracking was a primary feature of the noncumulative mode of fracture. He found that a slight amount of filament–matrix debonding in the vicinity of a broken filament could absorb a significant quantity of the elastic strain energy released by the filament to prevent cracking of the matrix. He could thus postpone the onset of noncumulative fracture by weakening the filament–matrix bond. The noncumulative fracture mode in B–Al composite sheet resulted from the transverse propagation of a stress wave emanating from an individual filament fracture. That stress wave was not damped by moderately weak bonding, and since it had already passed through the area, its effect was not diminished by subsequent local debonding due to shear stress concentrations at newly formed filament ends.

2. Composites with Extremely Weak Internal Bonding

Occasionally during the course of the investigation, the heated platens used in consolidation of the composite became warped. The warpage was detected by making several measurements of the thickness of each sheet of composite produced. Usually, the sheet was discarded when the maximum thickness variation exceeded three percent, and the platens were resurfaced. In one instance, however, during fabrication of the moderately weakly bonded composite, the platens became warped, and about one–half of each of three composite sheets was consolidated under somewhat less than the intended 9 ksi pressure. Instead of being discarded, the sheets were cut into tensile specimens, and four were obtained in which internal bonding

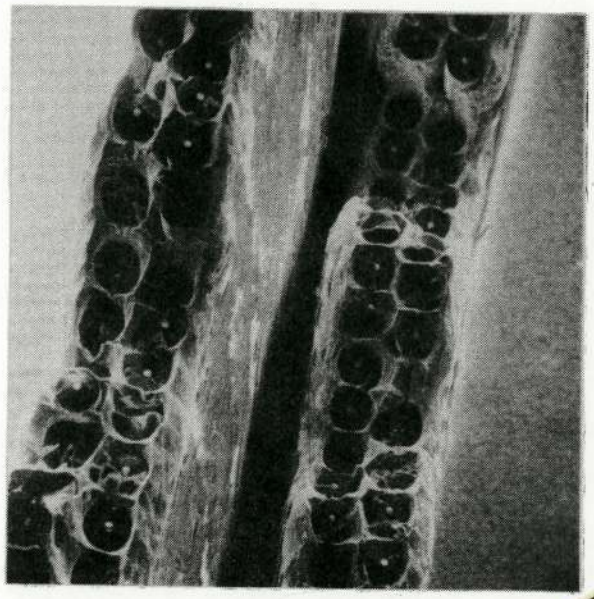

Figure 39. - General view of matching fracture surfaces in bilayer B-Al composite with moderately weak internal bonding, 3.5 mil filament diameter.

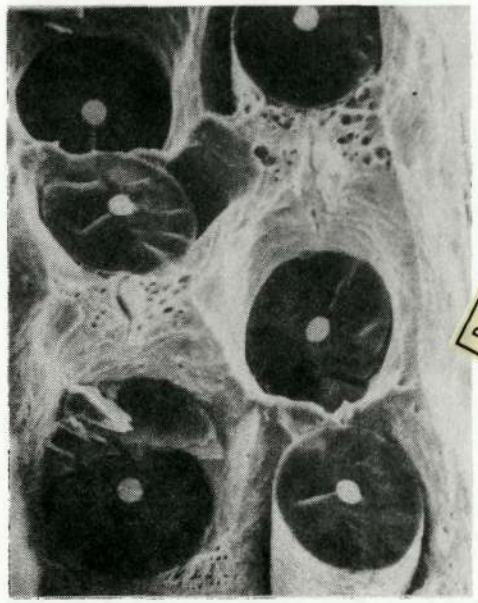

Figure 40. - Debonding around broken filaments in fracture surface of B-Al composite with moderately weak internal bonding, 3.5 mil filament diameter.

was extremely weak.

The extremely weakly bonded specimens fractured in a completely cumulative manner as shown in the radiograph of Figure 41. In contrast with the completely cumulative fracture shown previously in Figure 30, the gross lack of internal bond strength caused severe delamination of the matrix, and extensive filament pull-out. A typical fracture surface, presented as Figure 42, gives further indication of the extremely weak internal bonding between constituents. First, there was extensive protrusion of filaments from the surface, indicating the weakness of the filament-matrix bond. Second, the matrix-matrix bond was never formed at all. The consolidation pressure was so low that the aluminum foils were not even forced into contact in the spaces between filaments.

No practical significance is foreseen for composite sheet with such poor internal bonding. It is important to note, however, that unidirectional B-Al composite can be fabricated in such a way that it exhibits the cumulative mode of fracture, and at the same time does not contain severely degraded filaments.

F. Stress Criterion for Noncumulative Fracture

Based on radiographic analyses of tensile fracture in unidirectional B-Al composite sheet, a peculiar mechanism of non-cumulative fracture has been identified which severely limits the ultimate strength of the material. The mechanism has proven to be consistent with commonly observed features of composite tensile

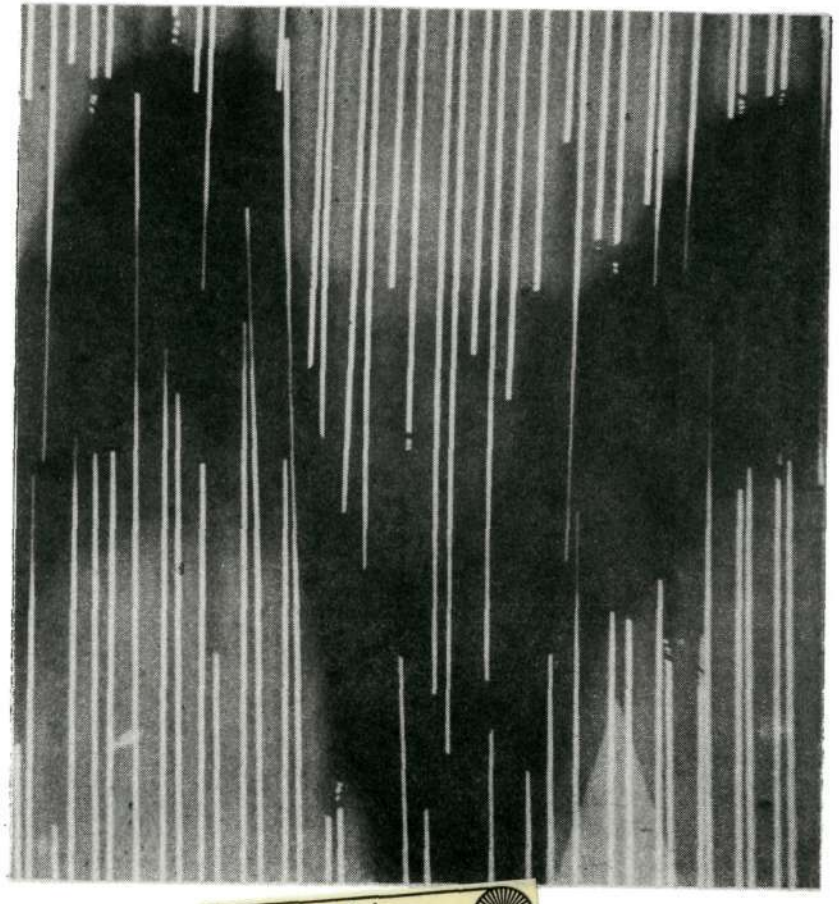

Figure 41. - Fractoradiograph showing cumulative fracture along with matrix delamination and filament pull-out in extremely weakly bonded bilayer B-Al composite, 0.6 mil core diameter.

Figure 42. - Typical fracture of bilayer B-Al composite with extremely weak internal bonds, 3.5 mil filament diameter.

fracture surfaces. It was observed during the course of the investigation that variation of the pressure used to consolidate well bonded composite caused the fracture mode to change, and it was assumed that the change resulted from a varying degree of filament degradation which occurred as a consequence of chemical reaction between boron and aluminum during consolidation. By comparing the average filament stress at the instant of composite fracture with the distributed strengths of filaments contained within that composite, the filament stress level required to initiate and sustain noncumulative fracture was determined. That comparison was made for six batches of well bonded composite with fracture modes varying from completely noncumulative to completely cumulative in order to establish a threshold value of average filament stress below which the noncumulative mechanism was not operative. The comparison was also made for the commercially fabricated composite and the moderately weakly bonded composite in an attempt to determine whether the results of the comparison for well bonded composites were generally applicable.

1. Comparison of Average Filament Stress at Composite Fracture with Strengths of Filaments in a Composite

This comparison was made for six batches of well bonded composite sheet, each with a different degree of filament degradation. Two batches exhibited completely noncumulative fracture, three batches failed by a combination of the noncumulative and cumulative modes, and one batch failed in a completely cumulative manner.

The comparison was also made for the commercially fabricated composite and one batch of moderately weakly bonded composite.

The first comparison is shown in Figure 43 for a monolayer composite containing 5.6 mil diameter boron filament. The composite was consolidated by hot pressing under 10 ksi pressure. Filament strength was characterized by the failure frequency histogram shown. The histogram was constructed by plotting the percentage of filament failures observed within 10 ksi stress intervals based on tensile tests of 150 filament specimens chemically removed from three typical composite tensile specimens. The weakest filament encountered exhibited a strength of approximately 250 ksi. Fifteen additional composite tensile specimens were prepared from the same batch, and tested to determine the average filament stress at fracture of the composite. That was done by assuming that the average filament strain was identical to the measured composite strain at failure of a specimen. Average filament stress was calculated by multiplying the measured ultimate strain value by Young's modulus of the boron filament (55×10^3 ksi). The results are shown as the vertical scatter band at the left side of the histogram. The average filament stress at composite fracture (represented by the vertical dashed line within the scatter band) was identical to the strength of the weakest filament in the composite.

The comparison given in Figure 43 is representative of well bonded composite in which the filaments are not too severely degraded. The strength distribution for virgin 5.6 mil diameter

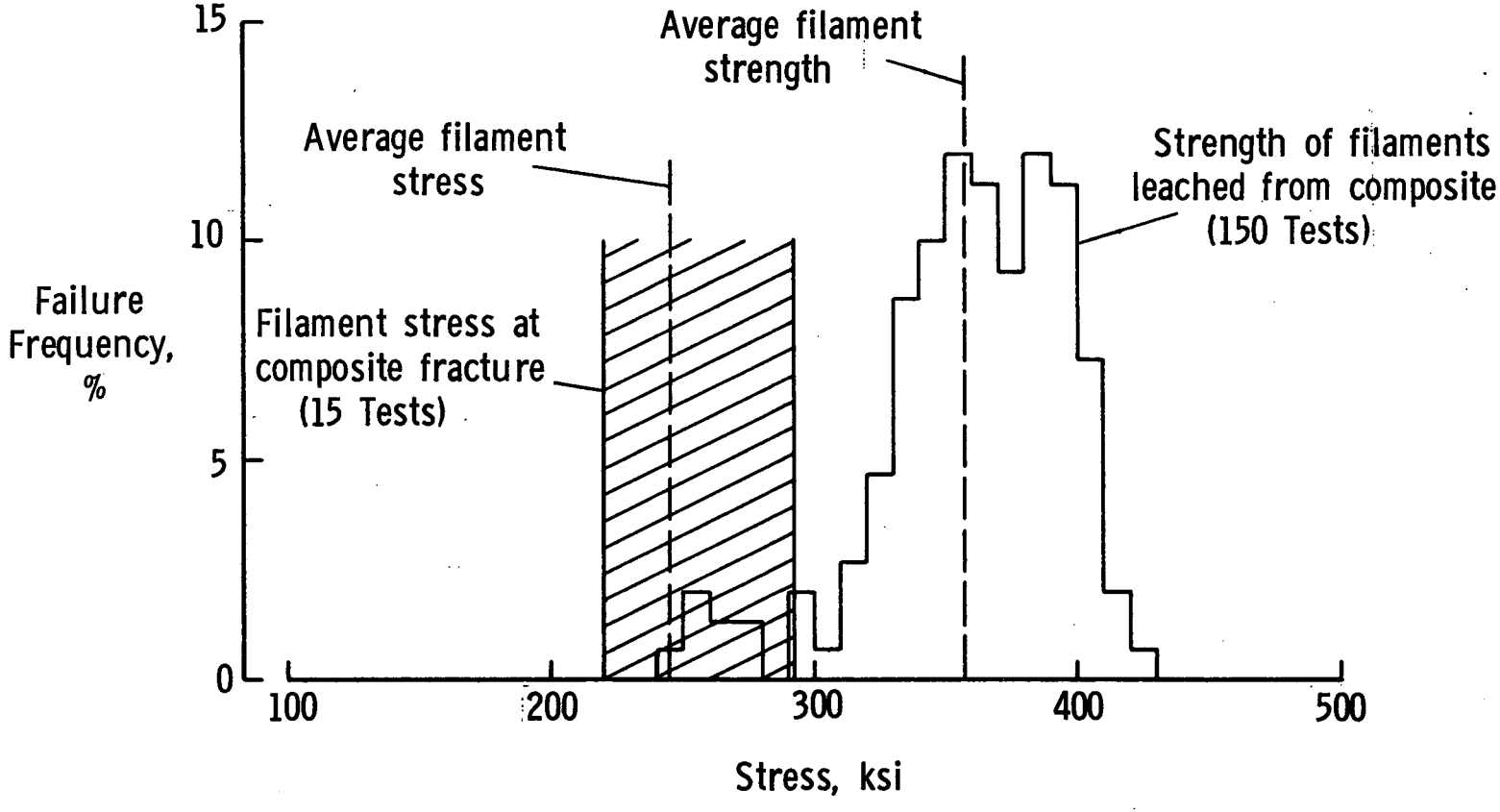

Figure 43.- Average filament stress at composite fracture compared with filament strength in composite for monolayer sheet containing 5.6 mil diameter boron filaments, consolidated under 10 ksi pressure at 1100°F.

filament is presented as Figure 44 to provide an indication of the actual degradation involved. For composite of this quality, enough energy is released by failure of the weakest filament to initiate and sustain catastrophic filament break propagation. Thus, fracture is completely noncumulative. Strength data from tests of virgin 5.6 mil diameter filament are listed in Table I. Similar data for the reclaimed filaments and from the composite tensile tests are presented in Tables II and III, respectively, identified with Batch 43.

Similar comparisons were made for five additional batches of bilayer composite containing 3.9 mil diameter boron filament. The virgin strength distribution for the 3.9 mil diameter filament is presented in Figure 45, plotted from data listed in Table IV. The additional composites were still well bonded, but filament degradation had been intentionally made progressively more severe in each successive batch. The second comparison is made in Figure 46 for a bilayer composite which contained slightly weaker filaments. The average filament in the composite had a strength of 300 ksi compared with 360 ksi for the previous batch represented by Figure 43. Both composites were consolidated under 10 ksi pressure, but the smaller initial filament diameter in the bilayer composite apparently made the degradation more effective in reducing the net filament section available to withstand load. The weakest filament had a strength of 190 ksi, and again, that value was identical to the average filament stress at failure of the composite. Fracture was still completely noncumulative. The histogram of Figure 46

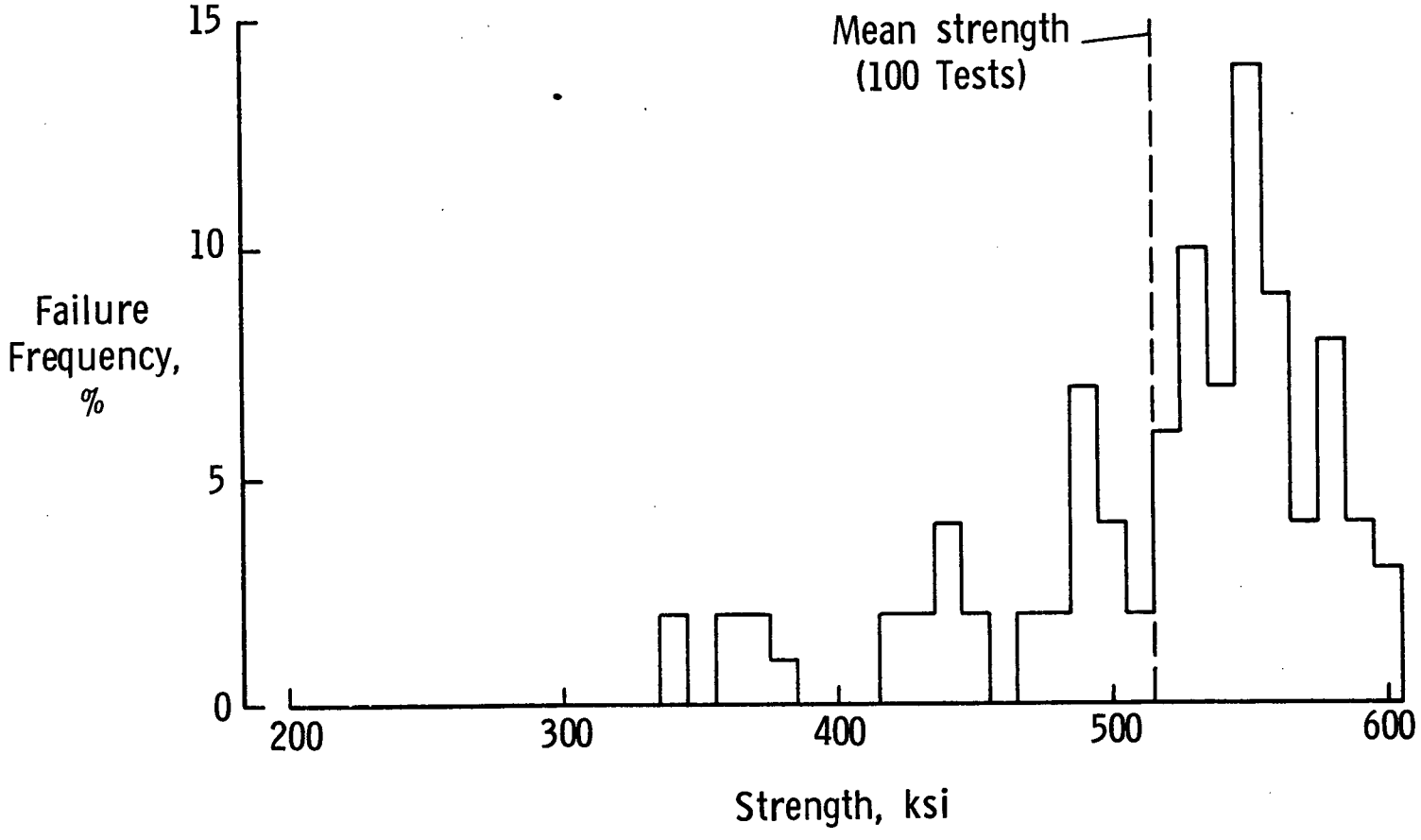

Figure 44. - Failure frequency histogram for virgin 5.6 mil diameter boron filament.

Table I. Strengths of Virgin 5.6 mils Diameter Boron Filament, ksi (Fig. 44)

342	490	534	557
344	492	535	559
357	493	539	560
359	494	541	560
368	495	542	562
369	496	542	564
370	499	543	566
375	504	544	570
417	508	545	571
423	512	545	573
429	(516) Mean	548	575
431	520	549	577
437	521	550	580
439	521	551	582
440	522	551	582
444	524	551	583
449	525	552	583
451	528	552	584
466	529	552	585
470	530	553	587
480	531	554	588
482	532	554	590
485	532	555	595
486	533	556	600
490	533	556	602

Table II. Strengths of 5.6 mils Diameter Boron Filament Reclaimed from Composite Batch 43, ksi (Fig. 43)

247	330	349	363	380	394
252	332	350	364	381	394
252	333	351	364	381	396
255	333	352	364	381	397
263	335	352	365	383	397
269	336	353	365	384	398
275	336	353	366	384	398
279	337	354	366	385	399
291	339	354	367	386	399
294	339	354	369	386	399
296	339	354	369	386	400
308	340	355	370	386	402
310	340	355	370	387	402
311	340	356	370	387	402
315	341	356	371	388	403
319	341	(357) Mean	373	388	403
321	343	357	374	389	403
323	343	359	375	389	406
326	345	359	375	390	407
326	345	361	375	391	408
327	345	361	375	391	408
328	347	361	377	391	410
328	347	361	379	392	413
330	348	362	379	392	419
330	348	362	379	392	427

Table III. Average Filament Stresses at Composite Failure for Composite Batches 43 and 46 through 50, Commercially Fabricated Composite, and Moderately Weak Bonded Composite, ksi (Figs. 43 and 46 through 52)

Batch 43	Batch 46	Batch 47	Batch 48	Batch 49	Batch 50	Commercially Fabricated	Moderately Weak Bonded
220	165	143	127	138	132	120	150
226	171	149	132	143	138	151	160
231	171	154	154	149	138	160	160
231	171	154	165	154	143	171*	160
231	171	170	165	154	143	179	165
237	176	171*	171*	154	143	200	165
242	176	171	176	165	149		171
242	182	171	187	171*	149		171
242	182	171	187	171	154*		171
242	187	182	198	171	165		171
248*	187	186	204	176	182		176*
259	193*	232	209	187	193		176
264	193			193			182
275	193			198			182
292	198			209			187
	209			231			198
	215						215
	226						225
	226						
	231						

* indicates approximate mean value

represents the results of 100 tensile tests of reclaimed filaments. The data are listed in Table V, identified with Batch 46. Twenty composite specimens were tested from the same batch to determine the average filament stress at composite failure. Those data are listed in Table III.

In Figure 47, data are plotted for a composite which had been consolidated under 11 ksi pressure. The average filament strength was reduced to 275 ksi, and the average filament stress at fracture of the composite was 171 ksi. For the first time there were filaments in the composite which had strengths less than the average filament stress at fracture of the composite, and those filaments failed cumulatively before the noncumulative mode was initiated. The data for Figure 47 are listed in Tables VI and III, identified with Batch 47.

The data in Figure 48 are from a composite in which the filaments were degraded to an even greater extent, exhibiting an average strength of 255 ksi. The average filament stress at composite failure, however, did not decrease, but remained essentially constant at 173 ksi. This material was hot pressed under 12 ksi pressure, and was designated as Batch 48. Data from filament and composite tests are presented in Tables VII and III, respectively, identified with the batch number.

The comparison made in Figure 49 is for composite which had been consolidated under 13 ksi pressure. The average strength of filaments leached from the composite was only 225 ksi. The average filament stress at fracture of the composite, however,

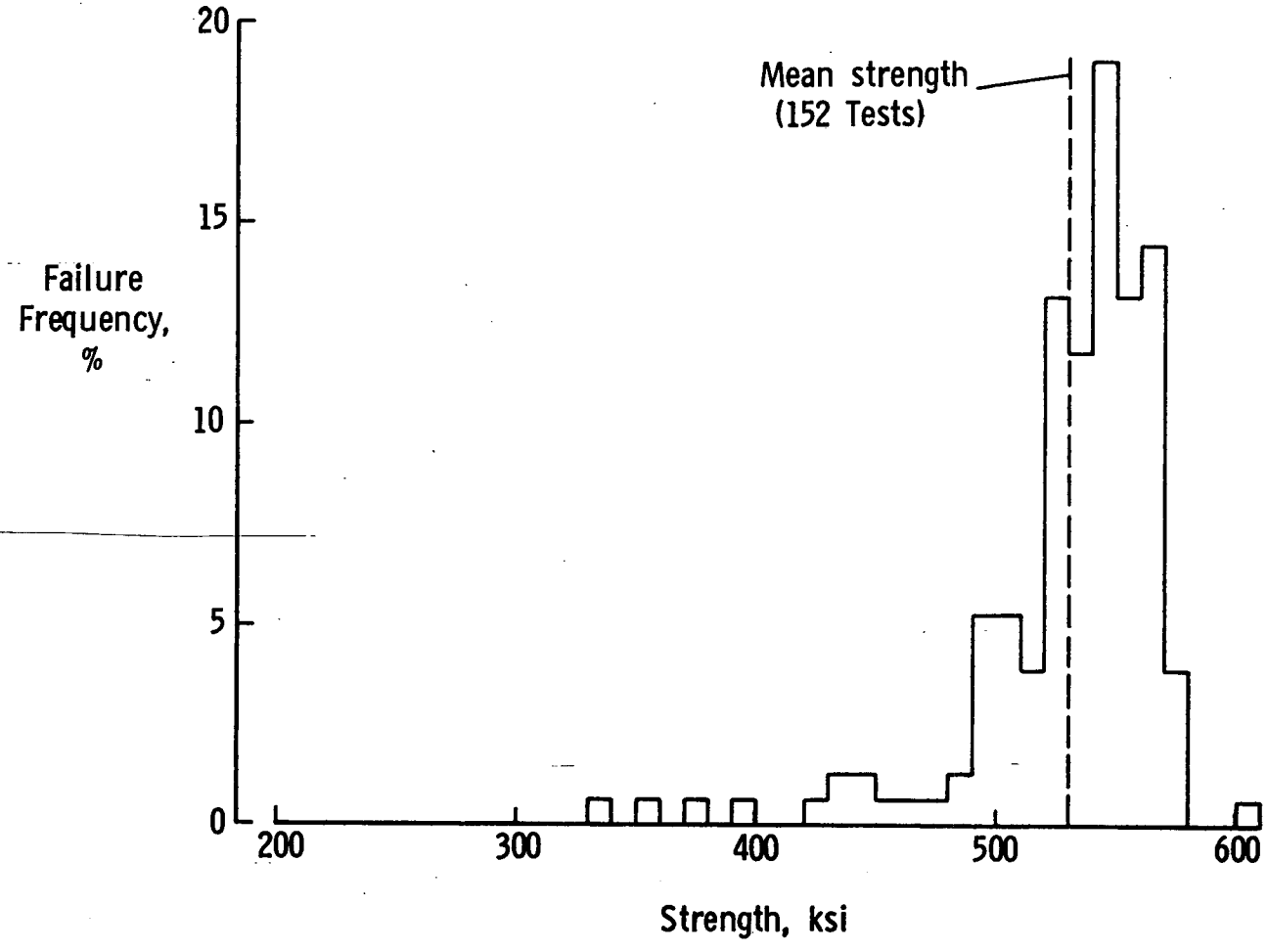

Figure 45. - Failure frequency histogram for virgin 3.9 mil diameter boron filament.

Table IV. Strengths of Virgin 3.9 mils Diameter Boron Filament, ksi (Fig. 45)

336	504	527	542	549	561
359	504	527	542	550	562
372	506	528	542	550	562
398	506	528	543	550	562
423	508	529	543	552	562
432	510	529	543	553	562
433	512	(530) Mean	544	553	563
445	514	531	544	553	563
447	516	531	545	553	564
453	517	533	545	553	564
468	518	533	545	553	564
476	520	534	545	554	564
480	521	535	545	554	565
485	522	535	545	554	565
492	523	535	545	554	566
493	523	536	546	555	567
494	523	536	546	556	569
495	523	436	546	556	569
495	524	537	546	557	570
495	524	537	546	557	570
497	524	538	546	558	573
499	525	538	547	560	577
501	525	539	547	560	578
502	526	539	547	561	579
504	527	541	549	561	608
		542	549		

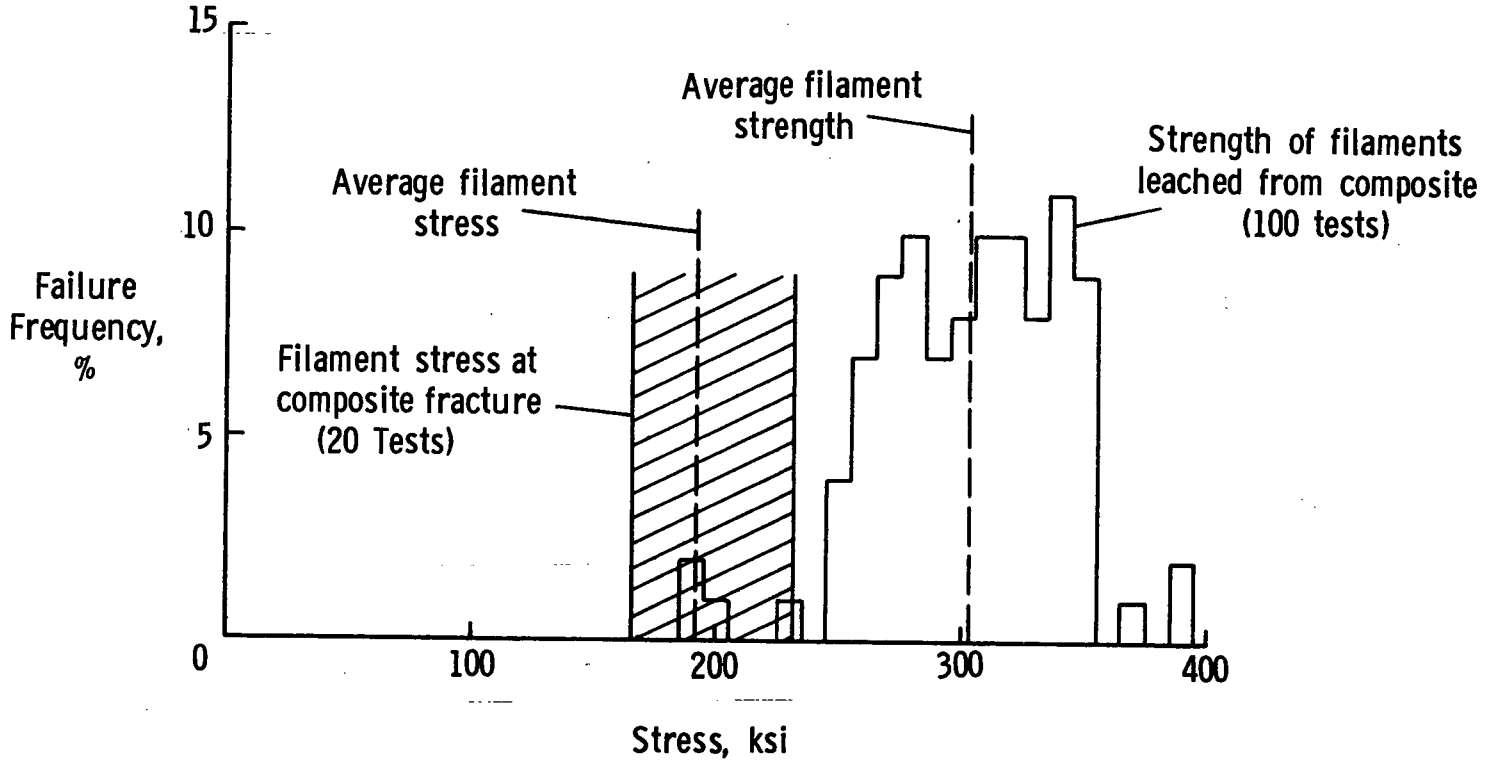

Figure 46. - Average filament stress at composite fracture compared with filament strength in composite for bilayer sheet containing 3.9 mil diameter boron filaments, consolidated under 10 ksi pressure at 1100°F.

Table V. Strengths of 3.9 mils Diameter Boron Filament Reclaimed from Composite Batch 46, ksi (Fig. 46)

191	277	311	331
193	278	312	331
210	279	312	335
225	281	312	339
248	283	312	340
252	283	312	340
252	284	313	341
253	284	313	341
255	284	314	341
257	286	317	341
259	289	318	342
259	290	318	343
260	293	319	343
263	293	319	345
264	293	321	345
265	294	322	346
265	295	323	346
270	298	323	349
270	299	324	351
270	299	325	351
272	300	326	351
273	300	327	351
274	(302) Mean	327	369
274	304	327	385
276	305	329	392

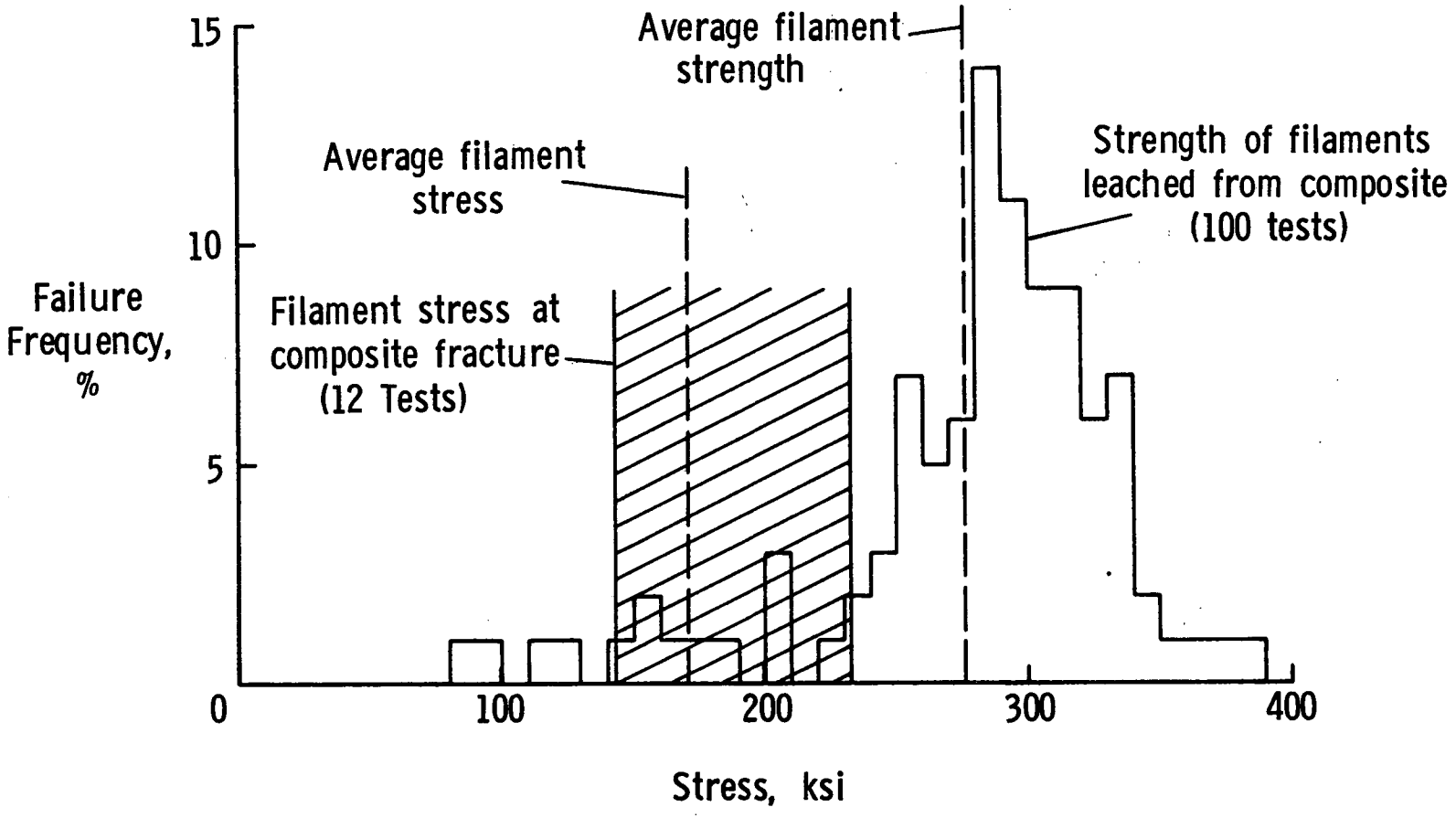

Figure 47.- Average filament stress at composite fracture compared with filament strength in composite for bilayer sheet containing 3.9 mil diameter boron filaments, consolidated under 11 ksi pressure at 1100°F.

still remained constant at a value of 173 ksi. The filament and composite tensile data for this composite are listed in Tables VIII and III, respectively, identified with Batch 49.

The final comparison for well bonded composite is made in Figure 50 for material which had been consolidated by hot pressing under 15 ksi pressure. Of all the composites tested, this material contained the most severely degraded filaments. Fracture of the composite was completely cumulative. The average filament in the composite had a strength of 235 ksi, which was slightly greater than the value of 225 ksi for the previous case of Batch 49, but the increased degradation was seen as a broadening of the range over which the filament strengths were distributed. The average filament stress at composite fracture was 152 ksi, significantly less than the value of approximately 170 ksi observed for composites which failed in a partially cumulative mode. Data from filament and composite tensile tests are listed in Tables IX and III, respectively, identified with Batch 50.

Similar comparisons were made for the commercially fabricated composite, and for the moderately weakly bonded composite which was consolidated at 950°F under 9 ksi pressure. Results from tests of the commercially fabricated composite are presented in Figure 51. The material contained five layers of 4.1 mil diameter silicon carbide coated boron filament in a 2024 aluminum alloy matrix. The average filament strength was reasonably high at 310 ksi, but the distribution was dispersed over a 460 ksi range. The average filament stress at composite fracture was 165 ksi, not greatly

Table VI. Strengths of 3.9 mils Diameter Boron Filament Reclaimed from Composite Batch 47, ksi (Fig. 47)

81	257	289	313
97	259	289	315
111	260	290	316
123	260	290	317
147	262	290	317
156	263	291	319
159	268	291	323
164	270	293	324
172	270	294	324
186	273	294	324
197	274	294	327
203	(276) Mean	297	329
203	276	298	331
209	280	300	331
221	282	300	331
238	282	302	331
239	283	304	336
241	283	305	338
246	284	307	338
247	284	307	346
250	284	308	348
251	286	309	354
253	287	312	367
253	287	312	377
253	289	313	381

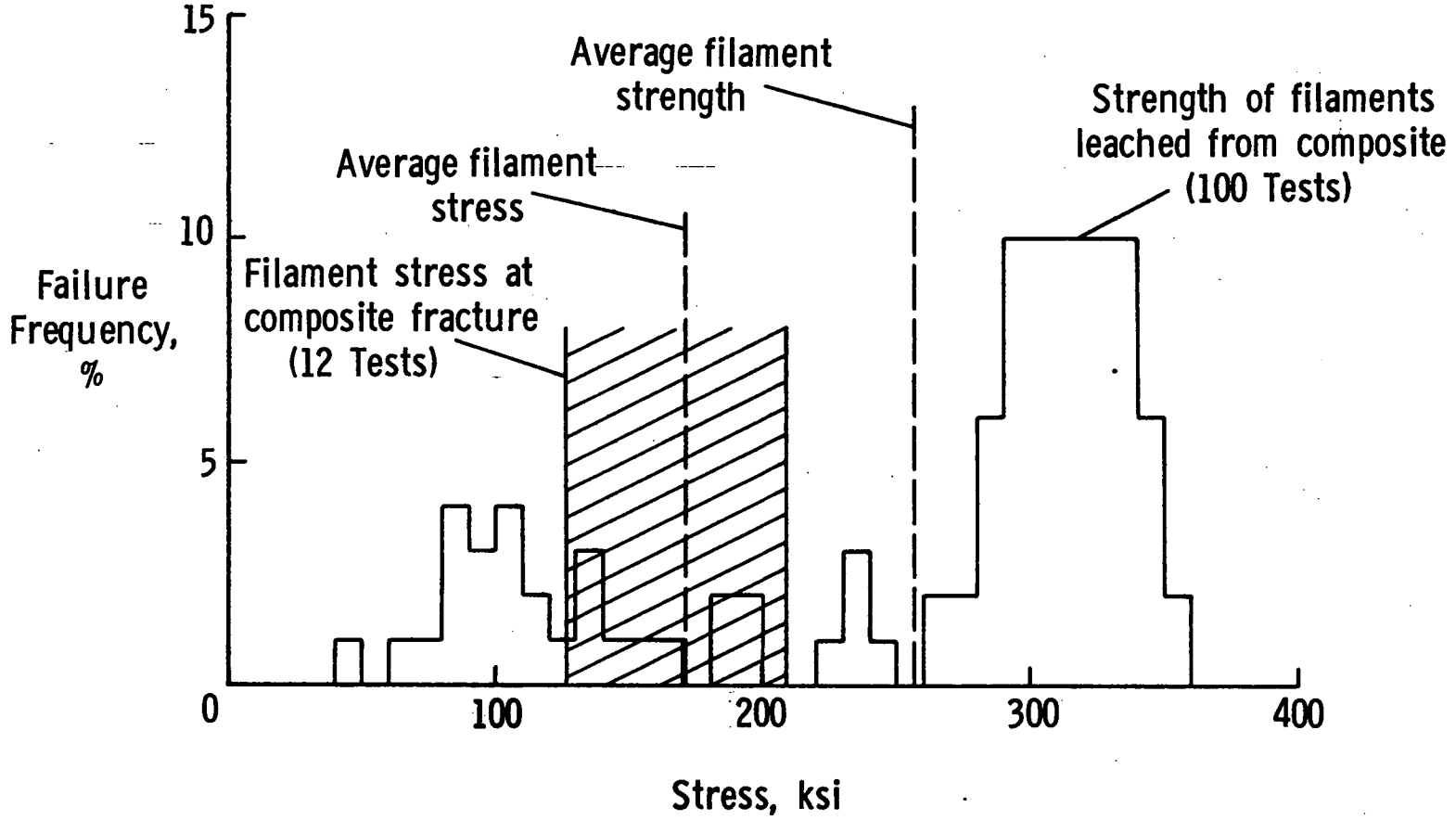

Figure 48. - Average filament stress at composite fracture compared with filament strength in composite for bilayer sheet containing 3.9 mil diameter boron filaments, consolidated under 12 ksi pressure at 1100°F.

Table VII. Strengths of 3.9 mils Diameter Boron Filament Reclaimed from Composite Batch 48, ksi (Fig. 48)

42	194	299	322
68	197	299	322
73	228	300	324
80	238	300	325
84	238	301	327
86	239	303	327
88	245	304	327
90	(260) Mean	304	331
92	269	305	332
95	270	305	333
101	278	306	333
101	280	308	333
104	280	311	334
105	285	311	335
115	285	311	336
118	289	312	336
121	289	313	336
133	290	315	340
135	290	316	341
139	291	316	341
143	293	317	341
158	293	318	344
161	294	320	344
183	298	320	350
189	298	321	354

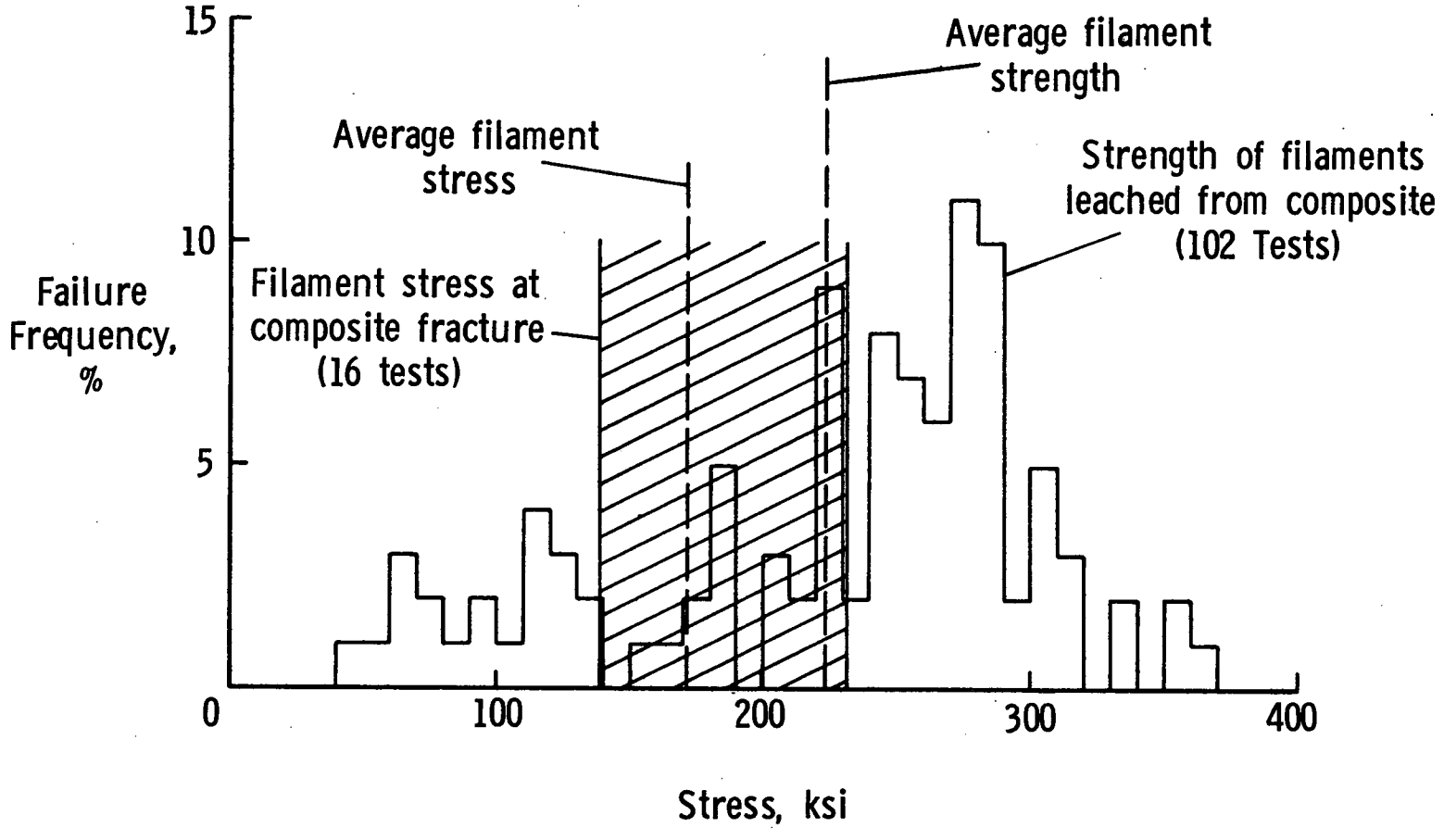

Figure 49. - Average filament stress at composite fracture compared with filament strength in composite for bilayer sheet containing 3.9 mil diameter boron filaments, consolidated under 13 ksi pressure at 1100°F.

Table VIII. Strengths of 3.9 mils Diameter Boron Filament Reclaimed from Composite Batch 49, ksi (Fig. 49)

43	183	248	281
52	184	248	281
64	185	250	282
64	189	251	283
64	202	252	284
70	205	258	284
73	206	259	286
88	212	259	286
92	218	259	287
93	221	260	287
106	(223) Mean	262	292
110	224	264	293
111	224	267	300
115	225	267	302
116	226	268	303
122	226	270	304
127	227	273	308
127	227	273	310
132	237	273	311
135	237	277	312
150	242	277	333
162	242	277	335
176	243	278	356
179	243	278	357
182	243	279	362
	244	279	

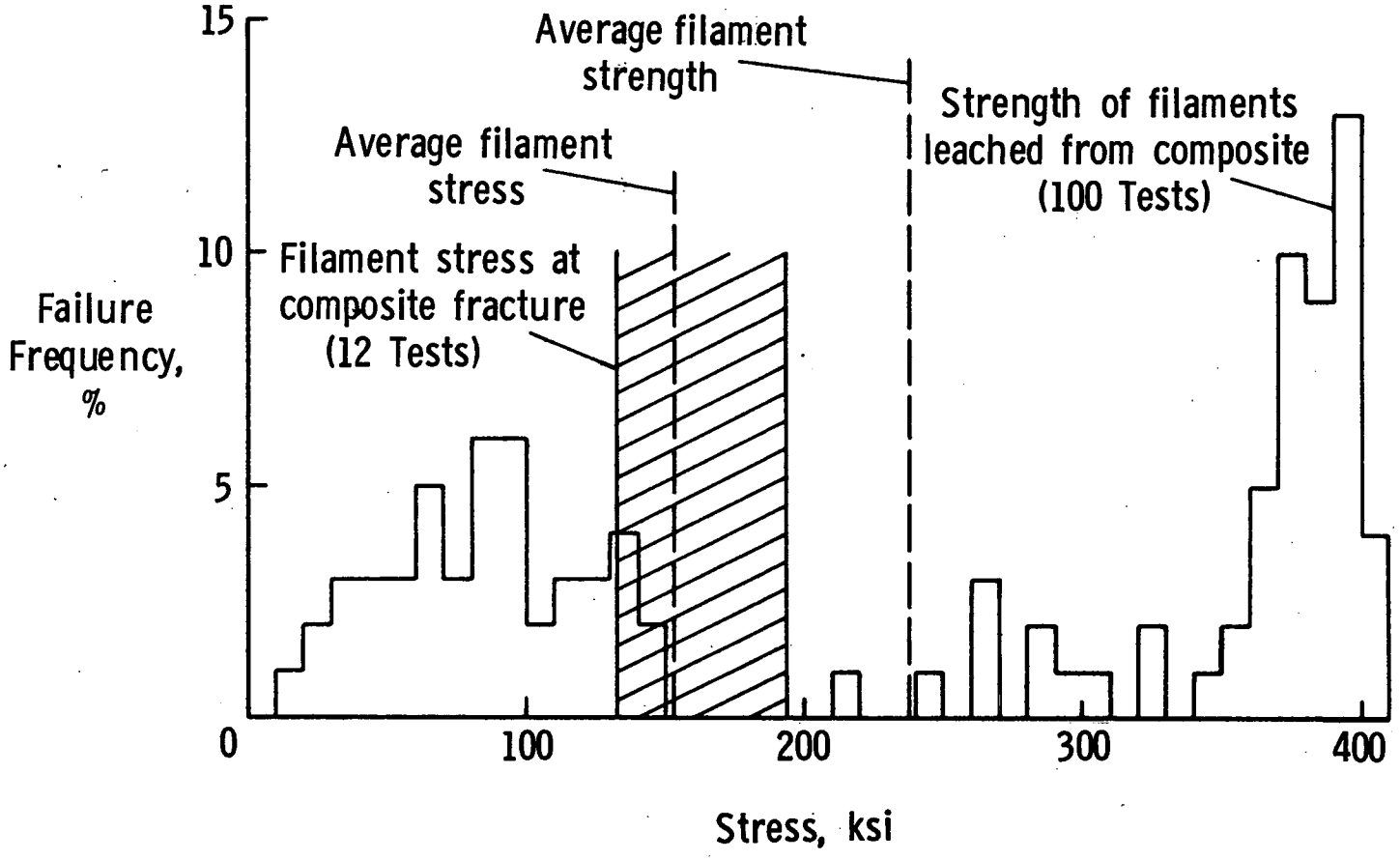

Figure 50. - Average filament stress at composite fracture compared with filament strength in composite for bilayer sheet containing 3.9 mil diameter boron filaments, consolidated under 15 ksi pressure at 1100°F.

different for the previously observed value for composites which failed in a partially cumulative manner. Data from commercial composite tests are listed in Tables X and III.

Results for the moderately weakly bonded composite are presented in Figure 52, plotted from data in Tables XI and III. The average filament strength in the composite was 270 ksi, and the average filament stress at fracture of the composite was 177 ksi. The average filament stress resulting from composite tensile tests was in reasonably good agreement with the previous results from composites which underwent partially cumulative fracture. However, the average filament strength was somewhat lower than had been expected considering the relatively mild hot pressing conditions. It should be recalled that the moderately weakly bonded composite contained 3.5 mil diameter boron filament which was known to possess erratic strength based on qualitative observations during filament winding. However, the virgin strength distribution was not quantitatively determined, and as a result, the true extent of degradation resulting from consolidation could not be evaluated.

2. Threshold Stress for Noncumulative Fracture

At this point it has been demonstrated that the tensile fracture mode for unidirectional B-Al composite sheet can be altered at will from completely noncumulative to completely cumulative through a range of mixed-mode fracture. It will now be shown that a threshold value of average filament stress exists above which

Table IX. Strengths of 3.9 mils Diameter Boron Filament Reclaimed from Composite Batch 50, ksi (Fig. 50)

18	90	275	381
24	92	277	381
28	93	299	382
32	96	303	385
32	97	325	386
40	98	327	388
42	100	345	388
49	105	350	389
54	113	356	391
57	114	360	392
58	115	360	392
63	122	363	395
64	123	368	396
64	124	369	396
64	130	370	397
69	133	370	397
70	135	371	397
71	139	372	397
77	140	375	398
80	147	377	398
84	210	377	399
85	(240) Mean	378	401
86	264	379	401
87	265	379	402
89	268	380	403

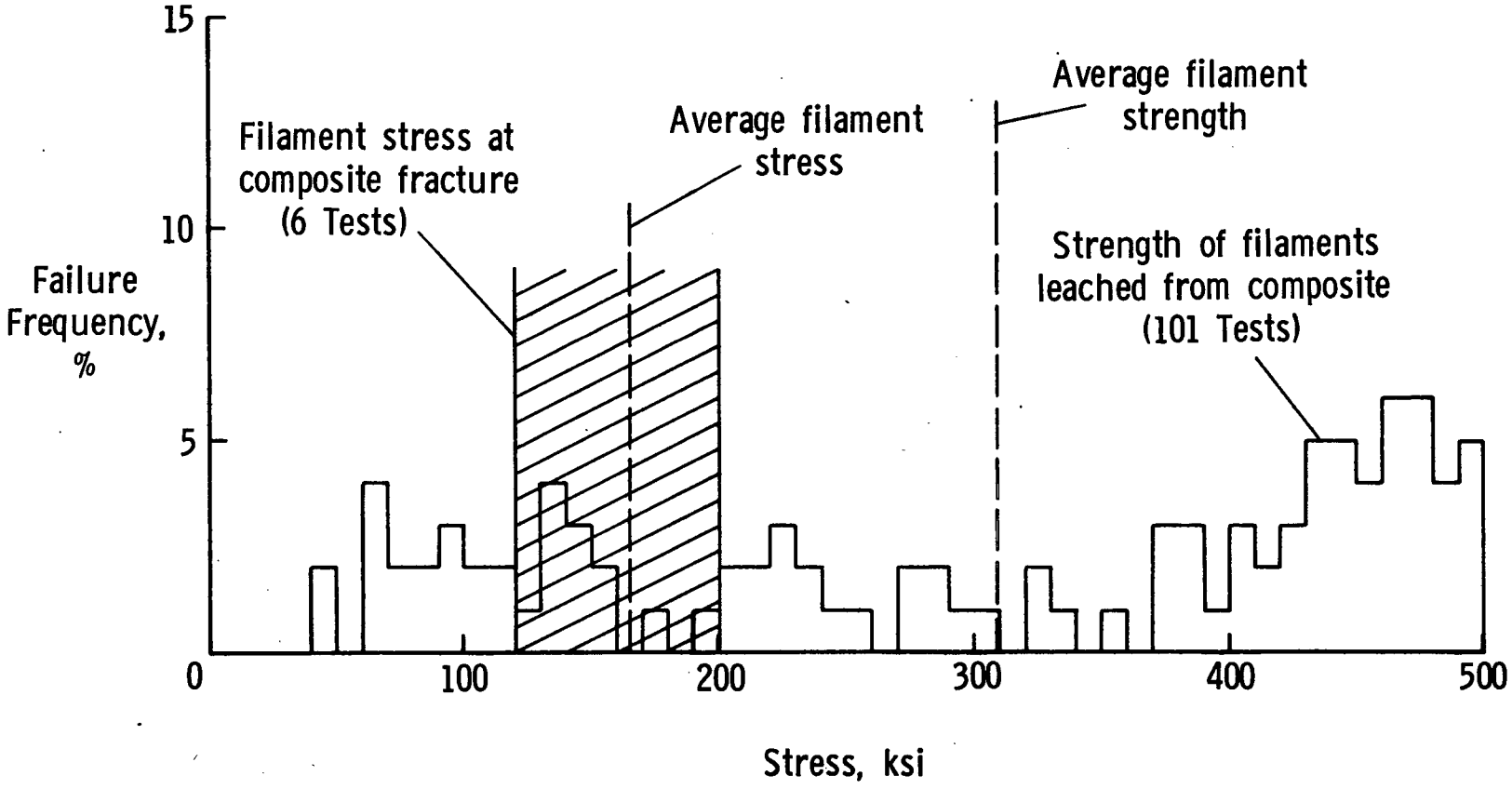

Figure 51. - Average filament stress at composite fracture compared with filament strength in composite for commercially fabricated five-layer sheet containing 4.1 mil diameter silicon carbide coated boron filaments.

Table X. Strengths of 4.1 mils Diameter Silicon Carbide Coated Boron Filament Reclaimed from Commercially Fabricated Composite, ksi (Fig. 51)

46	152	350	449
49	156	374	454
61	177	379	454
62	195	379	458
64	199	380	459
67	200	386	464
73	207	386	465
76	212	394	467
80	216	402	467
85	225	406	468
92	227	409	469
96	227	415	470
98	236	419	471
101	237	425	473
101	246	427	475
111	253	427	476
111	275	430	476
120	277	432	482
137	280	433	483
139	283	434	483
139	296	439	485
139	(307) Mean	442	490
142	321	447	491
143	324	448	494
147	335	449	495
			496

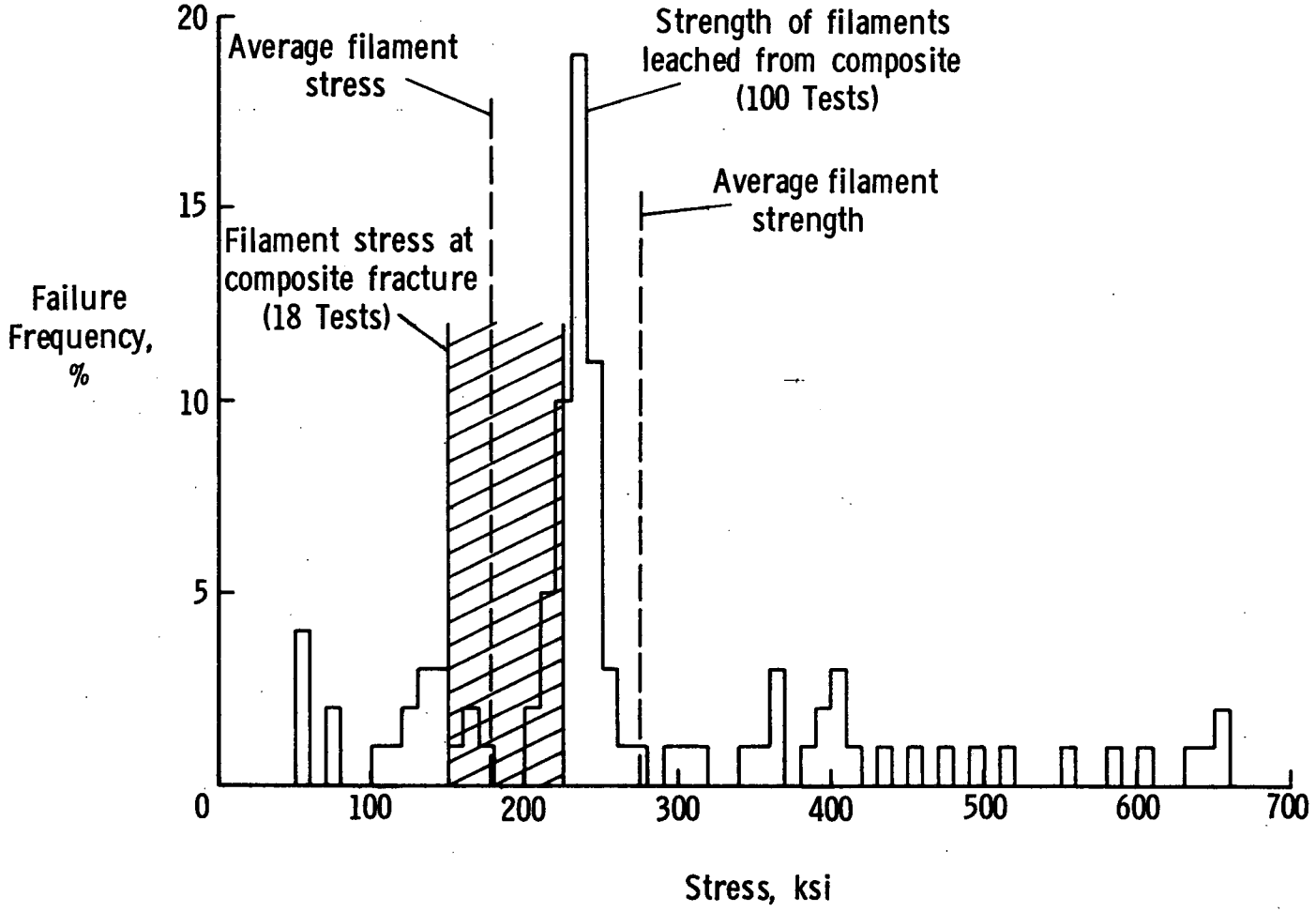

Figure 52. - Average filament stress at composite fracture compared with filament strength in composite for bilayer sheet containing 3.5 mil diameter boron filaments, consolidated under 9 ksi pressure at 950°F.

Table XI. Strengths of 3.5 mils Diameter Boron Filament Reclaimed from Moderately Weak Bonded Composite, ksi (Fig. 52)

55	218	237	329
56	219	237	342
57	220	237	353
58	221	238	361
72	222	239	365
74	224	239	367
100	225	240	385
112	226	240	393
122	227	242	395
128	228	243	400
135	229	244	403
135	229	245	405
136	230	245	418
141	230	245	431
146	230	246	456
147	230	247	474
158	231	249	493
162	231	250	513
162	231	252	556
176	232	255	585
201	232	260	602
208	233	(275) Mean	631
214	234	290	646
216	235	305	651
218	236	315	652

composite fracture is completely noncumulative, and below which fracture occurs in a completely cumulative manner. In order to do this, it is necessary to collectively represent the essential information presented in Figures 43 and 46 through 52 in a single graph. This is accomplished in Figure 53 where average filament stress at composite fracture is related to the strength distributions of filaments leached from the several composite batches.

In Figure 53, the average filament stress at composite fracture is plotted as a function of a degradation factor which is defined as that fraction of distributed filament strengths which were greater than or equal to the average filament stress at composite fracture. For completely noncumulative fracture, the degradation factor is unity. The data from Figure 43, for example, are represented by the uppermost point in Figure 53, and the degradation factor is unity since all of the filaments tested had strengths greater than the average filament stress when composite fracture occurred.

The data of Figure 53 seem to indicate, for all the composites represented, that unidirectional B–Al composite sheet will fail in tension as the result of completely noncumulative filament break propagation (see Figure 54) initiated by failure of its weakest filament, provided the average filament stress remains above approximately 170 ksi. That was the behavior observed for the composites represented by the upper two data points (composites of Figures 43 and 46). Since completely noncumulative fracture is apparently triggered by failure of the weakest filament in the

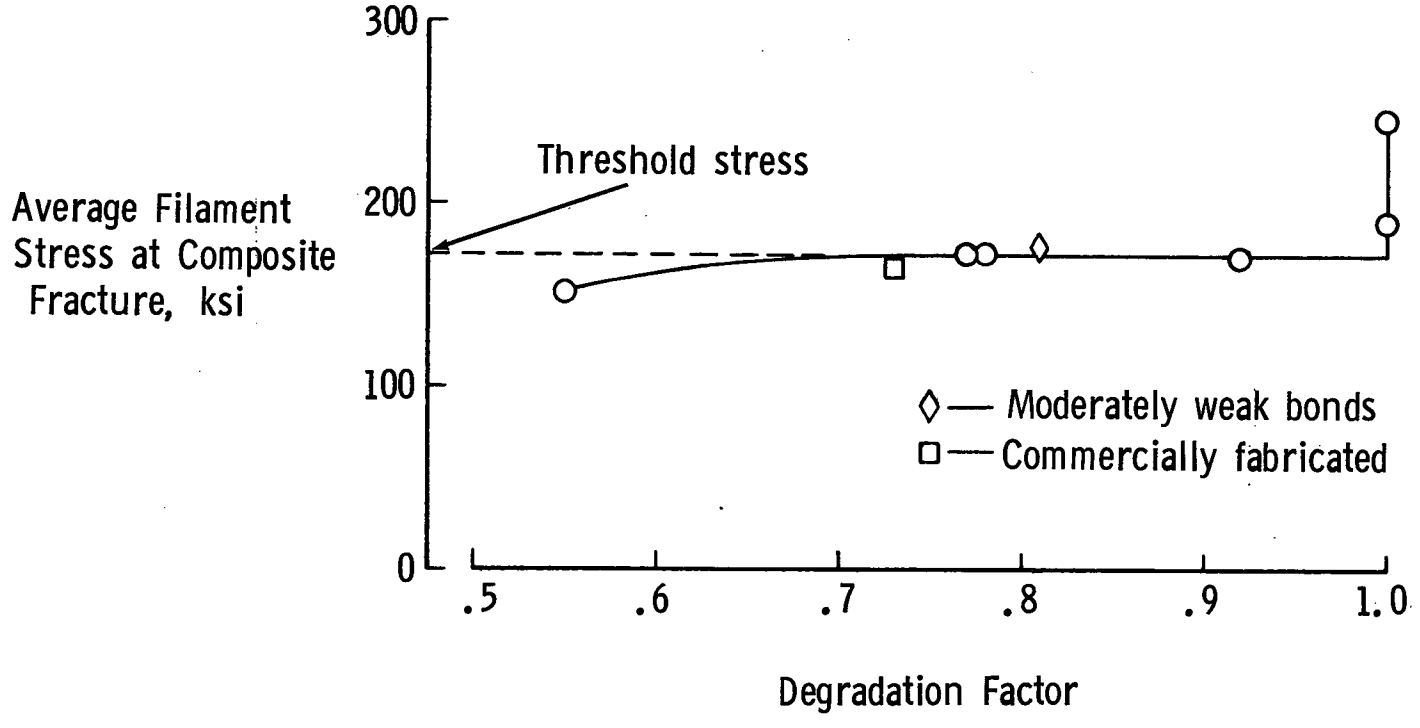

Figure 53. - Threshold stress for initiation and sustenance of noncumulative filament break propagation in unidirectional B-Al composite sheet.

Edge of specimen

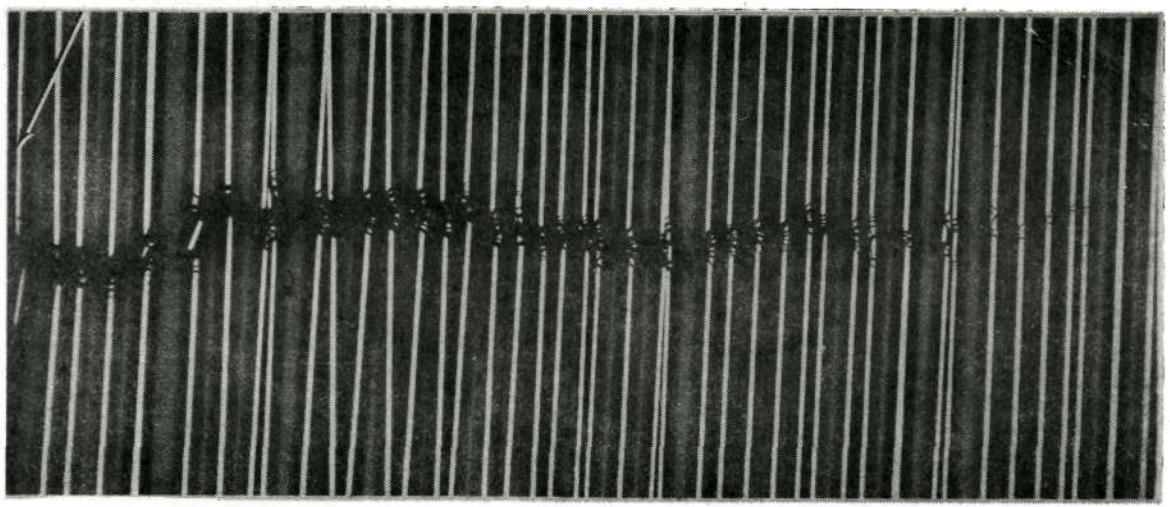

Figure 54. - Fractoradiograph illustrating the noncumulative fracture mode, 0.6 mil core diameter.

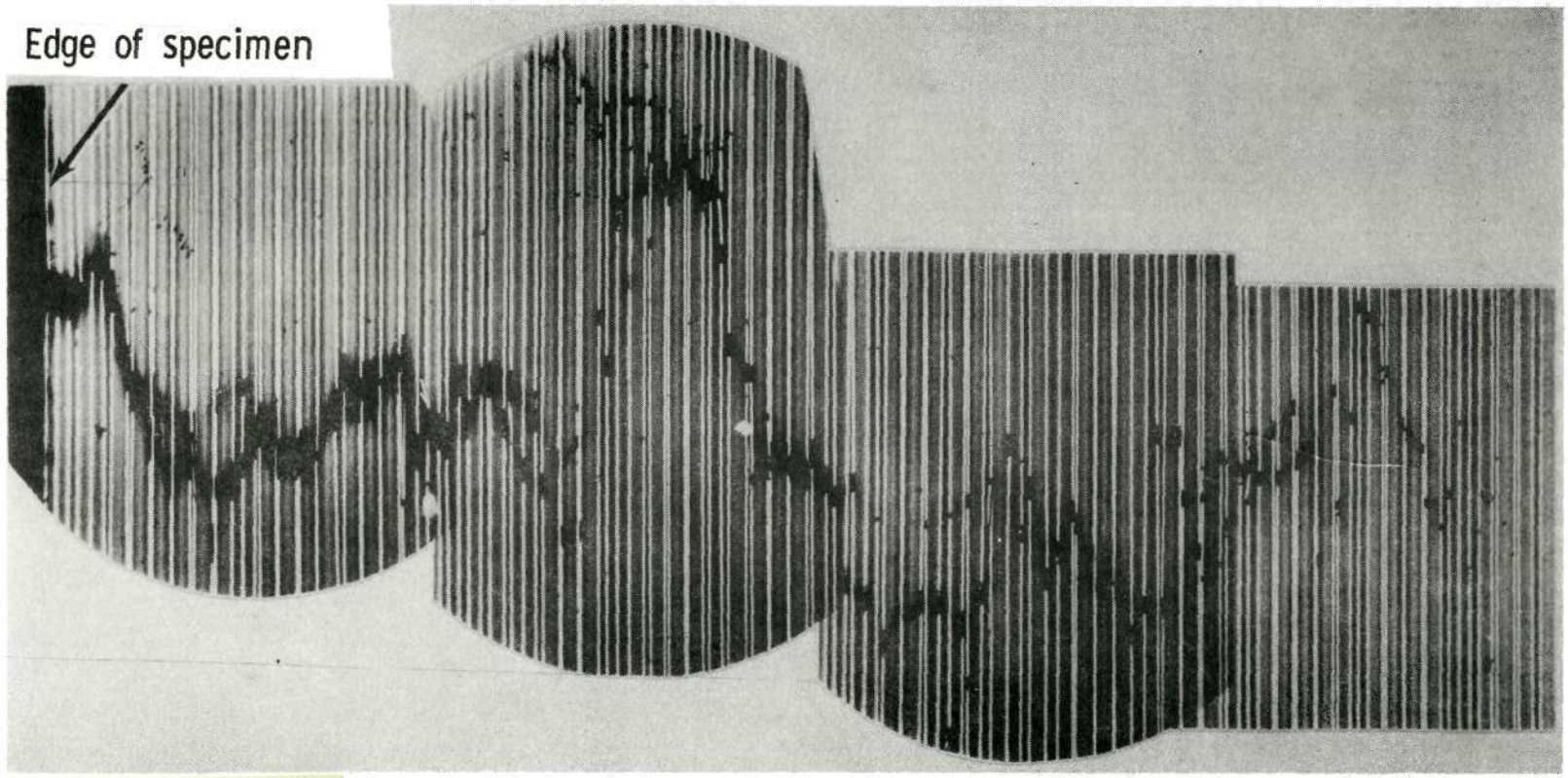

Figure 55. - Fractoradiograph illustrating the cumulative fracture mode, 0.6 mil core diameter.

composite, it would be essential to know what the strength of that filament is. A knowledge of the average filament strength would be of little value in predicting composite strength.

The lower data point on Figure 53 represents the well bonded composite of Figure 50 in which filaments were most severely degraded, and for which fracture was completely cumulative (see Figure 55). Isolated filaments in this composite were fragmented, but the average filament stress never reached the critical value required to sustain the noncumulative fracture mechanism.

The composites of Figures 47, 48, 49, 51, and 52 contained appreciable numbers of weaker filaments, but did not fracture until the average filament stress reached approximately 170 ksi. Those composites are represented in Figure 53 by the five data points associated with the horizontal line at 170 ksi. All five composites underwent fracture by a combination of the cumulative and non-cumulative modes. The weaker filaments failed cumulatively until the average stress in the remaining filaments reached the limiting value of 170 ksi. At that stress, the noncumulative filament break propagation mechanism was initiated and became self sustaining, resulting in abrupt failure of the remaining filaments and the composite. For composites which underwent mixed-mode fracture, the degradation factor could be defined as the fraction of filaments which were directly involved in the noncumulative mode of fracture.

The limiting value of 170 ksi appears to be the threshold stress for the initiation and sustenance of the noncumulative filament break propagation mechanism. On the average, any single

filament which fractures at a tensile stress greater than 170 ksi will liberate sufficient elastic strain energy to initiate a self sustaining progression of filament fractures similar to a chain reaction. Immediate composite fracture is the result. The strain energy from a filament which fractures at a stress less than 170 ksi will be absorbed without causing the immediate fracture of a sufficient number of adjacent filaments to initiate the noncumulative mechanism.

It is important to note that Figure 53 presents results from composites containing one, two, and five filament layers. The composites contained 3.5 mil, 3.9 mil, and 5.6 mil diameter boron filaments as well as 4.1 mil diameter silicon carbide coated boron filament. Both well bonded and moderately weakly bonded composites are represented containing two markedly different matrix alloys. None of these differences seems to affect the general applicability of the noncumulative filament break propagation fracture mechanism or the threshold stress for its initiation.

The composite with extremely weak internal bonding was not represented in Figure 53 because the strength distribution for filaments contained within it was not determined. As mentioned previously, the composite was not fabricated intentionally, and only four specimens were available. The material was unique in the sense that it failed in the completely cumulative mode at an average filament stress of 210 ksi, significantly greater than the value of approximately 170 ksi required to initiate the noncumulative mode in all the other composites tested.

The fracture characteristics of the extremely weakly bonded composite suggested that very weak internal bonding could prevent the occurrence of noncumulative filament break propagation. That would be reasonable to expect if the filament–matrix bond represented a sufficient mechanical discontinuity to prevent dynamic coupling of the two constituents. Stress waves produced by individual filament breaks would then be damped by internal friction within the composite, and their energy would be dissipated as heat.

Just how weak the internal bonding must be to take full advantage of the internal damping effect was not determined. The strengths of both moderately weakly bonded and commercially fabricated composites were found to be limited by noncumulative fracture, and the filament–matrix bonds in the commercial composite were certainly not well developed. However, the commercial material included in this study was not of prime quality, even though it was procured as such. Although the author has not personally tested the material, several manufacturers currently market unidirectional B–Al composite sheet with advertised tensile strength in the range from 150 ksi to 200 ksi. In order to develop those strengths in a composite with, say a 6061 aluminum alloy matrix, a minimum average filament stress on the order of 275 ksi would be required based on a rule of mixtures calculation. Average filament stresses of that magnitude could be obtained in two ways. First, the fabrication process could be controlled so as to ensure that the weaker filaments in the composite had strengths greater than 275 ksi, in which case fracture would be noncumulative. The second method would involve

precise and accurately controlled development of internal bonds in such a way that the threshold stress for noncumulative fracture would be elevated. It is suspected that the latter method would be very difficult to apply to the manufacture of large sheets, or to parts with complicated shapes because of the necessity for precise and uniform control of the consolidation process. Only slight local variations in consolidation parameters could result in regions of noncumulative fracture which could lead to serious problems in an engineering application.

G. Fracture of Internally Damaged Composites

Recent calculations by Zweben[19,20] have shown that stress concentrations in regions of minor filament damage would be expected to cause a significant reduction in the tensile strength of a composite. Zweben considered the matrix to behave elastically, and assumed that damage took the form of collinear cuts in adjacent filaments. His calculated results indicated that tensile fracture should occur through the damaged region. In the present investigation, an attempt was made to experimentally evaluate the effect of internal filament damage in unidirectional B-Al composite sheet. A primary objective was to determine the effect of matrix plasticity in reducing the stress concentration in a damaged area.

Fifteen composite tensile specimens were prepared with internal filament damage. An attempt was made to transversely cut a number of adjacent filaments in the center of the gage

section of each specimen prior to consolidation. Actually, instead of being cut, the affected filaments were crushed, and the internal damage after consolidation was much less localized than had been planned. The number of damaged filaments per specimen ranged from 4 to 20 from a total of 100 in an average specimen. A radiograph taken through the flawed region in a specimen containing four damaged filaments is represented as Figure 56. The matrix was continuous around the broken filaments, and the adjacent whole filaments showed some tendency to be washed into the flawed region by matrix flow during diffusion bonding. The flawed region of a specimen containing 14 damaged filaments is shown in the radiograph of Figure 57, against a background formed by a strain gage grid.

All 15 flawed specimens failed in their gage sections, but not one failure was associated with an internal flaw. Whatever stress concentrations there were associated with the internal filament breaks were made negligible by plastic flow in the matrix in the immediate vicinity of the breaks. Further, the broken filaments were rendered ineffective in carrying load only in the flawed region and over the short distance required to reassume the load by shear transfer through the matrix. So long as the matrix in a flawed region remained continuous, a relatively large number of broken filaments (up to 20 percent of the total number in the specimen in the present investigation) could be present in the region without directly influencing fracture of the specimen.

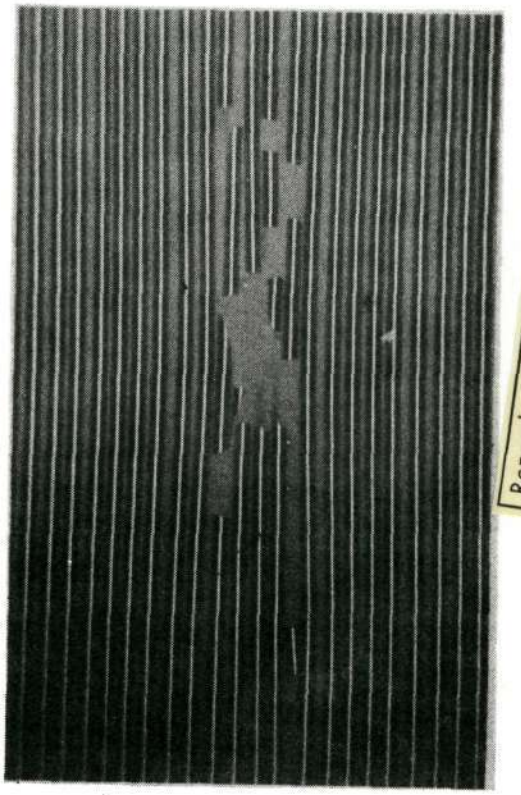

Figure 56. - Radiograph through gage section of monolayer B-Al composite tensile specimen containing four damaged filaments, 0.6 mil core diameter.

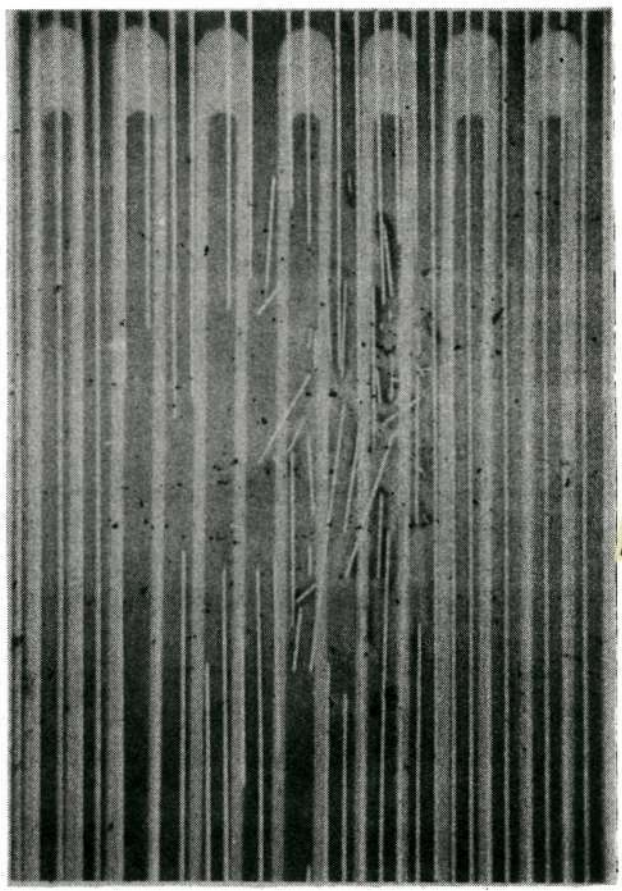

Figure 57. - Radiograph through gage section of monolayer B-Al composite tensile specimen containing 14 damaged filaments, 0.6 mil core diameter.

VI. CONCLUDING REMARKS

The results of this investigation have shown that the tensile strength of unidirectional B–Al composite sheet was generally limited by a noncumulative fracture mechanism which involved the initiation and sustenance of a chain reaction of filament fractures at a relatively low stress level. Matrix fracture followed in a completely ductile manner. The mechanism was apparently initiated by the first few filaments to break above a threshold stress level of approximately 170 ksi, and was perpetuated by the transverse propagation of compressive stress waves within the composite which caused rapid fracture of the remaining filaments. Within the limited ranges investigated, the threshold stress for initiation of the noncumulative mechanism was not altered by variations in filament diameter, number of filament layers, or the identity of the matrix alloy. The threshold stress could be elevated by making internal bonding between constituents of the composite extremely weak. There were apparently sufficient mechanical discontinuities created between filaments and matrix to prevent dynamic coupling, and thus to cause internal stress waves to be damped.

A comprehensive analysis of tensile fracture surfaces revealed that characteristic features of the surfaces were determined by the mode of fracture: cumulative, partially cumulative, or noncumulative. The characteristic features were categorized, and

related to the responsible fracture mechanisms in such a way that subsequent fractographic analyses of B–Al tensile failures will be greatly facilitated by direct comparison with the results of this investigation.

Tests of specimens which contained flaws in the form of internally broken filaments revealed that a relatively large proportion (up to 20 percent in this investigation) of the filaments in a given specimen may be broken without directly affecting fracture. Local stress concentrations resulting from internal filament breaks were apparently alleviated by matrix plasticity.

Future research designed to improve the strength of B–Al composite should be concerned with the problem of internally damping the stress waves produced by the failure of individual filaments. Also, it would seem wise to consider means for narrowing the range over which the strengths of boron filaments are spread. Even the strength of good quality, well bonded composite with minimal filament degradation is apparently limited by the strengths of its weakest few filaments. The least understood facet of the overall problem of tensile fracture in B–Al composite is probably the role of the filament. The present investigation has raised the question of whether the filament itself has two tensile fracture modes, especially after being subjected to the composite consolidation operation. One mode could be initiated at the filament surface and result in fragmentation, and the other could begin at the core and produce no fragments. A related question might be concerned with the exact nature of the degradation which results from consolidation.

No evidence of gross interfacial chemical reaction between filaments and matrix was observed in the present study, yet filament strength was greatly reduced. The strength reduction may have been associated with an increase in the frequency of occurrence of the core–initiated mode of failure. Filament behavior should certainly be a fertile subject for future research.

VII. REFERENCES

1. Herring, H. W.; Carri, R. L.; and Webster, R. C.: Compressive Behavior of Titanium Alloy Skin-Stiffener Specimens Selectively Reinforced with Boron-Aluminum Composite Attached by Brazing. NASA TND-6548, 1971.

2. Zweben, C.: Tensile Failure Analysis of Fibrous Composites. AIAA J., vol. 6, no. 12, December, 1968, pp. 2325-2331.

3. Zweben, C.: Tensile Strength of Fiber Reinforced Composites: Basic Concepts and Recent Developments. ASTM STP 460, 1969, pp. 528-539.

4. Zweben, C.; and Rosen, B. W.: A Statistical Theory of Material Strength with Application to Composite Materials. J. Mech. Phys. Solids, vol. 18, 1970, pp. 189-206.

5. Rosen, B. W.: Mechanics of Composite Strengthening. Fiber Composite Materials, Am. Soc. Metals, Metals Park, Ohio, 1965.

6. Mullin, J. V.; Berry, J. M.; and Gatti, A.: Some Fundamental Fracture Mechanisms Applicable to Advanced Filament Reinforced Composites. J. Comp. Mat., vol. 2, no. 1, January, 1968, pp. 82-103.

7. Gatti, A.; Mullin, J. V.; and Berry, J. M.: The Role of Bond Strength in the Fracture of Advanced Filament Reinforced Composites. ASTM STP 460, 1969, pp. 573-582.

8. Mullin, J. V.; and Mazzio, V. F.: Basic Failure Mechanisms in Advanced Composites. Final Report, Contract NASw-2093, NASA, April, 1971.

9. Steele, J. H., Jr.: A Microradiographic Study of Fracture in Boron Filament-Aluminum Matrix Composite. Proc. Third Ann. Meeting, International Metallographic Soc., November, 1970. (To be published.)

10. Steele, J. H., Jr.; and Herring, H. W.: Fracture of Boron Filaments in an Aluminum Matrix. Proc. Symposium on Advanced Materials: Composites and Carbon, Am. Cer. Soc., April, 1971. (To be published.)

11. Coleman, B. D.: On the Strength of Classical Fibres and Fibre Bundles. J. Mech. Phys. Solids, vol. 7, 1958, pp. 60-70.

12. Weibull, W.: A Statistical Distribution Function of Wide Applicability. J. Appl. Mech., vol. 18, September, 1951, pp. 293–297.

13. Daniels, H. E.: The Statistical Theory of the Strength of Bundles of Threads I. Proc. Royal Soc., Series A, vol. 183, 1945, pp. 405–435.

14. Gücer, D. E.; and Gurland, J.: Comparison of the Statistics of Two Fracture Modes. J. Mech. Phys. Solids, vol. 10, 1962, pp. 365–373.

15. Hedgepeth, J. M.: Stress Concentrations in Filamentary Structures. NASA TN D-882, 1961.

16. Hedgepeth, J. M.; and Vandyke, P.: Local Stress Concentrations in Imperfect Filamentary Composite Materials. J. Comp. Mat., vol. 1, no. 3, July, 1967, pp. 294–309.

17. Jones, R. C.: Fractography of Aluminum-Boron Composites. ASTM STP 460, 1969, pp. 512–527.

18. Taylor, R. J.; Shimizu, H.; and Dolowy, J. F., Jr.: Mechanical Behavior of Aluminum-Boron Composites. AFML-TR-68-385, August, 1969.

19. Zweben, C.: The Strength of Notched and Damaged Composites. J. Comp. Mat., vol. 3, October, 1969, pp. 713–714.

20. Zweben, C.: On the Strength of Notched Composites. J. Mech. Phys. Solids, vol. 19, June, 1971, pp. 103–116.

21. Herring, H. W.: Selected Mechanical and Physical Properties of Boron Filaments. NASA TN D-3202, 1966.

22. Cooper, G. A.; and Kelly, A.: Tensile Properties of Fibre-Reinforced Metals: Fracture Mechanics. J. Mech. Phys. Solids, vol. 15, 1967, pp. 279–297.

VIII. VITA

The author was born in [redacted] He attended public schools in Virginia and graduated from Poquoson High School in 1957. He attended Virginia Polytechnic Institute and State University, and in 1962 received the B.S. degree in metallurgical engineering. He has been employed by the National Aeronautics and Space Administration, Langley Research Center since 1962 where he has been involved in research programs in the areas of materials, mechanics, and structures with special emphasis on structural applications of advanced filamentary composites. He has published several technical papers in these fields.

The author served a six year enlistment in the United States Marine Corps Reserve, being honorably discharged in 1963. He was married in 1958 to the former Mary Elaine [redacted] of Hillsboro, North Carolina, and has a son, Gary, aged 10 years, and a daughter, Helen, aged 6 years.